# The surface of helium crystals

Sébastien Balibar*

*Laboratoire de Physique Statistique de l'Ecole Normale Supérieure, associé au CNRS et aux Universités Paris 6 et 7, 24 rue Lhomond, 75231 Paris Cedex 05, France*

Harry Alles†

*Low Temperature Laboratory, P.O. Box 2200, FIN-02015 HUT, Espoo, Finland*

Alexander Ya. Parshin‡

*P.L. Kapitza Institute for Physical Problems, Kosygina ul. 2, 119334, Moscow, Russia*

(Published 18 May 2005)

Helium crystals exhibit faceting as do ordinary crystals, but no other crystals can grow and melt sufficiently fast to make the propagation of crystallization waves possible at their surfaces. After nearly two decades of controversy, it is now generally accepted that helium crystals are model systems for the general study of crystal surfaces, but also exceptional in having unique quantum properties. This review, which summarizes 25 years of research on the surface of helium crystals, treats both what is general and what is particular to helium. A central issue among the general properties is the "roughening transition," the phase transition from a smooth faceted state of the crystal surface at low temperature to a rough and fluctuating state at high temperature. This review describes the series of experiments that have significantly improved our understanding of this transition and its related critical phenomena. Some attention is paid to the experimental techniques, which are rather unusual in many cases. The Nozières renormalization theory of roughening is also described in some details and compared with experiment. Other general properties of crystal surfaces have also been studied in helium, such as the energy of steps on the facets and their mutual interactions, and several instabilities. The relevant experiments are presented together with their theoretical interpretation. The quantum mechanisms that control the growth dynamics of helium crystals are also reviewed. Here, too, theory is compared with experiment, not only in the matter of crystallization waves, but more generally on the mass and heat flows in nonequilibrium situations, including the two stable helium isotopes $^4$He and $^3$He, which behave in quite different ways. Finally, a list of open questions is presented for future research.

## CONTENTS



*Electronic address: balibar@lps.ens.fr
†Electronic address: harry@boojum.hut.fi
‡Electronic address: parshin@kapitza.ras.ru

 

## I. INTRODUCTION

Helium crystals are model systems. Their study has revealed crucial information on very general properties of all crystal surfaces. But this is not the only reason they are interesting: some of their other properties are exceptional and surprising, as is often the case when quantum mechanics plays a major role (Balibar and Nozières, 1994).

Why exceptional? At low enough temperature, for example, below 0.5 K, $^4$He crystals grow and melt so easily that "crystallization waves" can propagate at their surface. Imagine that you have a cryostat with optical access and that the experimental cell inside contains a $^4$He crystal in equilibrium with its liquid phase. Then, shake the cryostat. You will see waves propagating at the liquid-solid interface just as if you looked at the free surface of water (see Fig. 1). These waves propagate because $^4$He crystals grow and melt very fast. This was predicted in 1978 (Andreev and Parshin, 1978) and the phenomenon observed a year later (Keshishev *et al.*, 1979). Moreover, the lower the temperature, the faster $^4$He crystals grow. No classical crystal behaves in this manner.

As we shall see in this review, the spectacular phenomena of crystallization waves and the unusual growth dynamics are linked to the quantum properties of liquid and solid helium at low temperatures. When crystal growth takes place from a superfluid, there are situations in which no dissipation at all takes place at the moving interface; this would be impossible in a classical liquid, where the sticking of individual atoms necessarily dissipates energy because of a momentum exchange at the moving crystal surface.

At a temperature of 0.1 K, the growth of $^3$He crystals is slower than the growth of $^4$He crystals by 11 orders of magnitude (Graner *et al.*, 1989). If one compared classical crystals made of different isotopes of the same element, one would find that they had very similar properties. In contrast, because $^3$He atoms are Fermi particles while $^4$He atoms are Bose particles, the growth dynamics of $^3$He crystals are very different from those of $^4$He crystals.

Given all this, how can it be that helium crystals are ideal for the study of universal properties of crystal surfaces? As temperature goes down, in any crystal, the surface is covered with more and more facets, which are smooth and flat states of the surface (see Fig. 2). Of course, in helium everything happens at lower temperature than in other systems because the interaction energy between atoms is much smaller, but the physical mechanism for the existence of facets is the same as in other systems. Furthermore, the fast dynamics allows the use of unusual experimental methods for the measurement of quantities that are difficult to access with ordinary crystals. This is particularly true for the surface tension and step energies, which are the quantities controlling faceting and roughening, that is, the appearance and disappearance of facets at the crystal surface.

Suppose that you pour some liquid into a glass. The liquid occupies the bottom of the glass and its free surface quickly reaches an equilibrium shape minimizing the sum of the surface and gravitational energies. Suppose now that you pressurize a cell which contains superfluid $^4$He at low temperature. At a pressure of 25.3 bars, a crystal appears. Now stop the pressurization. The helium in the cell will relax to its thermodynamic equilibrium within a very short time. In equilibrium, the shape of the liquid-solid interface also minimizes the effects of gravity and surface tension: the crystal occupies the bottom part of the cell, with a horizontal surface in the middle and with some capillary effects at the edges, just as if it were a liquid. This relaxation is fast because both liquid and solid $^4$He have large thermal conductivities and also because the latent heat of crystallization is

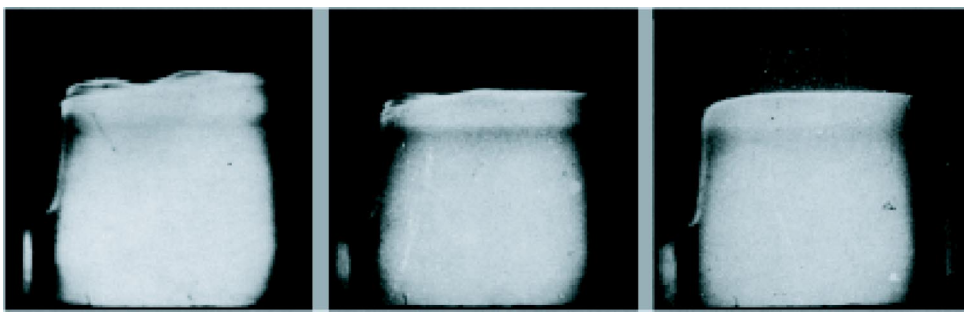

FIG. 1. Crystallization waves in $^4$He. Keshishev *et al.* discovered crystallization waves in 1979 by shaking their cryostat: the interface between a $^4$He crystal and superfluid $^4$He moves so easily by growth and melting that it looks like a free liquid surface. From Keshishev *et al.*, 1979.

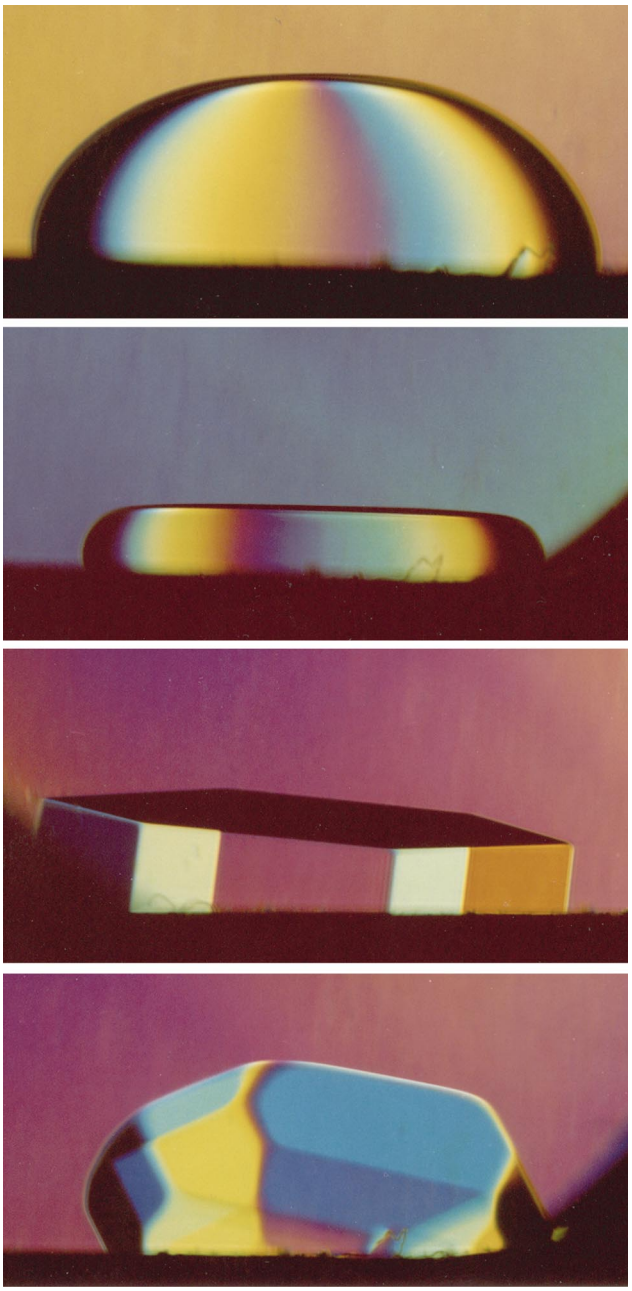

FIG. 2. (Color) Faceting of $^4$He crystals. As temperature goes down, more and more facets appear at the surface of $^4$He crystals. From top to bottom, the temperature is successively 1.4, 1, 0.4, and 0.1 K. The size of the facets is larger than on equilibrium shapes, due to the slow growing from the surrounding superfluid (see Fig. 20). The colors are real, obtained by Balibar, Guthmann, and Rolley (1994) with a prism, a lens, and a small mask (see Sec. II.B.1).

small, so that the crystal shape is not perturbed by any temperature inhomogeneity as in classical systems. Furthermore, since mass transport occurs easily in a superfluid, the crystal evolves very quickly by melting in one place and freezing in another (except in the faceted areas). Its shape evolution does *not* include any deformation of the lattice. All the mass transport takes place in the liquid. In Sec. IV we shall see more precisely how these dynamics proceed, but one result is clear: capillary phenomena show up in helium crystals as if they were liquids, although they are among the highest-quality crystals one can find in nature.

In fact, crystallization waves are manifestations of the same capillary phenomena, and evidence has been found that they propagate from zero frequency up to thermal frequencies ($10^{11}$ Hz). Of course this would never happen with classical crystals, in which heat and mass diffuse slowly. Usually, surface phenomena are hidden by bulk diffusion, but not in helium. This allows important comparisons of experimental results with theoretical predictions, particularly for the renormalization-group (RG) theory of roughening, which has been improved thanks to comparison with experiments in helium (Balibar and Nozières, 1994).

The existence of facets at crystal surfaces has been a long-standing problem in theoretical statistical physics. As early as 1949, Landau was interested in it, and he predicted that, at $T=0$, the crystal surface would be covered with facets in all crystalline directions having rational Miller indices (Landau, 1965).[1] In 1949–1951, Burton, Cabrera, and Frank then predicted that all facets would disappear at the successive "roughening temperatures," which they calculated using an approximate theory (Burton and Cabrera, 1949; Burton *et al.*, 1951). As temperature increased, crystal surfaces should be more and more rounded, with "smooth" facets only in a decreasing number of high-symmetry directions and with "rough" surfaces in all other directions.

The modern theory of roughening was developed only after Wilson introduced the renormalization-group theory (Wilson, 1971). van Beijeren, Knops, and Chui and Weeks solved the first models (van Beijeren, 1975, 1977; Chui and Weeks, 1976, 1978; Knops, 1977) and their work was soon extended by many other authors (for a review, see Weeks, 1980). Some predictions of the RG theory have been tested with metallic crystals such as copper (Mochrie, 1987; Lapujoulade, 1994), nickel (Conrad and Engel, 1994), and silver (Hoogeman *et al.*, 2000), but it seems that the most complete and quantitative check of this theory, or this class of theories, has been performed with the hexagonal facets of $^4$He crystals. These experiments spurred later developments of the theory itself (Nozières and Gallet, 1987; Nozières, 1992). The RG theory of roughening is now well established and can be universally applied to predict the existence of facets at the surface of crystals, as shown by the recent case of some liquid crystals (Nozières *et al.*, 2001).

As we shall see, a smooth facet becomes a rough surface at its roughening temperature $T_R$ when the energy of steps between successive crystal planes decreases to zero. The long-range order of facets is destroyed by the proliferation of steps. But at low temperature, facets are

[1]Editor's note: For his argument, Landau considered the energy associated with individual steps on a crystal surface and an interaction energy between steps due to van der Waals forces.

well-ordered surfaces whose size and growth rate are controlled by steps with nonzero energies. For a complete understanding of the properties of facets, it is important to know not only the energy of steps at this surface, but also their width, fluctuations, and mutual interactions. Here again, helium crystals have allowed precise measurements of all the above properties of steps, while with ordinary crystals measurement is usually rather difficult.

Helium crystals have thus provided an interesting model system for the general study of crystal growth and shapes. No less interesting are the quantum mechanisms underlying many aspects of their dynamics. A classical crystal grows or melts more slowly as temperature decreases. This is because the microscopic processes are thermally activated, so that, as temperature decreases, they become exponentially slow. With helium at low temperature, atoms can go through energy barriers by quantum tunneling (Andreev and Parshin, 1978). As a result, the growth dynamics of crystals are limited only by the scattering of the moving crystal surface with thermal excitations, on either side of the liquid-solid interface (Andreev and Parshin, 1978; Andreev and Knizhnik, 1982; Bowley and Edwards, 1983). At low temperature, where the dominant thermal excitations are phonons, the resistance of $^4$He crystals to growth has been predicted to vanish proportionally to $T^4$ (Andreev and Parshin, 1978; Andreev and Knizhnik, 1982; Bowley and Edwards, 1983). This behavior was observed experimentally by Keshishev *et al.* (1979, 1981). It is reminiscent of the electrical resistivity of a metallic crystal at low temperature. Electrons tunnel through the lattice of positive ions and, in a certain temperature range, their mobility is limited by collisions with phonons, so that the resistivity decreases as temperature goes down.

It was also predicted (Andreev and Parshin, 1978; Puech *et al.*, 1986a), and observed later (Graner *et al.*, 1989) that, in $^3$He, the scattering of Fermi quasiparticles leads to a much higher growth resistance than in $^4$He. The study of the growth dynamics of helium crystals has illustrated another general problem, the motion of surfaces in quantum systems. Below 1 mK, where liquid $^3$He is superfluid and solid $^3$He is a nuclear antiferromagnet, new properties are currently under investigation.

For most of these studies, it has proven very useful to be able to vary the temperature over a substantial range. This is possible in helium because of particular features of its phase diagram. As shown in Figs. 3 and 4, there is no triple point in helium where the liquid, solid, and gas phases would coexist. Instead, the liquid exists down to absolute zero and the solid is stable only above about 25 bars in $^4$He (30–35 bars in $^3$He). As a result, the crystal surface that we consider in this review is a liquid-solid interface. Experiments have been performed in a temperature domain that extends over nearly four decades, from $5\times10^{-4}$ K to 2 K, without much change in pressure or density. Liquid $^4$He is superfluid below 2.17 K, while liquid $^3$He becomes superfluid at temperatures a thousand times lower. There is a transition from the hexagonal-close-packed (hcp) structure to the body-centered-cubic (bcc) one in $^4$He at 1.46 K. At low temperature, $^3$He crystals have a bcc structure, with a nuclear antiferromagnetic phase below $T_N=0.93$ mK (see Fig. 4).

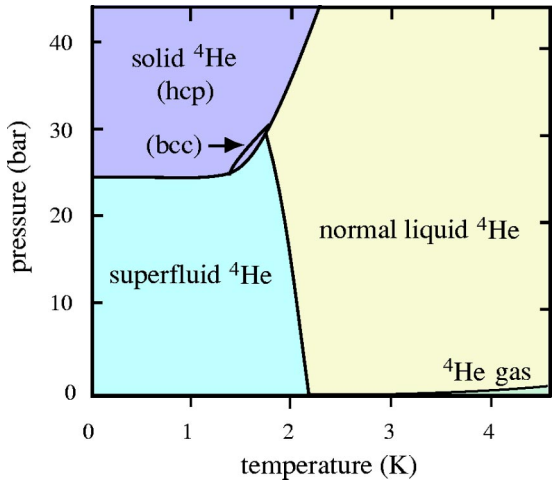


FIG. 3. (Color in online edition) Phase diagram of $^4$He. There is no triple point where the liquid, solid, and gas phases would meet. On the melting curve at low temperature, solid $^4$He has a hcp structure; between 1.46 and 1.76 K, it is bcc.

This review article is organized as follows. In Sec. II, we describe experimental techniques that have been developed for the study of helium crystals. Section III is devoted to the roughening transitions. We present various theories with special emphasis on the Nozières RG theory. We then describe various measurements of quantities such as the surface tension, crystal curvature, step energy, and surface mobility, and compare experimental results with theoretical predictions. We continue with other aspects of crystal shapes, in particular, with step-step interactions. This section ends with a discussion of

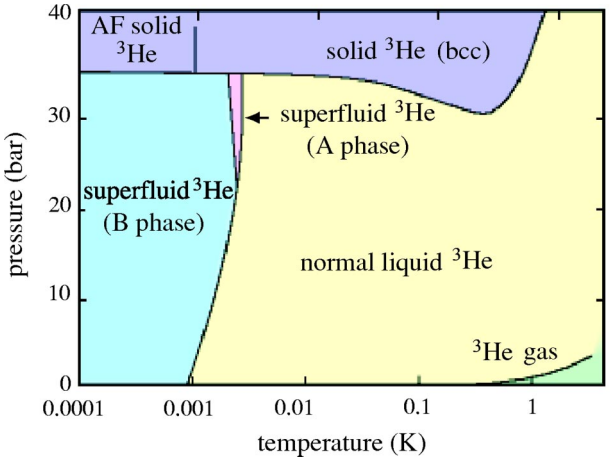


FIG. 4. (Color in online edition) Phase diagram of $^3$He. As in $^4$He, there is no liquid-solid-gas triple point. Two distinct superfluid phases exist below $T_c=2.5$ mK, and the bcc crystal is antiferromagnetic below $T_N=0.93$ mK.

$^3$He crystals, in which the study of roughening is more difficult than in $^4$He, but for which additional information on the step-step interactions has been obtained, thanks to the variety of facets seen on these crystals. In this section, as in all others, we not only describe the well-understood properties, but also mention open questions that deserve further study.

Section IV describes the dynamics—that is, the growth and melting—of rough crystal surfaces. We start with a description of crystallization waves at the rough surfaces and explain how their study has led to accurate measurements of the surface tension (more precisely, the surface stiffness), step energies, and mutual interactions between steps. In the same section, we consider the damping of crystallization waves as a function of temperature. This damping is one aspect of a more general problem of nonequilibrium thermodynamics. We also describe sound transmission and heat flow through the liquid-solid interface, as well as crossed effects of temperature and chemical potential differences in the frame of the relevant Onsager matrix. After considering $^4$He, we present the dynamic properties of $^3$He crystals, which are quite different.

Section V is devoted to the dynamics of smooth faceted surfaces, which is related to the motion of steps and much slower than the dynamics of rough surfaces. Here again, some of the observed mechanisms, such as spiral growth, are common to all crystalline surfaces, while others are particular to helium, for example, critical velocities for the motion of steps.

In Sec. VI, we review various instabilities that have been studied in helium, which further illustrate the role of helium as a model system for other crystal surfaces. One example is the Asaro-Tiller-Grinfeld instability, which concerns the shape of a crystal surface when a nonhydrostatic stress is applied. Corrugations appear above some threshold value, a phenomenon that has been related to spontaneous pattern formation in heteroepitaxy. We describe both the theory of this instability and the experiments with $^4$He crystals that provided the first evidence for its existence. We then consider the dendritic instability and describe the case of $^3$He crystals. We also mention briefly a few other instabilities that are of interest.

Our conclusion contains a list of open questions for future work.

## II. EXPERIMENTAL TECHNIQUES

### A. Optical cryostats

When Keesom discovered solid helium ($^4$He), he tried to observe the liquid-solid interface, but he failed. Through the walls of his glass Dewar, "… there was nothing peculiar to be seen …" (Keesom, 1926). Thirty-five years later, Shal'nikov grew good-quality helium crystals and took the first pictures of the liquid-solid interface down to 1.2 K, for both $^4$He and $^3$He (Shal'nikov, 1961, 1964). However, the quantitative study of the surfaces of helium crystals really began with the work of three different groups, in Moscow (Keshishev *et al.*, 1979), Paris (Balibar *et al.*, 1979), and Haifa (Landau *et al.*, 1980). Although many experiments could be done with blind cells, for example, in Paris (Balibar *et al.*, 1979; Castaing *et al.*, 1980), at Brown University (Huber and Maris, 1981; Graf *et al.*, 1984), in Texas (Wang and Agnolet, 1992a), in Grenoble (Puech and Castaing, 1982; Amrit and Bossy, 1990), and in Kyoto (Nomura *et al.*, 1994; Kawaguchi *et al.*, 2002), the use of cryostats with good-quality optical access proved to be very useful because the direct observation of crystal shapes permitted determination of the crystal orientation, its surface state, and the quality of the surface before performing measurements.

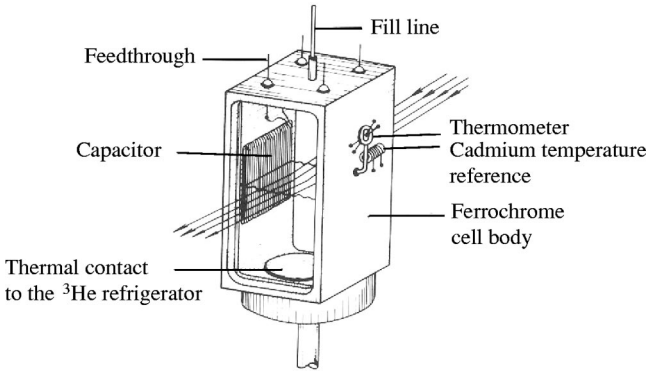


FIG. 5. Experimental cell used in Moscow. From Keshishev *et al.*, 1981.

One has to avoid looking through liquid nitrogen, which usually boils, and even through an ordinary liquid-helium bath at 4 K, where convection takes place and snowflakes of frozen air are often found. Conventional optical cryostats have windows attached to the low-temperature screens and optics outside (see Fig. 6 as an example). They allow easy adjustments or even complete changes of the optical setup in the course of experimental runs, but their lowest temperature is limited by the heat leak due to thermal radiation from the outside world at 300 K through the windows.

Keshishev *et al.* (1979, 1981) modified Shal'nikov's apparatus and observed crystals through five pairs of windows, at 300 K, on the 77-K shield, on the two sides of a 4.2-K liquid-helium bath, and on the experimental chamber, which was cooled down by a $^3$He refrigerator. These windows were glued with Stycast 1266 epoxy glue. In order to minimize the risk of leaks, the cell was built out of ferrochrome, so that the differential thermal contraction was not too large between the cell body and the large chemical glass windows ($12\times28$ mm$^2$), which were glued onto it (see Fig. 5). For their later experiments in Paris, Wolf *et al.* (1985) and Rolley, Guthman, *et al.* (1995) preferred sealing the windows with indium rings on stainless-steel or copper flanges, a technique that was also used in Mainz (Savignac and Leiderer, 1982), Konstanz (Thiel *et al.*, 1992), Helsinki (Manninen *et al.*, 1992; Babkin *et al.*, 1995; Ruutu *et al.*, 1998; Tsepelin *et al.*,

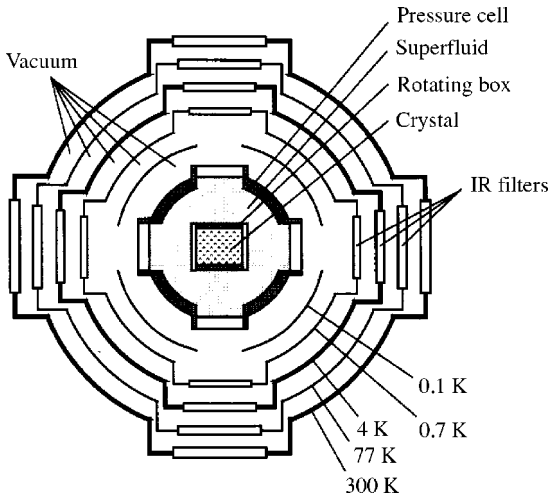


FIG. 6. Optical setup of the Paris group. From Rolley, Guthmann, *et al.*, 1995.

2002a), etc. The Leiden group successfully glued fused silica windows with Stycast 1266 onto a cell made out of Araldite (Wagner *et al.*, 1994; Marchenkov *et al.*, 1999; van Rooijen *et al.*, 2001). In Tokyo, Nomura *et al.* (1994) used Kovar seals with glass windows and a stainless-steel cell.

In conventional optical cryostats, low temperatures are not reached without filtering the incoming infrared radiation. This is particularly important when the cell sees a room-temperature environment. Radiation with wavelengths larger than 0.8 $\mu$m can be efficiently filtered by suitably coating the windows. In order to improve this, the Paris group used Pyrex glass for the window material (except for their cell, where the use of sapphire, which is stronger, allowed the windows to be thinner). In their latest cryostat, the total absorption of radiation by the cell was about 10 $\mu$W, with four sets of large windows ranging from 34 mm diameter on the cell to 70 mm at 300 K (see Fig. 6). By using only one set of windows, reducing the size of the windows, and improving the infrared filtering, this radiative power could probably be reduced to 1 $\mu$W, which would be compatible with temperatures of a few mK.

Above its superfluid transition temperature $T_c$ (2.5 mK on the melting curve), liquid $^3$He is a Fermi liquid with poor thermal conductivity, and the latent heat of crystallization is large. As a consequence, $^3$He crystals behave similarly to classical crystals at such temperatures. However, below $T_c$, the superfluid-solid interface of $^3$He is expected to behave differently, and, at $T_N = 0.93$ mK, the effect of the magnetic ordering transition in the solid is also expected to be interesting. Thus different groups have built special cryostats for optical studies in the submillikelvin range (Manninen *et al.*, 1992; Wagner *et al.*, 1994; Tsepelin *et al.*, 2002a).

The Helsinki group was able to observe the free surface of superfluid $^3$He down to about 0.7 mK by using optical fibers to communicate between room temperature and the low-temperature part of their cryostat

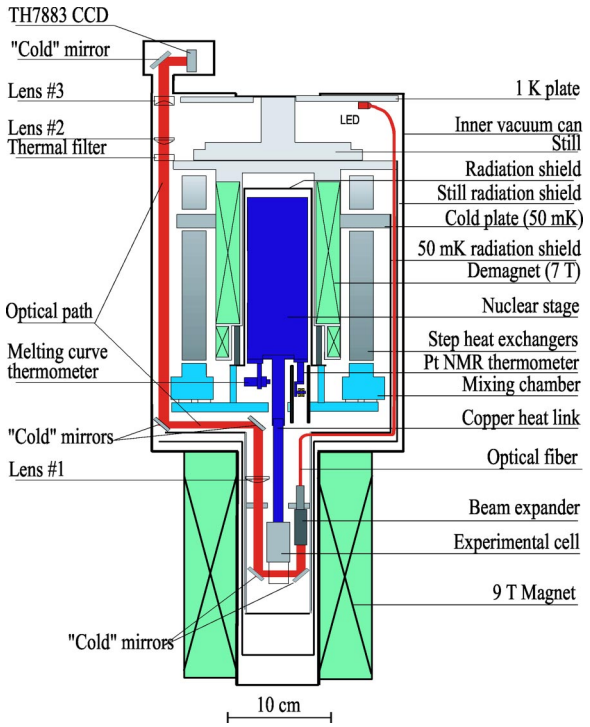


FIG. 7. (Color in online edition) Leiden optical setup for studies of $^3$He crystals in a high magnetic field. From van Rooijen *et al.*, 2001.

(Manninen *et al.*, 1992). The Leiden group designed and constructed a new type of optical cryostat with a charge-coupled device (CCD) camera sensor inside its vacuum can (Wagner *et al.*, 1994). Their latest setup is presented in Fig. 7. This sensor works around 60 K and with slow scanning (one image every 4 s), in order to improve the sensitivity and allow the use of less light. The illumination is provided by a light-emitting diode (LED), which is also located inside the cryostat. In their later setups, the Helsinki group also adopted a low-temperature CCD camera because the resolution ($576 \times 384$ pixels) was better than with a bundle of 30 000 fibers (Babkin *et al.*, 1995; Ruutu *et al.*, 1998; Tsepelin *et al.*, 2002a). For laser light illumination a single-mode optical fiber is used as before. After filtering the thermal radiation from the CCD sensor with two filters made of $CaF_2$ and sapphire (see Fig. 9), the radiative power into the experimental cell was reduced to a few nW (Alles and Parshin, 2004).

### B. Imaging techniques

#### 1. Black and white or color imaging

The polarizability of helium is weak and the difference in density between liquid and solid helium is small, so that the difference in their refractive indices is also small. However, in $^4$He the incidence angle for total reflection is 85° from the solid side, so that the liquid-solid interfaces are visible at grazing incidence. A He crystal immersed in liquid He is a transparent object in a transparent medium; when looking at it with the naked eye, it

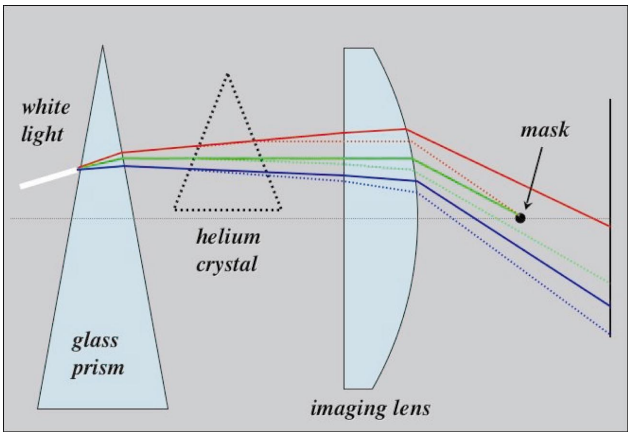


FIG. 8. (Color) Principle of the color imaging technique used by Balibar, Guthmann, and Rolley in Paris (not to scale). In practice, the mask was a small black cylinder with a diameter of 2 mm. By moving this mask in the focal plane of the imaging lens, one could change the color of the background. Each pair of facets forms a helium prism whose angle determines the refraction and thus the color.

looks like an ice cube in water: one sees its profile but not its three-dimensional shape. Growth shapes may have facet edges that are sharp enough so that diffraction takes place and makes these edges visible (see Fig. 36 below). In practice, infrared (IR) filters on the windows usually absorb some red light, so that images look greenish, especially if photographed with ordinary cameras whose films are sensitive to IR radiation and thus not supposed to give real colors if IR is suppressed. Video or digital cameras are not so sensitive to IR problems.

Simple imaging techniques can be used to improve the observation of the crystal shape. If the crystal is observed in transmission with white light, a dark background can be obtained by stopping the light with a little mask at the focal point of the imaging lens. Due to the index difference, the light is deviated when passing through the crystal and it converges in the focal plane but not through the focal point; thus the crystal looks bright on a dark background. A spectacular improvement of this dark-background technique can be obtained by dispersing the white light with a glass prism before it reaches the helium crystal (see Fig. 8). In this case, each couple of facets forms a helium prism, which refracts light at an angle that depends on the opening angle of the helium prism. As a result, each couple of facets appears with its own uniform color, which is different from the background color, except of course if the two facets are parallel (see Fig. 2). All these colors can be easily changed by moving the mask in the focal plane.

### 2. Interferometry

Conventional imaging techniques can be used to demonstrate the qualitative properties of crystal surfaces. Quantitative studies require interferometry. The refractive indices are given by the Clausius-Mossotti relation,

$$n^2 = \frac{1+2\eta}{1-\eta}, \tag{1}$$

where

$$\eta = \frac{4\pi\rho\alpha_M}{3M}, \tag{2}$$

and where $M$ is the molar mass (4.0026 g/mole for $^4$He and 3.0160 g/mole for $^3$He), $\rho$ is the density, and the polarizability $\alpha_M$ depends slightly on frequency. From the work of Cuthbertson and Cuthbertson (1932), Edwards (1958), Harris-Lowe and Smee (1970), and Donnelly and Barenghi (1998), $\alpha_M$ is found to be 0.1233 at zero frequency, 0.1241 for red light (632.8 nm), and 0.1245 for green light (515 nm) (Chavanne *et al.*, 2001). As a result, in $^4$He on the melting curve at low temperature, where $\rho_L = 0.172\,45$ g/cm$^3$ and $\rho_C = 0.190\,76$ g/cm$^3$, one has $n_L = 1.0338$ and $n_C = 1.0374$ for red light (1.0339 and 1.0375 for green light). The index difference $\delta n = n_C - n_L$ equals $3.6\times10^{-3}$. For $^3$He in the very-low-temperature limit, one finds $\delta n = 1.0324 - 1.0307 = 1.7 \times 10^{-3}$ for red light.

Pipman *et al.* (1978) and Landau *et al.* (1980) applied a differential holographic technique, which proved very complicated to use. All other groups have installed an interferometric cavity inside their cryostat. For example, Bodensohn *et al.* (1986) and Gallet *et al.* (1987) were able to measure 1-$\mu$m height changes of a liquid-solid interface. For this, they had to analyze fringe patterns within one hundredth of a fringe. In such cavities, the fringe structure depends on the reflection coefficients of the walls. For small coefficients one has two-beam interferometry and sinusoidal fringes, which is suitable for studies of large surface areas. Small surface areas, such as facets, need sharper fringes for analysis, and this can be obtained by using surfaces with larger reflection coefficients (in the limit of a Fabry-Pérot interferometer, the fringes are delta functions).

It is also possible to use the helium interface itself as one of the walls of the optical cavity. In this case, one gains a factor $(n/\delta n) \approx 10^3$ in sensitivity but, since the reflection coefficient of the crystal surface is very small ($10^{-6}$–$10^{-7}$), the other cavity wall, which is a glass plate, has to be covered with an antireflection coating in order to obtain a reasonable contrast. With the best available coatings, which have reflection coefficients of about $10^{-4}$, the contrast between bright and dark fringes is about 1.5, quite sufficient for good measurements (Hakonen *et al.*, 1995). However, this technique can only be used when the crystal surface is nearly parallel to the glass plate.

For their studies of $^4$He crystals, the Helsinki group used the optical setup shown in Fig. 9. A He-Ne laser light ($\lambda = 632.8$ nm) enters the cryostat through a single-mode optical fiber (leak-tight feedthroughs are made with Stycast 1266 epoxy). From the end of the fiber, the beam is expanded with two lenses, and a parallel beam with an 8 mm diameter illuminates the experimental cell. Most of the light is transmitted through the cell and

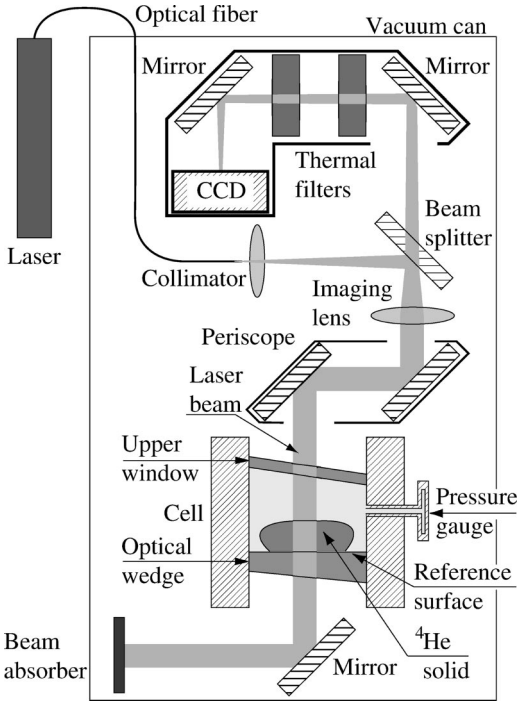


FIG. 9. Interferometric setup of the Helsinki group for the studies of $^4$He crystals built inside the 4-K vacuum can of the nuclear demagnetization cryostat. From Ruutu *et al.*, 1998.

absorbed by a black surface, which is thermally anchored to the 0.7-K still of the dilution refrigerator. Only about 1 ppm of light is reflected back from the liquid-solid interface and about 100 ppm from the reference plane, which is the antireflection-coated upper surface of the lower window of the cell. These two reflected beams form the interference pattern, which is focused to a cooled CCD sensor inside the vacuum can.

The optical cell of Ruutu *et al.* is a cylindrical copper volume with an inner diameter of 17 mm. The upper window is tilted and the lower window wedged by about 2° with respect to the cylinder axis in order to prevent reflections from the corresponding surfaces from reaching the CCD sensor. The optical volume is connected to the silver heat exchanger at the top of the nuclear stage (not shown in Fig. 9). The pressure in the cell is measured using a sensitive capacitive gauge (Straty and Adams, 1969). With this setup $^4$He crystals were imaged down to about 2 mK (Ruutu *et al.*, 1998).

Subsequently, the Helsinki group concentrated on the study of $^3$He crystals and modified the setup of Ruutu *et al.*; they built a multiple-beam interferometer inside their nuclear demagnetization cryostat (see Fig. 10). Multiple-beam interferometry was chosen in order to determine the orientation of small facets from fringe spacings in a small area.

This interferometer consists of two nearly parallel mirrors with 50% and 70% reflectivities, placed above and below the optical part of the cell and thermally anchored to the mixing chamber. The vertical resolution of the interferometer is a few $\mu$m, while the horizontal resolution of about 15 $\mu$m is limited by the pixel size of

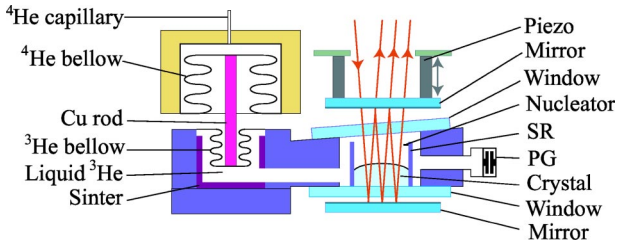


FIG. 10. (Color in online edition) Compressional cell and a Fabry-Pérot type of interferometer for the studies of $^3$He crystals. From Tsepelin *et al.*, 2002a.

the CCD sensor. Crystal surfaces with a slope of up to 70° with respect to the bottom mirror of the interferometer could be resolved.

A typical interferogram taken with this multiple-beam interferometer is shown in Fig. 37, below, where a growing $^3$He crystal has been imaged at 0.55 mK. The adjacent fringes correspond to multiples of $\lambda/2(\delta n)$ in the optical path length, which corresponds to 190 $\mu$m in crystal thickness. The facets show up in the interferograms as sets of equidistant parallel straight lines; the background pattern is due to the liquid wedge and less-than-perfect alignment of mirrors.

### C. Nucleation and orientation of crystals

The liquid-solid transition being discontinuous, there is an energy barrier against the nucleation of crystals. In most experiments in helium, an overpressure of a few mbar is enough to overcome the barrier. Crystals typically nucleate on local defects which might be graphite dust particles attached to the walls (Balibar *et al.*, 2000). Once nucleated, the crystals grow and fall to the bottom of the cell as soon as they feel the effect of gravity, that is, when they are larger than the capillary length $l_c \approx 1$ mm. After a given crystal has been melted by reducing the cell pressure, it often happens that a new nucleation leads to a crystal with the same orientation as the previous one. This is usually attributed to the possibility that the wall defects retain crystal seeds even at pressures below the melting pressure $P_m$. These seeds could be eliminated by reducing the pressure further, sometimes very far below $P_m$, or by warming up the cell.

Keshishev *et al.* invented a clever method for obtaining oriented crystals. They noticed that nucleation could be forced to occur at a particular place in the cell by using an electric field (Keshishev *et al.*, 1979). For that purpose, they made a double winding of 30-$\mu$m-diameter insulated wires and applied a high voltage, typically 800 V, between the two wires. In this manner they obtained a region of high electric field. Due to electrostriction, the solid density being larger than the liquid one, crystals preferably nucleated on the coil when the pressure inside the cell was increased. By locating this coil on the top of the cell, they then forced the crystals to fall to the bottom through superfluid helium. At a fraction of a kelvin, the shape of $^4$He crystals is often flat, with large hexagonal facets, so that they land with

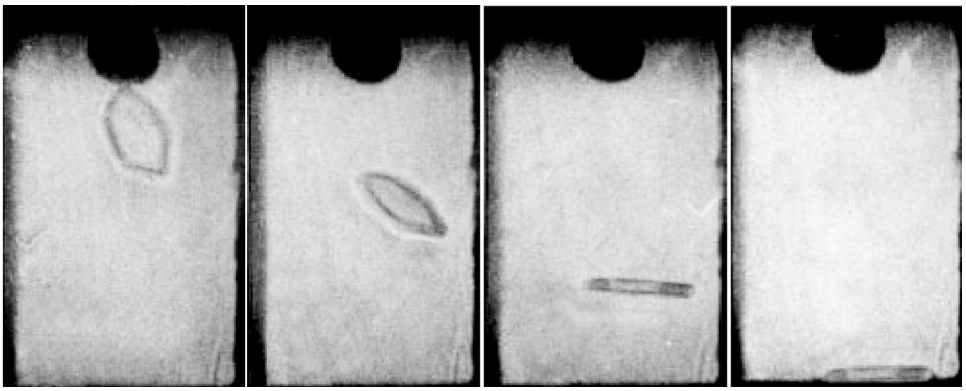

FIG. 11. Sequence of photographs showing a $^4$He crystal falling from the top, where it nucleates, to the bottom of the cell. If its shape is a flat prism, the crystal flies like a sheet of paper and lands horizontal. From Babkin *et al.*, 1985.

one of these facets nearly horizontal (see Fig. 11). This method has been successfully used by other groups (Rolley, Guthmann, *et al.*, 1995; Ruutu *et al.*, 1998); the double winding could be replaced by an interdigital evaporated layer or by a sharp needle (Tsymbalenko, 1995). Eventually, since $^4$He crystals were shown to grow epitaxially on graphite substrates (Balibar *et al.*, 1980; Eckstein *et al.*, 1980; Ramesh and Maynard, 1982; Wang and Agnolet, 1992a), it was found possible to obtain oriented crystals by placing a small piece of clean graphite in the cell. Balibar *et al.* (1980) showed that this graphite piece had to be properly degassed to work.

In order to study crystals with different orientations, one can repeat the nucleation procedure several times, so that a random distribution of orientations is obtained. With ordinary crystals, one usually gets surfaces with different orientations by cutting new crystals at different angles. With $^4$He crystals, it was found possible to do this in a completely different way (Andreeva and Keshishev, 1987; Rolley, Guthmann, *et al.*, 1995). If crystals are larger than the capillary length, their upper surface is forced by gravity to be horizontal. As a result, when a crystal is rotated together with the cell, it melts on one side and grows on the other side. This change in shape occurs within much less than a second at temperatures well below 1 K. As a consequence, the crystal surface remains horizontal but it changes orientation because the lattice orientation rotates together with the cell walls. Using this method, very precise studies of the angular variation could be performed with a single $^4$He crystal. Andreeva and Keshishev (1987) could rotate their cell by as much as ±60° around one axis. Rolley, Guthmann, *et al.* (1995) could rotate their cell by ±6° around two perpendicular axes (see Fig. 12).

What about crystal quality? At low temperature, the melting pressure $P_m$ of solid helium is nearly independent of temperature, so that helium crystals can be grown only by applying a small overpressure. As, Shal'nikov showed, the quality of helium crystals was not good when they were grown by cooling a cell that had first been filled at high temperature and then closed to follow an isochore. This was presumably because, above 1.2 K or so, the melting pressure of $^4$He increases significantly with temperature, so that varying the temperature leads to stresses in the crystal. These stresses lead to an instability of the crystal surface, which has been carefully studied in $^4$He by the Konstanz group (Bodensohn *et al.*, 1986; Thiel *et al.*, 1992; see Sec. VI.A).

To obtain high-quality helium crystals, one has to grow them from a small seed. After nucleation, the crystal has to be melted to the smallest possible size in order to eliminate as many defects as possible. These defects can be dislocations, which are important for the growth of faceted surfaces (see Sec. V). They can also be stacking faults, in which case the crystal surface shows macroscopic grooves like those on the skin of an orange. This is because stacking faults have a surface energy comparable to the energy of the liquid-solid interface, so that they create cusps with finite angles when they emerge at the crystal surface. Rolley, Guthmann, *et al.* (1995) showed that, by growing $^4$He crystals around 0.1 K, from a 1-mm seed and not faster than 0.1 $\mu$m/s, it was possible to obtain liquid-solid interfaces without defects. Ruutu *et al.* (1996) obtained dislocation-free crystals by nucleating them spontaneously and growing them at 20 mK without special care. It thus seems that grow-

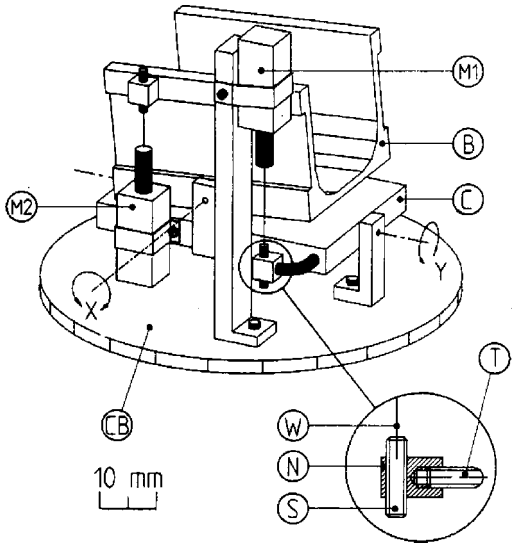


FIG. 12. Rotating box in the Paris setup. Two micromotors (M1 and M2) allow rotation by ±6° around the $X$ and $Y$ axes. The motors are coupled to the box (B) and to the plate (C) thanks to flexible metallic wires (W) attached to screws (S). From Guthmann *et al.*, 1994.

ing crystals by applying a small overpressure (a few mbar) at the lowest possible temperature leads to the highest quality.

The required overpressure is usually applied through the fill line of the cell, from the outside of the cryostat. The Moscow group used a buffer volume outside the cryostat, whose temperature was regulated around 300 K, sometimes modulated in order to produce successive growth and melting (Keshishev *et al.*, 1979, 1981). The Paris group used a high-pressure cylinder containing high-purity helium gas and electronic flow regulation (Rolley, Guthmann, *et al.*, 1995). It should be noted here that this fill line does not usually become blocked (unless the helium is not sufficiently pure), although the melting curve of $^4$He has a shallow minimum near 0.8 K, so that the melting pressure in a low-temperature cell is higher than in some part of the fill line. Liquid $^4$He thus has to be in a metastable state somewhere in this fill line. This looks to be marginally possible since experiments have shown that the metastability can extend about 10 mbar above $P_m$ in the presence of ordinary walls, while the depth of the melting curve minimum is 8 mbar. However, in the case of $^3$He, where the depth of the minimum in the melting curve is about 6 bar, crystals can neither be grown nor melted at low temperature by varying the pressure from the outside, and deformable cells have to be used, either with bellows or with diaphragms (Sydoriak *et al.*, 1960; Osheroff *et al.*, 1972; Rolley *et al.*, 1989; Nomura *et al.*, 1994; Wagner *et al.*, 1994 Tsepelin *et al.*, 2002a).

Since the negative slope of the melting curve is large in $^3$He, it is possible to nucleate $^3$He crystals with a small heat pulse (Osheroff *et al.*, 1991). Osheroff *et al.* first cooled the liquid down to about 0.4 mK while keeping the cell pressure at least 200 mbar below the liquid-solid equilibrium pressure $P_m$. After that, the $^3$He pressure was slowly increased up to 1.2 mbar above $P_m$ and a heat pulse (1 ms, 2 erg) applied. Tsepelin *et al.* (2002b) nucleated $^3$He crystals with an electrical field, as in $^4$He. By growing their crystals in a narrow tube, Osheroff *et al.* (1991) could keep only one magnetic domain of the antiferromagnetic structure. The correlation between magnetic domains and crystal growth was later studied in Kyoto (Kawaguchi *et al.*, 2002).

### D. Surface-tension measurements

The surface tension of ordinary crystals is rarely accurately known. In contrast, with helium crystals, the rapid growth dynamics allows for simple measurements of capillary effects as if these crystals were liquids. Three different methods have been used to measure either capillary rise, their capillary length (from the shape of large crystals), or the dispersion relation of crystallization waves.

In their early experiments, Balibar *et al.* (1979) measured a capillary rise between the two electrodes of a cylindrical capacitor, inside a blind cell. In fact, this rise was negative—it was a capillary depression because the copper wall was preferentially wet by the liquid. They found a contact angle of typically 135° between the cell wall and the liquid-solid interface (see Fig. 13). This was attributed by Dash (1982) to the existence of large stresses in the solid $^4$He near the wall, especially if this wall was rough, and about the same angle was later observed with most other types of walls, and with $^3$He. Graphite walls are exceptional, since some matching of the crystal lattice leads to epitaxial growth of hcp $^4$He on it, indicating complete wetting by solid $^4$He. A similar matching has been reported by Eckstein *et al.* (1980) for bcc $^3$He crystals on cubic MgO substrates. Despite further studies by Markovitz and Polturak (2001), it is not yet clear whether there exist other substrates on which helium crystals could grow by epitaxy. Balibar *et al.* (1979) also measured the minimum overpressure necessary for the liquid-solid interface of $^4$He to pop through a circular hole. Balibar and Castaing (1980) later understood that, if facets were well developed at the crystal surface, the rather high measured overpressure was not directly related to the surface tension of the crystal. Instead, it was an indirect indication that $^4$He crystals are faceted below 1 K.

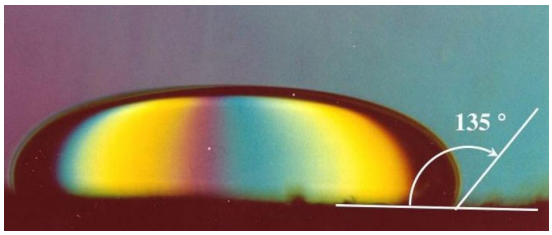


FIG. 13. (Color in online edition) Contact angle of the liquid-solid interface of $^4$He. As shown by this photograph, taken by Balibar, Guthmann, and Rolley (1994), the contact angle of the liquid-solid interface of $^4$He is about 135°; the walls are preferably wet by the liquid phase (Balibar *et al.*, 1979). $^3$He crystals show a similar property (see Fig. 34).

The surface tension can also be measured by studying equilibrium shapes if crystals are larger than their capillary length. This was first done by Landau *et al.* (1980) in $^4$He, and later by Rolley *et al.* (1989) in $^3$He (see Fig. 34). The most precise method uses the dispersion relation of crystallization waves, as described below.

### E. Excitation and detection of crystallization waves in $^4$He

Crystallization waves were discovered in 1979 by Keshishev *et al.* when shaking their cryostat. However, for an accurate measurement of the properties of crystallization waves, it was necessary to excite plane waves at known frequencies. For that purpose, Keshishev *et al.* used an electrostatic method: they made a small flat capacitor by winding two 30-$\mu$m-diameter copper wires around a Fiberglass plate. This capacitor was placed on one side of the cell (see Fig. 5) and they applied to it a dc voltage in the range from 400 to 800 V plus an ac voltage (from 20 to 200 V).

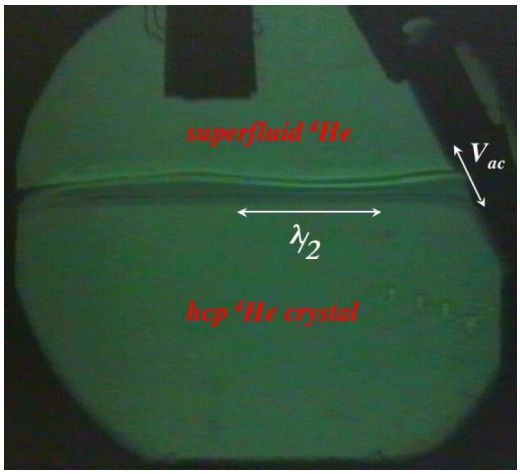


FIG. 14. (Color in online edition) Standing crystallization waves in $^4$He. The photograph is from a video sequence taken in 1994 by Balibar, Guthmann, and Rolley and shows the experimental cell with the oscillating interface between the crystal in the lower part and the superfluid above it. The wave was excited with an interdigital capacitor on the tilted plate on the right and it resonated across the width of the cell. The excitation frequency was about 30 Hz, so that the wavelength was close to 2/3 of the cell width (24 mm).

A similar method was used by Wang and Agnolet (1992a) and by Rolley, Guthmann, *et al.* (1995), except that the double winding was replaced by an interdigital structure evaporated on a borosilicate glass plate, so that smaller voltages could be used. Rolley, Guthmann, *et al.* (1995) found that the dissipation was about 30 $\mu$W at 1 kHz, with 100 V peak to peak for the wave excitation. They attributed this dissipation to dielectric losses in the glass, and this limited the lowest temperature at which they could study these waves. In Moscow as well as in Paris, the dc voltage was used to adjust the contact angle of the liquid-solid interface to the glass plate. Figure 14 shows a standing wave that was excited near 30 Hz and had a macroscopic amplitude. At higher frequency, or close to faceted directions as in Fig. 15, the damping is higher, so that the reflection of waves from the opposite wall is negligible, except at very low temperature.

In order to detect the waves, more precisely to measure their amplitude as a function of time or distance, Keshishev *et al.* (1979) first used the diffraction of light, but this method was not very sensitive due to the large mechanical vibrations of their apparatus. They improved the detection sensitivity by using a light transmission technique and a lockin amplifier. A 1-Å resolution in height was achieved by Rolley, Guthmann, *et al.* (1995) who measured the deflection of a laser beam at the oscillating surface (see Fig. 15), as had been previously done by Boldarev and Peshkov (1973) and Leiderer *et al.* (1977) in measuring the surface tension of liquid-helium mixtures. Of course, none of these experiments worked if the surface had facets or surface defects on the path of the waves, so that special care had to be taken with the quality and orientation of crystals. Wang and Agnolet (1992b) used the same interdigital capacitor for the emission and detection of waves in a resonant cavity.

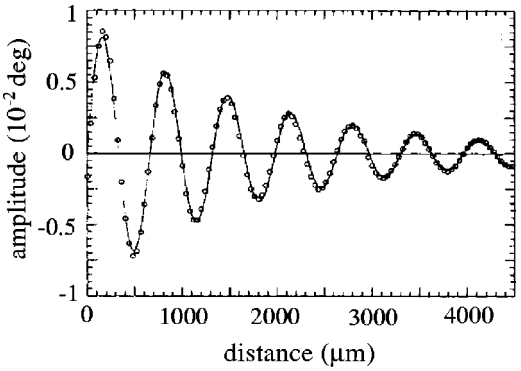


FIG. 15. Profile of a crystallization wave propagating at the surface of a $^4$He crystal, as measured by Rolley, Chevalier, *et al.* (1994). In this particular case, $T=280$ mK, the surface was oriented 3° away from the (0001) plane, and the frequency was 1946 Hz, so that the wavelength was 0.660 mm. The recorded quantity is the local tilt angle of the crystal surface with respect to the horizontal plane. From Rolley, Chevalier, *et al.*, 1994.

### F. Electrons at the liquid-solid interface

Leiderer and his group used electrons to study the liquid-solid interface of $^4$He (Bodensohn *et al.*, 1986; Leiderer, 1995). Electrons were first injected into the liquid with a field-emission tip or with a radioactive source. Once the electrons had slowed down, they formed a bubble with a radius of the order of 17 Å. In the solid, the energy of the electron bubble is higher by about 200 K, so that there is a large energy barrier against the penetration of electrons from the liquid into the solid. With a properly oriented electric field $E_z$, the layer of electrons can be pressed against the crystal surface. If the electrons are confined horizontally in some region of the crystal surface, for example, in the center as shown in Fig. 16, and if the electron charge density there is $\sigma_{\rm el}$, then this part of the crystal melts down by an amount $h=\sigma_{\rm el}E_z/g(\rho_C-\rho_L)$. Any change in the applied electric field produces a local change in the crystal height, which can be accurately measured with interferometric techniques. From the relaxation time of this height change, Leiderer and his group measured the growth dynamics of rough crystal surfaces (see Fig. 43 below) in a temperature region where crystallization waves were too heavily damped to be used (Bodensohn *et al.*, 1986; Leiderer, 1995). Eventually, they found the same instability of the crystal shape as in the case of the free surface of liquid $^4$He: beyond some critical electric field, a lattice of dimples appears (see Fig. 17 and Savignac *et al.*, 1983).

## III. ROUGHENING TRANSITIONS

### A. Historical observations of facets on helium crystals

Facets were first seen at the surface of slowly growing $^4$He crystals by Landau *et al.* (1980) in Haifa and by

FIG. 16. Interference pattern of a charged interface between liquid and solid $^4$He. Here the electrons are concentrated in the central region to enhance the visibility of the deformation. The parallel fringe pattern outside the center results from a small angle between the two interferometer plates. The field of vision is about 2 cm in diameter. From Savignac and Leiderer, 1982.

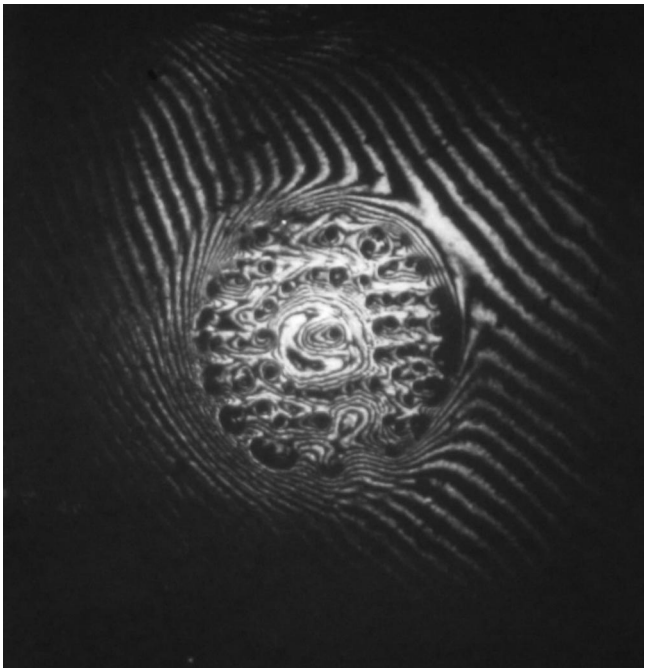

FIG. 17. Charge-induced instability of a superfluid-hcp $^4$He interface, as observed by Savignac *et al.* (1983) above the critical electric field. The instability develops in the form of a lattice of dimples, where electrons accumulate (dark spots on the image). The diameter of this pattern is about 1.5 cm. From Savignac *et al.*, 1983.

Keshishev *et al.* (1979) in Moscow. Balibar and Castaing (1980) then proposed the existence of a roughening transition around 1 K in order to understand the apparent discrepancy between the measurements of the surface tension of $^4$He crystals by Balibar *et al.* (1979), by Keshishev *et al.* (1979) and by Landau *et al.* (1980) below this temperature. These three groups had studied different capillary effects. Balibar *et al.* had measured the minimum pressure necessary for a $^4$He crystal to grow through a small hole. Landau *et al.* had measured the shape of a large liquid-solid interface that was governed by both gravity and surface tension. Keshishev *et al.* had measured the dispersion relation of crystallization waves.

It was soon confirmed by Keshishev *et al.* (1981) that facets existed not only on growth shapes but also on the equilibrium shapes of the crystals (see Fig. 18). Furthermore, both Landau *et al.* (1980) and Keshishev *et al.* (1981) had seen that facets existed in the "*c*" or [0001] direction, on the basal planes of the hexagonal structure (see Fig. 19), and in the "*a*" direction perpendicular to "*c*," which was later identified as the $[10\bar{1}0]$ direction (Wolf, Balibar, and Gallet, 1983; Andreeva and Keshishev, 1990).[2] A third type of facet was discovered by Wolf, Balibar, and Gallet (1983) below about 0.36 K; it was identified as the $[10\bar{1}1]$ direction, which is tilted by 58.5° with respect to the [0001] direction, by Andreeva and Keshishev (1990). All these facets can be seen in Fig. 2.

As for the maximum temperatures at which facets could be observed, they increased with time. It is now understood that the roughening transition is continuous, so that the facets are very small and fragile in a definite temperature domain below the roughening temperature $T_R$. As a consequence, improved measurement techniques revealed the existence of facets at higher and higher temperatures.

Some of the first measurements were done on equilibrium crystal shapes. However, it was soon realized that, close to $T_R$, the facets were too small to be detected. This is because the equilibrium facet size is proportional to the step free energy, which vanishes exponentially [see Landau, 1965; Nozières, 1992; Eq. (13), and Fig. 23 below]. In fact, when the state of a crystal surface changes from rough to smooth, its mobility drops by several orders of magnitude, so that the growth shapes are highly anisotropic below the roughening temperature and reveal the slowly growing parts of the surface. In contrast, melting shapes tend to be more rounded, and this can be understood from a simple geometric construction (see Fig. 20). Most facets have been seen dur-

[2]Note that, for the hcp structures, one uses sets of four Miller indices where the last index refers to the sixfold symmetry axis. The projection in the basal planes is decomposed over three equivalent vectors of the hexagons, so that the notation is symmetric and the sum of the first three indices has to be zero; the notation $\bar{1}$ means "–1."

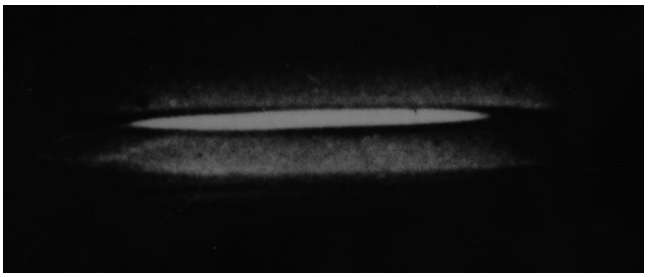

FIG. 18. Horizontal $c$ facet at the surface of a $^4$He crystal as seen by Keshishev *et al.* From Keshishev, Parshin, and Babkin, 1981.

ing growth, both in $^4$He and in $^3$He. Note, however, that the growth has to be slow enough to avoid "dynamic roughening" as explained below.

The first measurements of facet sizes (Avron *et al.*, 1980) led to a roughening temperature $T_{R1}=1.08$ K in the [0001] direction, but the analysis of Wolf *et al.* (1985), Gallet *et al.* (1987), and Balibar *et al.* (1993) progressively concluded that $T_{R1}=1.30$ K. Wolf *et al.* (1985) found that, for the $(10\bar{1}0)$ facets, $T_{R2}$ may be as high as 1.07 K, and Andreeva and Keshishev (1990) claimed that, for the $(10\bar{1}1)$ facets, $T_{R3}$ is higher than 0.43 K. Although some indication has been found for the existence of a fourth type of facet at 0.21 K (Puech *et al.*, 1983), there is not yet a clear proof for the existence of more than three types of facets in $^4$He.

As for the bcc $^3$He crystals, the measurements by Rolley *et al.* (1986, 1989) in Paris showed that (110) facets exist up to 100 mK. Later, (100) and (211) facets were found by the Leiden group (Wagner *et al.*, 1996) and many others [(310), (111), (321), (411), (210), (510), (431), and (311)] by the Helsinki group (Alles *et al.*, 2001; Tsepelin *et al.*, 2001).

Among all these facets, only the (0001) facet in $^4$He has been studied with enough accuracy to check that the precise value of its roughening temperature $T_{R1}$ is correctly predicted by the theory, as well as the critical behaviors near the roughening transition. The first purpose of the next section is to present this theory and its comparison with experiment. For the other roughening temperatures, although the measurements have been much less precise and somewhat incomplete, we shall also compare experimental observations with theoretical predictions.

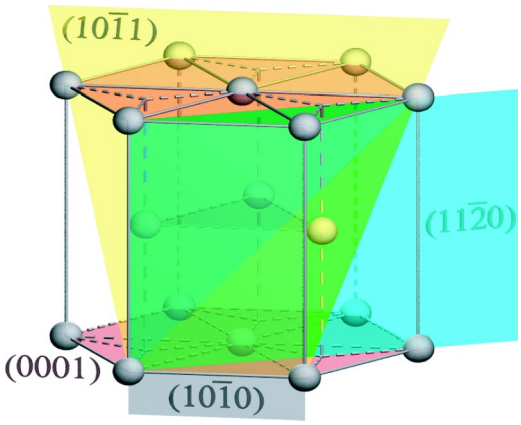


FIG. 19. (Color in online edition) Unit cell of the hcp $^4$He crystals. The plane containing three atoms in the center of the unit cell has the same energy as the bottom and top (0001) planes, so that the step height is half the lattice period in the [0001] direction.

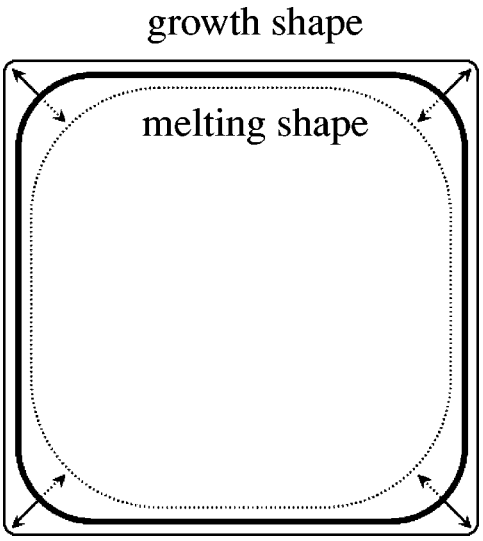


FIG. 20. Growth and melting shapes of a crystal. Facets grow and melt more slowly than rough corners; as a consequence, facets are larger on growth shapes than on melting shapes.

### B. Main theoretical predictions

#### 1. Static properties of simple surfaces

Why are there roughening transitions at the surface of crystals? This question has motivated intense theoretical activity in recent years. At zero temperature, the crystal energy is minimized with smooth surfaces in all directions, as predicted by Landau in 1949 (see Landau, 1965). As temperature increases, thermal fluctuations create defects such as terraces bounded by steps. At high enough temperature, the crystal surface will be invaded by steps and it will become independent of the underlying lattice as illustrated by numerical simulations (Leamy *et al.*, 1975; see Fig. 21).

In fact, it is not only the density of steps that increases, but also the average step length and the size of the thermally activated terraces. This is because the free energy of these steps tends to zero at a critical temperature, as can be expected for the following reason: Consider a simple cubic crystal with a lattice spacing $a$, as in Leamy's simulations. Now, let us estimate the free energy $\beta$ of a step with a length $Na$. The step is like a random walk with three possibilities at each site. The step entropy is thus $k_B\ln(3^N)$, and the step free energy can be written as

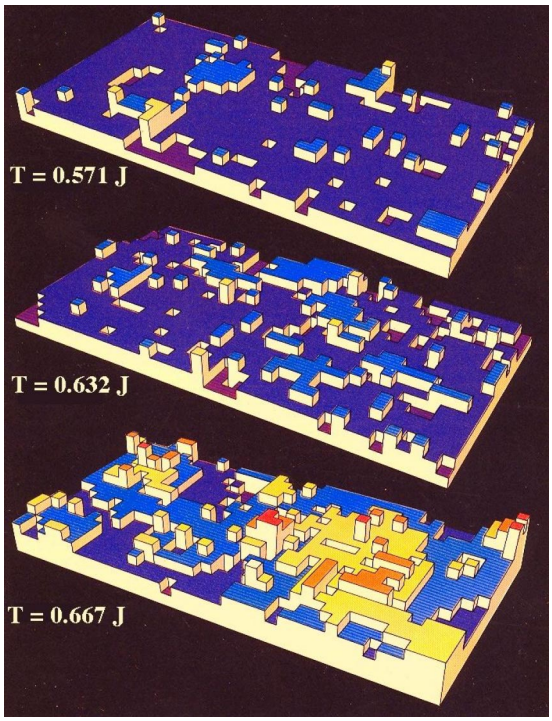


FIG. 21. (Color in online edition) Numerical simulations by Leamy *et al.* (1975) illustrating the basic physics of a roughening transition. The crystal has a simple cubic lattice and each atom is represented by a cube. At low temperature, there are very few defects such as adatoms, surface vacancies, steps, and terraces. As temperature increases, steps proliferate and the crystal surface loses reference to the lattice. The temperature is expressed as a function of the bond energy $J$. The roughening transition occurs at $T_R = 0.632J$. From Leamy *et al.*, 1975.

$$\beta = N[a\beta_0 - k_B T \ln(3)], \tag{3}$$

where $\beta_0$ is the internal energy per unit length of the step and $a\beta_0$ is approximately one-half of the bond energy $J$ between two neighboring atoms. The above equation predicts that the step free energy vanishes at the critical temperature $T_R = a\beta_0/[k_B \ln(3)] \approx 0.45J$, at which both the density of steps and the typical size of terraces should diverge.

In fact, the existence of a roughening transition was first predicted by Burton, Cabrera, and Frank within a model that was nearly as simple (Burton and Cabrera, 1949; Burton *et al.*, 1951). These authors considered the surface of a cubic crystal as the last lattice plane where sites are either occupied or empty. They introduced an interaction only between nearest neighbors, so that the surface they considered was strictly analogous to a two-dimensional (2D) Ising model of spins. Burton, Cabrera, and Frank then used Onsager's solution of the 2D Ising model to predict that a transition would take place at $T_R = 0.57J$, where $J$ is the bond energy. However, they realized that the crystal surface was not confined to only one atomic layer. Terraces can pile up on top of each other (see Fig. 21). As a consequence, later calculations showed that the above formulas were only rough approximations, and critical behaviors near $T_R$ were different from those found with the Ising model.

Further progress was made from the exact solutions of various models through equivalence to other 2D systems whose transitions were known. In particular, Chui and Weeks (1976) found a transition in the *discrete Gaussian solid-on-solid model* (DGSOS) which was equivalent to that found in the 2D Coulomb gas. "Gaussian" refers to the quadratic variation of the energy of local columns of atoms with their height, and solid-on-solid means that the atoms pile up without overhangs. The 2D Coulomb gas is a layer containing positive and negative charges; it has an insulating phase at low temperature, where charges bind as neutral molecules, and a conducting phase at high temperature, where molecules are ionized. It is known to belong to the Kosterlitz-Thouless class of transitions which are of "infinite order." For these transitions critical behaviors are exponential, with no discontinuity in any of the temperature derivatives of the free energy. Chui and Weeks thus predicted that the roughening transition was even more continuous than the second-order phase transition of the Ising model. At the same time, van Beijeren (1977) demonstrated that the "body-centered solid-on-solid model" was equivalent to the "six-vertex model," and Knops (1977) found an equivalence with the $XY$ model of spins. These are all members of the Kosterlitz-Thouless class of transitions, which also include the superfluid transition of films, and some liquid-solid transitions.

When it appeared possible to compare theory and experiment in helium, more theoretical work was needed, to include a few adjustable parameters in the theory, so that a real crystal surface could be described. This is what Nozières and Gallet (1987) achieved. For a detailed presentation of this theory, we refer the reader to Nozières' lecture notes at the Beg-Rohu summer school (Nozières, 1992). Here we only summarize its principle, starting point, approximations, and main results, so that one can understand how it could be compared with experimental results.

Nozières starts by writing an effective Hamiltonian to describe the energy of a surface deformation:

$$H = \int\int d^2r \left[ \frac{1}{2}\gamma(\nabla z)^2 + V \cos\frac{2\pi z}{d} \right]. \tag{4}$$

In this expression, $z(r)$ is the height of the crystal surface at a position $r$ and the cosine term describes the periodic influence of the underlying lattice; the quantity $d$ is thus the periodicity of the surface energy as a function of height and it is also the step height in the smooth faceted state. Note that, in the direction under consideration, $d$ can be different from the lattice spacing $a$. The lattice potential $V \cos 2\pi z/d$ anchors the crystal surface to the lattice planes at low temperature. As for the quantity $\gamma$, it is the surface stiffness of a crystal and deserves comment.

The Laplace equation shows that the curvature of a free liquid surface is equal to the ratio of the pressure difference across the surface to the surface tension $\alpha$, which is the free energy per unit area. A crystal, being

anisotropic, has not only a surface tension which tends to minimize the surface area, but also a torque which tends to rotate the surface towards a direction with minimum surface energy (see Herring, 1953 or Nozières, 1992). As a result, the equilibrium curvatures of the crystal surface are governed by the surface stiffness tensor,

$$\gamma_{ij} = \alpha + \frac{\partial^2 \alpha}{\partial \phi_i \, \partial \phi_j}, \tag{5}$$

where $\phi_{i,j}$ are the reference angles. In the case of a liquid-solid interface, one can write a generalized Laplace equation as

$$\left(\frac{\rho_C}{\rho_L} - 1\right) \delta P = \frac{\gamma_1}{R_1} + \frac{\gamma_2}{R_2}, \tag{6}$$

where $\gamma_1$ and $\gamma_2$ are the two components of the surface stiffness tensor after diagonalization and $R_1$ and $R_2$ are the two radii of curvature in the corresponding directions. The pressure difference $\delta P = (P_L - P_{L0})$ is the departure from the liquid-solid equilibrium pressure $P_{L0}$ when the interface is flat.[3] Once multiplied by the density factor in Eq. (6), this pressure term is a generalization of the pressure difference across the interface (the problem here is that, unless the solid is under hydrostatic equilibrium, its stress tensor is not isotropic, so that the solid pressure is not a well-defined quantity). In the case of the (0001) surfaces of hcp $^4$He crystals, and in the absence of gravity, the surface has a cylindrical symmetry axis [0001]. Thus $\gamma_1 = \gamma_2$, and the right-hand side of Eq. (6) simplifies to $2\gamma/R$ with $\gamma = \alpha + \partial^2 \alpha / \partial \phi^2$.

The Hamiltonian in Eq. (4) is often called a *continuous sine-Gordon* Hamiltonian because it uses continuous variables and a sinusoidal potential. Its form calls for a few more remarks. The roughening transition is a macroscopic phenomenon, and one is interested in the properties of the crystal surface at a large scale. This is what justifies the use of continuous variables. At these large scales, the fluctuation amplitude is always smaller than the wavelength, so that the local slopes are small ($\nabla z \ll 1$). This is why only the leading term with $(\nabla z)^2$ is kept in the expansion for the surface shape. Furthermore, it is assumed that $V/\gamma < 1$: the crystal surface is weakly coupled to the lattice. This weak-coupling approximation is shown to be valid close to the roughening transition temperature, where critical behaviors are calculated. It also justifies the use of only the first harmonic, a cosine term, instead of a periodic function of arbitrary shape (see Nozières, 1992).

Although the algebra involved in the renormalization calculation of the roughening transition is tedious, its principle is simple. One calculates the free energy of the surface by averaging over fluctuations of larger and larger scale. At each scale $L$, the Hamiltonian keeps the same form, Eq. (4), but its coefficients $\gamma(L)$ and $V(L)$ become scale dependent, when fluctuations with larger and larger wavelengths are progressively accounted for through the process of renormalization. By comparing coarse graining at scale $L$ and at scale $L + dL$, one obtains coupled differential equations for $\gamma(L)$ and $V(L)$; their integration gives the scale dependence of these two quantities: the *renormalization trajectories*. The important result of this theory is that there are two different behaviors, depending on the temperature.

If $T > T_R$, the potential energy $U = VL^2$ renormalizes to zero at large $L$. The interface becomes free from the influence of the crystal lattice, like a free liquid surface. Its fluctuations diverge at large distance, as described by the height-height correlation function,

$$G(r) = \langle [z(r) - z(0)]^2 \rangle = \frac{k_B T}{2\pi\gamma} \ln \frac{r}{L_0}, \tag{7}$$

which is the same as for a free liquid surface ($L_0$ is the cutoff of fluctuations at small scale). Physically this means that the fluctuations are so large that the crystal surface wanders over many periods $d$, so that the potential $V \cos(2\pi z/d)$ is averaged to zero.

In contrast, if $T < T_R$, the potential energy $U$ diverges at large scale. Actually, as soon as $U$ becomes larger than $k_B T$, one understands that it should kill the fluctuations and the renormalization should stop. This renormalization is "truncated" at the maximum scale $L_{\max}$ which appears in the problem. As a result, the height-height correlation function saturates:

$$\lim_{r \to \infty} G(r) = \frac{k_B T}{2\pi\gamma} \ln \frac{L_{\max}}{L_0}. \tag{8}$$

We thus see that the crystal surface is "rough" like a free liquid surface at high temperature, and "smooth" at low temperature. The difference between these two states is *not* at the atomic scale. It is at the larger scale $L_{\max}$ where fluctuations are either free or killed by the lattice. It is thus preferable to avoid expressions like "atomically smooth" or "atomically rough," which have been used by many authors in the past.

The quantity $L_{\max}$ appears in Eq. (8) as a correlation length, but one usually defines the correlation length $\xi$ from the step profile, which can be calculated within this sine-Gordon model. The step that we consider here is a *macroscopic step*. It is the surface defect whose existence is forced by pinning the crystal surface, say, at the height $z = 0$ on the left ($x = -\infty$) and at $z = +d$ on the right ($x = +\infty$). Its profile is given by

$$z(x) = \frac{2d}{\pi} \arctan\left[\exp \frac{x}{\xi}\right]. \tag{9}$$

Close to $T_R$, the theory predicts that $\xi \approx L_{\max}/2$, but the exact value depends on the way in which the renormalization is truncated (see below and Balibar *et al.*, 1993). $L_{\max}$ is the minimum size for a smooth state to be defined, and it is not surprising to find that it is related to the step width, but, here again, there are numerical factors that need to be considered for a comparison with

[3] $P_{L0}$ is also called the melting pressure $P_m$ of the solid: For a gas-solid interface, just replace liquid by gas in the above expressions.

experiment. If one defines a step width $w$ as the horizontal distance necessary for the surface height to go from $0.1d$ to $0.9d$, then Eq. (9) implies that

$$w \approx 4\xi \approx 2L_{\max}. \tag{10}$$

At $T=T_R$, the renormalization goes to a *fixed point*, where $U=0$ and the surface stiffness has the universal value $\gamma(T_R)$ given by

$$k_B T_R = \frac{2}{\pi}\gamma(T_R)d^2. \tag{11}$$

This is known as the *universal roughening relation*. It was first obtained by Fisher and Weeks (1983) and by Jayaprakash *et al.* (1983). It is universal in the sense that it does not depend on any microscopic detail such as interatomic interactions. Note that $\gamma(T_R)$ is the critical value of the surface stiffness in the right direction and exactly at the critical temperature $T_R$. Equation (11) refers to a surface with cylindrical symmetry. For an arbitrary symmetry, when there are two different stiffness components, Fisher and Weeks (1983) showed that the universal relation has to be written as

$$k_B T_R = \frac{2}{\pi}(\gamma_1\gamma_2)^{1/2}d^2. \tag{12}$$

There are two other predictions about critical behaviors near $T_R$. The first one concerns the step free energy $\beta$, which is predicted to vanish exponentially according to

$$\beta \propto \exp\left[-\frac{\pi}{2\sqrt{tt_c}}\right]. \tag{13}$$

Here $t=1-T/T_R$ is the reduced temperature and the parameter $t_c$ is defined as

$$t_c = \frac{2\pi^2\sqrt{A(2)}U_0}{\gamma_0 d^2}, \tag{14}$$

where $A(2)\simeq 0.4$ and the index "0" in $\gamma_0$ and $U_0=V_0L_0^2$ means the unrenormalized value at the microscopic scale $L_0$. The parameter $t_c$ indicates the strength of the coupling of the crystal surface to the underlying lattice. It is weak if $t_c<1$. Note that the critical domain in temperature is large if this coupling is weak and vice versa. It has been found that the correlation length $\xi$ diverges exponentially near $T_R$, since

$$\xi \approx \frac{k_B T_R}{\pi\beta}. \tag{15}$$

The theory also predicts that the magnitude of $t_c$ controls the amplitude of the renormalization of the surface stiffness, since

$$\gamma(T_R) = \gamma_0(1 + t_c/2). \tag{16}$$

Another important prediction concerns the temperature dependence of $\gamma$. Below $T_R$ the stiffness is infinite, so that the crystal curvature is zero (the facet is flat). This is because, the step free energy being nonzero, the angular variation of the surface energy $\alpha(\phi)$ has a linear cusp,

$$\alpha(\phi) = \alpha_0 + \frac{\beta}{d}|\phi|, \tag{17}$$

around the smooth ($\phi=0$) direction. Above $T_R$, the surface stiffness reaches its universal value $\gamma(T_R)$ with a square-root cusp:

$$\frac{\gamma(T)}{\gamma(T_R)} \approx 1 - \sqrt{|t|t_c}. \tag{18}$$

Consequently, as temperature decreases, the crystal curvature exhibits a square-root cusp until it reaches a universal value, where it jumps to zero. Such square-root cusps and universal jumps can be found in all Kosterlitz-Thouless transitions. Depending on the system under consideration, the physical quantity showing this remarkable behavior is different. For example, it is the superfluid density for the superfluid transition of films, the shear modulus for the melting of 2D crystals, the magnetization in the $XY$ model of spins, the dielectric constant in the Coulomb gas, etc.

### 2. Vicinal surfaces and dynamic roughening

Several experiments called for predictions on the properties of vicinal surfaces whose orientations were tilted by a small angle $\phi$ with respect to the high-symmetry faceted ones. Nozières calculated the properties of such surfaces within a slightly modified version of his original theory. He replaced the potential term $V\cos(2\pi z/d)$ in Eq. (4) by $V\cos[2\pi(z-\phi x)/d]$. A new scale appeared in the problem, which was the average distance between steps, $l=d/\phi$. At a scale larger than $l$, the surface extends over more than one period $d$, so that the lattice potential is zero and the renormalization stops. In other words, the tilt angle introduces a "finite-size effect" in the renormalization procedure. The exact scale at which it stops has been found numerically to be $L=l/6$ (Nozières and Gallet, 1987), and we shall see below that this numerical factor of 6 is important. The RG theory was thus able to predict the angular variation of $\gamma(\phi)$ at small $\phi$ and near $T_R$.

Another kind of finite-size effect appears when the crystal grows or melts at a finite velocity $v=\dot{z}$. Nozières's theory of this dynamic situation follows an approach first introduced by Chui and Weeks (1978). It uses the same RG technique, but now applies it to the Langevin equation of motion of the surface position $z(x,y)$:

$$\frac{\rho_C}{k}\dot{z} = \rho_C\delta\mu + \gamma\Delta z - \frac{2\pi}{d}V\sin\frac{2\pi z}{d} + R(z,t) \tag{19}$$

instead of the Hamiltonian of Eq. (4). In this new equation, the important coefficient $k$ is the *surface mobility*, sometimes called the *growth coefficient* ($1/k$ is consequently the friction coefficient or the growth resistance, which is discussed more extensively in Sec. IV). $R(z,t)$ is the random force at the origin of fluctuations and $\delta\mu$

$=\mu_L-\mu_C$ is the difference in chemical potential between the liquid and the crystal, which drives the net growth.

In the limit of $\delta\mu$ tending to zero (zero growth velocity), Nozières and Gallet (1987) found a critical behavior for the mobility $k$, which has a square-root cusp similar to the one found for the surface stiffness:

$$\frac{k(T)}{k(T_R)} \approx 1 - \sqrt{5.66|t|t_c}. \tag{20}$$

This time the mobility $k(T_R)$ is not universal. As soon as a finite departure from equilibrium produces a net growth with some average velocity $v$, the roughening transition is blurred. Indeed, a time scale appears that is $\tau=d/v$, the time necessary for the crystal surface to move by one layer $d$. During $\tau$, the surface fluctuations diffuse over a distance $(k\gamma\tau/\rho_C)^{1/2}$ according to Eq. (19), which is a diffusion equation. As a consequence, renormalization cannot proceed beyond this new scale. If it is larger than the correlation length $\xi$, there is no change. If it is smaller, then the renormalization stops before the lattice potential diverges, and the surface is dynamically rough. The criterion for this *dynamic roughening* is thus $\xi\approx(k\gamma\tau/\rho_C)^{1/2}$, which can be rewritten as

$$\frac{\beta^2}{d\rho_C\delta\mu k_B T_R} \approx 1. \tag{21}$$

There is a simple physical interpretation of this criterion. On a smooth facet, and if the step free energy is small enough, as happens close to $T_R$, the growth of a crystal proceeds by nucleation of terraces. In order to grow in size, these terraces need to have a radius larger than a critical value

$$r_c = \frac{\beta}{d\rho_C\delta\mu}. \tag{22}$$

Equation (21) means that this critical radius is comparable to the correlation length $\xi\approx k_B T_R/\beta$. Dynamic roughening occurs if the critical radius for nucleation is smaller than the step width, which is also the minimum size for the definition of a smooth state. Let us finally remark that this dynamic roughening is different from another type of roughening (Kardar *et al.*, 1986), as explained by Balibar and Bouchaud (1992).

### C. $^4$He crystals

#### 1. The (0001) surface

Balibar *et al.* (1993) summarized and discussed the comparison by the Paris group of the RG theory of roughening with the surface properties of $^4$He crystals in the [0001] direction. Wolf *et al.* (1985) had measured the equilibrium shape of $^4$He crystals at a known overpressure $\delta P$. From this they found that the large-scale angular variation of the surface stiffness of crystals was

$$\gamma_0(\phi) = 0.245(1-12\phi^2)\ \text{erg/cm}^2. \tag{23}$$

They found that this angular variation was independent of temperature, as expected, since they had to calculate the second derivative of the profile, and this could not be done in an angular domain smaller than about 10°. This was not small enough to catch the critical behavior of $\gamma$. Indeed, at the end of the analysis, the Paris group found the critical angular domain to be only about 2°–3°. They considered 0.245 erg/cm$^2$ as the value of the nonrenormalized quantity $\gamma_0$ in Eq. (16).

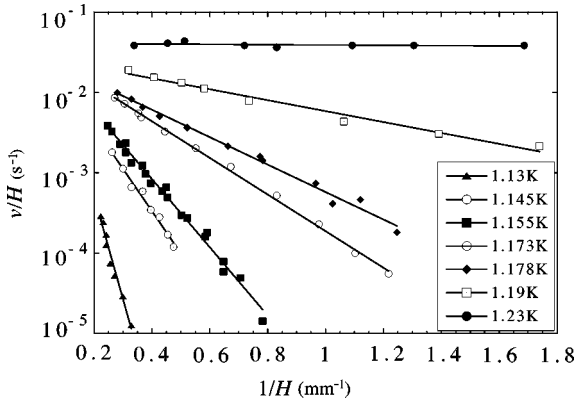


FIG. 22. Experimental measurement by Wolf *et al.* (1985) of the growth characteristics of the *c* facet in $^4$He: semilog plot of the growth velocity $v$ divided by a departure of the height $H$ from the equilibrium position ($H=0$), as a function of $1/H$. The difference in chemical potential across the interface is $\delta\mu=(\delta\rho/\rho_C)gH$. Good agreement was found with Eq. (24), from which values of the step free energy were obtained. From Wolf *et al.*, 1985.

Wolf *et al.* (1985) and Gallet *et al.* (1987) also measured the step free energy of the *c* facets. This was done by studying the relaxation of a horizontal crystal surface towards its equilibrium height. In this case, in Eq. (19), the difference in chemical potential $\delta\mu$ is due to the hydrostatic equilibrium in the liquid; it is proportional to the departure $H$ from the equilibrium height. The visual observation technique of Wolf *et al.* was improved by Gallet *et al.*, who used interferometry (see Sec. II.B.2). In the temperature range from 1.13 to 1.23 K, they found that the crystal growth apparently proceeded by 2D nucleation of terraces. If true, the growth velocity had to be given by

$$v = k\delta\mu \exp\left(-\frac{\pi\beta^2}{3d\rho_C\delta\mu k_B T}\right). \tag{24}$$

In this equation, the factor of 3 indicates that terraces coalesce to form new atomic layers. As shown in Fig. 22, good agreement with this exponential behavior was found over several decades in velocity, and this allowed them to determine the step free energy $\beta$.

Figure 23 shows measurements of the step free energy close to $T_{R1}$ (Wolf *et al.*, 1985; Gallet *et al.*, 1987). In this figure, the solid line corresponds to a numerical integration of the Nozières renormalization equations, which tend to the exponential form of Eq. (13) near $T_R$. The best fit was obtained by Balibar *et al.* (1993) with the following set of parameters:

$$T_{R1} = 1.30\ \text{K}; \quad t_c = 0.58; \quad L_0 = 4d \approx 2\xi_0. \tag{25}$$

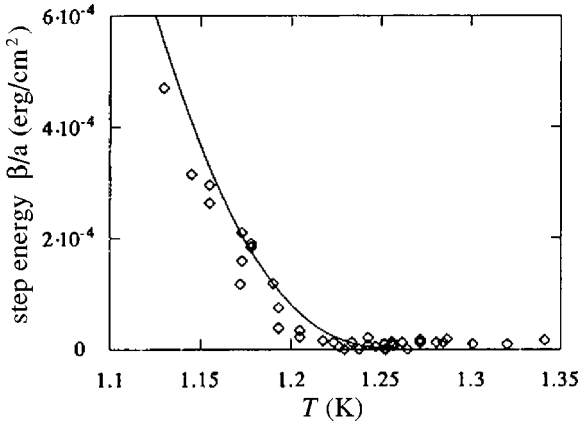


FIG. 23. Temperature variation of the step free energy $\beta$ for $c$ facets in $^4$He. The symbols correspond to the successive experiments of Wolf *et al.* (1985) and Gallet *et al.* (1987). The solid line is the last fit to the RG theory of Nozières and Gallet (1987) that was done by Balibar *et al.* (1993) using the parameters of Eq. (25). From Balibar *et al.*, 1993.

In reality, these three parameters were determined not only by fitting the $T$ dependence of the step free energy, but also by the critical variation of the growth velocity. The temperature 1.2 K appeared to be the threshold for dynamic roughening in these experiments, so that Eq. (24) could not be used above this temperature. Figure 24 shows that the growth characteristics $v(\delta\mu)$ are still slightly nonlinear at 1.2 K and evolve continuously into a linear regime near 1.3 K. This kind of evolution of growth is a central characteristic of a roughening transition, and it is described by the dynamic part of Nozières's theory, as shown in Fig. 25. In this figure, the two sets of data correspond to two different values of $\delta\mu$. The growth velocity in the [0001] direction has been normalized by the velocity of rough surfaces in

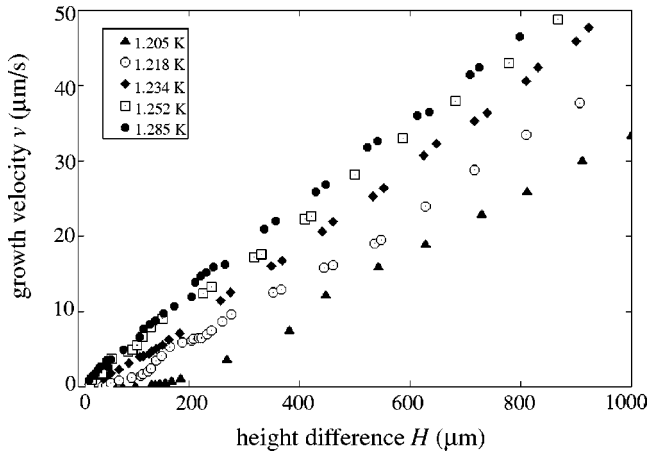


FIG. 24. Growth characteristics of $^4$He crystals in the [0001] direction. As the temperature approaches the roughening temperature $T_{R1}=1.3$ K, the growth characteristics evolve smoothly from nonlinear to linear behavior. These measurements were made by Gallet *et al.* (1987) and were analyzed using the RG theory of dynamic roughening (see Fig. 25). From Gallet *et al.*, 1987.

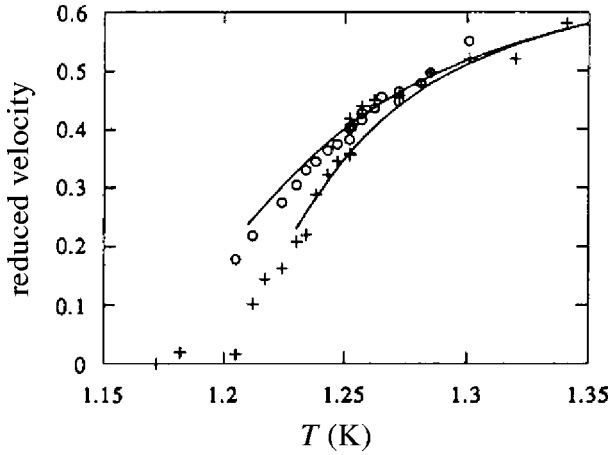


FIG. 25. Measurements by Gallet *et al.* (1987) of the growth velocity of $c$ facets: ○, height difference of 0.7 mm; +, height difference of 0.07 mm. The "reduced velocity" is the ratio of the velocity $v$ of the (0001) surface to the velocity $v_r$ of a typical rough surface at the same temperature (taken in another crystalline direction). The two solid lines are theoretical fits by Balibar *et al.* (1993), who used the theory of dynamic roughening by Nozières and Gallet (1987) and the parameters from Eq. (25). From Balibar *et al.*, 1993.

other directions. The parameters used for the theory are the same as those in Eq. (25).

Figure 25 illustrates dynamic roughening: when subjected to a larger driving force $\delta\mu$, the transition from large growth velocity (in the rough state) to small growth velocity (in the smooth state) is broader than in the case when the driving force is small. At the intermediate temperature of 1.23 K, the applied force drives the surface into growing faster because of enhanced roughness. In the limit of a vanishingly small force, the velocity would jump sharply to zero at $T_R$. Note also that the normalized velocity depends on $\delta\mu$ only below the roughening transition: this is where the growth is nonlinear.

Once this agreement was found and the parameters adjusted [Eq. (25)], Balibar *et al.* (1993) compared the RG theory with other measurements of the surface stiffness that had been carried out in Moscow (Babkin *et al.*, 1985; Andreeva *et al.*, 1989). The solid line in Fig. 26 is a numerical calculation of the angular variation of $\gamma$ at 1.2 K, the temperature of Babkin's measurements. The stiffness variation has an inflexion point between 2 and 3 degrees, where it departs from Wolf's measurement of its noncritical behavior [Eq. (23)]. This angular range is directly connected to the value of $L_0$. Indeed, as explained above, the renormalization stops at the scale $L_{\max}=l/6=d/6\phi$. With $L_0=4d$, Nozières's theory predicts no renormalization if $\phi$ is larger than $1/24$ rad $=2.4°$. This is remarkably consistent with Fig. 26. As we shall see in Sec. III.C.5, it has been further checked by later studies of stepped surfaces (Rolley, Chevalier, *et al.*, 1994; Rolley, Guthmann, *et al.* 1995), again with excellent agreement.

Finally, the amplitude of renormalization of $\gamma$ is also correct: Babkin's data tend to the universal value of

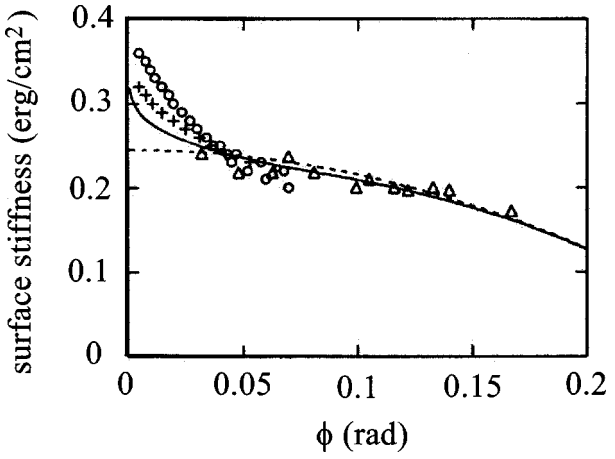


FIG. 26. Angular variation of the surface stiffness of hcp $^4$He crystals close to the [0001] direction: ○, +, measurements by Babkin *et al.* (1985) at 1.2 K; △, measurements by Andreeva *et al.* (1989) at 0.4 K; dashed line, measurements by Wolf *et al.* (1985) in the interval from 1.18 to 1.41 K [Eq. (23)]. Given the scatter in the data, the agreement is good with the result from the RG theory at 1.2 K [solid line, calculated by Balibar *et al.* (1993)]. It confirms that the critical angular domain is small, about 2° or 3°, the only region where the surface feels the formation of the facet and where the stiffness has some temperature dependence. From Balibar *et al.*, 1993.

$$\gamma(T_{R1}) = 0.315 \text{ erg/cm}^2 = 0.245\left(1 + \frac{0.58}{2}\right) \text{ erg/cm}^2 \tag{26}$$

at $\phi=0$, or more precisely, to a slightly larger value because the measurements were unfortunately done at 1.2 K instead of 1.3 K (at that time, the exact value of $T_{R1}$ was not yet known). This further confirms the values of $t_c$ and $T_{R1}$. Despite the scatter in the data, Babkin's measurements can be considered as the best experimental evidence of the universal roughening relation [Eq. (11)].

At the time of their publications, the Moscow group considered their results to be inconsistent with the RG theory [see, for example, Keshishev and Andreeva (1991)]. They first considered the value of $\gamma$ to be too high by about 20%, but this was because they took $T_{R1}$ as 1.20 K. However, with $T_{R1}=1.30$ K, good agreement was found with the Moscow measurements, whose typical error bar is at least 10%, given the scatter in their experimental data. Furthermore, they said that no temperature dependence of $\gamma$ was observed. This was because they did not look at a sufficiently small angle, nor at temperatures low enough to be in the critical domain. Later Rolley *et al.* (Rolley, Chevalier, *et al.*, 1994; Rolley, Guthmann, *et al.* 1995) performed experiments down to 40 mK and between 0.3° and 6°. Their results showed a drastic change as soon as the step width was small enough, once more in very good agreement with the predictions from the RG theory (see Sec. III.C.5).

Although rather good agreement was found between RG theory and the properties of the *c* facet in $^4$He, so that the validity of this theory appears well established, there remain at least two problem areas that need to be clarified. The first was pointed out by Balibar *et al.* (1993). As explained above, the renormalization is truncated, stopping at the maximum scale $L_{\max}$ if $T<T_R$. In their analysis, the Paris group stopped the renormalization when the lattice potential $U$ equaled $k_BT$. Gallet *et al.* (1987) found this physically correct because, beyond the corresponding length scale, the lattice potential is too large and kills the fluctuations. This implies the relation $\xi \approx L_{\max}/2$. However, as later explained by Nozières (1992), the weak-coupling approximation requires $4\pi U/k_BT \ll 1$, so that the renormalization should perhaps be stopped when $U=k_BT/4\pi$ rather than when $U=k_BT$.

Balibar *et al.* (1993) obtained a good fit to the experimental results by changing the maximum scale slightly, but not if the renormalization was stopped when $U=k_BT/4\pi$. The exact maximum scale is in fact an additional adjustable parameter, which is not explicit. In order to determine it, one would need independent measurements of both the correlation length $\xi$ and the step free energy $\beta$. The exact scale at which renormalization has to be stopped could then be more accurately determined and the other parameters slightly modified. The correlation length $\xi$ could perhaps be obtained from a measurement of the height-height correlation function in an x-ray scattering experiment. This looks difficult but challenging. Another experiment was suggested by Giorgini and Bowley (1995) to obtain more information on the best truncation scale, namely, a measurement of the response of the interface to an external drive at a few kHz, near the roughening transition temperature.

The second problem emerged very recently from criticism by Todoshchenko *et al.* (2004) of the way the experimental data were analyzed in the work of Wolf *et al.* (1985), Gallet *et al.* (1987), and Balibar *et al.* (1993). Todoshchenko's argument is that the assumption of a 2D nucleation mechanism is not well justified because the step mobility should be larger by a factor $\xi/d$ than the mobility $k$ of rough surfaces, as Gallet *et al.* (1987) erroneously assumed. If facets have no dislocations at all, then, of course, Gallet's assumption holds; but if the mechanism is in fact spiral growth due to Frank-Read sources, then a fit with a quadratic law leads to new values for the step free energy $\beta$ that are larger than previously thought. From new fits with the RG theory, where the renormalization was stopped when $U=k_BT/4\pi$, Todoshchenko *et al.* obtained values for the three parameters $T_{R1}$, $t_c$, and $L_0$ slightly smaller than those obtained by the Paris group [Eq. (25)]. This recent criticism calls for further examination of the critical behaviors near the roughening transition temperature, especially for new independent measurements of both $\beta$ and $\xi$.

#### 2. Quantum roughening and mean-field theories

A certain number of other theoretical ideas have been proposed. Andreev and Parshin (1978) first introduced the idea of quantum kinks. They had noticed that, as

with other point defects in quantum systems (see Andreev and Lifshitz, 1969), kinks on steps behave as delocalized quasiparticles. The energy of the ground state of such quasiparticles is always lower than that of a localized state. According to Andreev and Parshin, this effect is strong enough to make the net kink energy negative, so that *zero-point kinks* should exist. A step with such kinks, a *quantum rough step*, should be very mobile at low temperatures, in contrast to classical steps. For a further discussion of the properties of quantum kinks and steps, see Secs. IV.C.3 and V.A.2.

The presence of zero-point kinks decreases the step energy. Therefore Andreev and Parshin (1978) further proposed that this effect could be strong enough to make the step energy negative and create "zero-point steps." In such a case the smooth state of a given facet would be unstable against quantum roughening, even at $T=0$. However, Fisher and Weeks (1983) have shown that this is impossible: the step energy cannot be zero at $T=0$. Here we meet with a fundamental difference between the roles of quantum fluctuations in 1D and 2D cases, first suggested by Fisher and Weeks (1983). Roughening originates in the divergence of fluctuations at large enough scale. In the 2D case the integral of quantum fluctuations leads to a finite contribution to the height-height correlation function, which cannot diverge at $T=0$, so that the thickness of the crystal surface is always finite. As a consequence, the crystal surface is always sensitive to the periodic potential of the lattice; the energy of the above defined *macroscopic steps* is always positive at $T=0$, whatever happens to the steps at a microscopic scale. In contrast, in the 1D case the height-height correlation function of quantum fluctuations may diverge at a large scale, the pinning of a step to the lattice potential may be eliminated, and the step may indeed be quantum rough. The absence of quantum roughening in the 2D case was further demonstrated by solving various quantum models of crystal surfaces (Fradkin, 1983; Iordanskii and Korshunov, 1983, 1984, 1985; Bol'shov *et al.*, 1984). Iordanskii and Korshunov (1984) predicted that quantum fluctuations lead to a step energy that is nonzero at $T=0$ but decreases exponentially with the step height.

We now understand that quantum effects enter the determination of the surface thickness and the step width at $T=0$, and an *a priori* calculation of the parameters $t_c$ or $L_0$ would have to consider them: with more quantum fluctuations the crystal surface and the steps at it are thicker at $T=0$ and the length $L_0$ is also larger, so that the surface should be more weakly coupled to the lattice (the coupling parameter $t_c$ should be smaller, as well as the step energy at $T=0$). But the universal relation does not depend on this. Iordanskii and Korshunov (1984) mention a small dependence of the surface stiffness on quantum effects, but the quantity they consider is $\gamma_0$, not $\gamma(T_R)$.

There is one more theoretical question of general interest: whether facets can appear as a result of a phase transition other than the Kosterlitz-Thouless transition. Of course faceting could be caused by a first-order transition in the bulk, but not necessarily (Knops, 1979; Keshishev *et al.*, 1982; Fisher and Weeks, 1983; Nozières, 1992). There is no evidence for such transitions in helium. In 1981, Andreev proposed a mean-field theory of faceting, similar to the Landau theory of second-order phase transitions. In Andreev's approach, the rough surface plays the role of the symmetric phase and the step free energy the role of the order parameter. He predicted that the step free energy should vanish near $T_R$ according to the square-root law $\beta \propto \sqrt{T_R - T}$ and that the surface stiffness should continuously diverge to infinity as a function of angle at $T_R$. Furthermore, Andreev predicted the existence of surfaces with one zero curvature only, that is, with a cylindrical shape. None of these predictions were observed in experiments (Babkin *et al.*, 1984; Wolf *et al.*, 1985; Gallet *et al.*, 1987). In fact, as clearly stated by Iordanskii and Korshunov (1984), the mean-field theory "has no range of applicability because of the governing role played by fluctuations."

### 3. Other facets in $^4$He

Let us now consider other facets in $^4$He. This has been another controversial subject. The study of the (0001) facets showed that several measurements are needed for a precise comparison with the RG theory. In the case of $(10\bar{1}0)$ and $(10\bar{1}1)$ facets, the comparison is more difficult because there are two components of the surface stiffness tensor instead of one. Not only it is hard to obtain a crystal with vertical $[10\bar{1}0]$ or $[10\bar{1}1]$ axes, but even this would be insufficient: one would need to rotate the crystal around this vertical axis and find the values of the two principal components of the stiffness tensor at the right temperature and in the precise directions where facets appear. One hopes that this might be done in the future, but let us consider the currently available data.

Supposing that the roughening temperature $T_{R2}=1$ K for the $(10\bar{1}0)$ surfaces, it would be consistent with the RG theory if the geometric mean $(\gamma_1\gamma_2)^{1/2}$ of its two surface stiffness components were 0.21 erg/cm$^2$ at 1 K, since the step height is 3.18 Å in this direction. Wolf *et al.* (1985) have measured the average value $\gamma=0.19$ erg/cm$^2$ for this direction at 0.95 K and Andreeva *et al.* (1989) have measured 0.36 erg/cm$^2$ 1.5° away from the $[10\bar{1}0]$ direction at 0.4 K. Andreeva and Keshishev (1990) have also measured 0.21 erg/cm$^2$ 13° away from the $[10\bar{1}0]$ direction, while Edwards *et al.* (1991) have estimated the two surface stiffness coefficients to be 0.2 and 0.16 erg/cm$^2$. Clearly, more precise measurements are needed in this direction, but there is no contradiction with the universal relation: the measured values of the surface stiffness components have roughly the right order of magnitude.

As for the $[10\bar{1}1]$ direction, the lack of precise measurements is similar. If one assumes that $T_{R3}=0.43$ K, as proposed by Keshishev and Andreeva (1991), then the mean surface stiffness $(\gamma_1\gamma_2)^{1/2}$ should be 0.11 erg/cm$^2$

for this third direction, where the step height is 2.80 Å. Only one component, $\gamma_1 = 0.22$ erg/cm$^2$, has been measured by Keshishev and Andreeva (1991). Agreement with the RG theory would require the other component $\gamma_2$ to be much smaller, but this is not unreasonable, since a value as low as 0.08 erg/cm$^2$ has been measured in the $[11\bar{2}0]$ direction by Keshishev and Andreeva (1991). In fact, the study of the $[10\bar{1}1]$ direction would perhaps be easier to do than of the $[10\bar{1}0]$ direction because the stiffness could be measured from the dispersion of crystallization waves around 0.4 K (at 1 K and above, they are overdamped).

What about other directions? How can it be that no more than three types of facets have yet been observed in $^4$He? In the $[11\bar{2}0]$ direction, the step height is 1.83 Å. Thus if the average stiffness is about 0.2 erg/cm$^2$, the facets should appear below $T_{R4} = 0.3$ K [below 0.15 K if $(\gamma_1\gamma_2)^{1/2} = 0.1$ erg/cm$^2$]. Puech *et al.* (1983) have found an anomaly at 0.21 K which might be due to this fourth roughening transition, but no systematic search of higher-order facets has as yet been done in $^4$He. When crystals grow (slowly enough that no dynamic roughening occurs), the facet sizes are enhanced because they grow more slowly than the adjacent rough surfaces (see Fig. 20). Since the growth rate depends on the step energy, the facets with large Miller indices grow faster than those with small indices, and they are more difficult to see on the growth shapes. Furthermore, the hcp structure is highly anisotropic, so that the growth shapes of hcp $^4$He crystals are usually dominated by the [0001] and $[10\bar{1}0]$ facets. The $[10\bar{1}1]$ facets are very often absent on the growth shapes, and usually not as clearly visible as in Fig. 2. Is this a sufficient argument to explain why only three facets have been observed in $^4$He? Perhaps, but a more systematic study would be useful.

If one looked at the equilibrium shapes, it would be also difficult to see facets because the equilibrium facet size is proportional to the step free energy. For the (0001) facet in the low-temperature limit, Rolley, Guthmann, *et al.* (1995) found that the step energy $\beta/d$ was equal to 0.014 erg/cm$^2$, less than one-tenth of the surface tension value, so that the radius of the equilibrium facet should be less that one-tenth of the typical crystal radius. The sizes of facets with higher Miller indices would be even smaller, and thus these facets would be even more difficult to see on the equilibrium shapes of crystals. One possibility would be to enhance the facet size with the help of gravity, by adjusting the orientation of the crystal. This might produce a picture similar to the one shown in Fig. 18.

Note finally that, for bcc $^4$He crystals that exist above 1.46 K and have a surface tension value less than 0.12 erg/cm$^2$ (Balibar *et al.*, 1979; Gallet *et al.*, 1984), the universal relation [Eq. (11)] predicts that the first roughening transition for the (110) surfaces will take place below 0.45 K. This is, of course, consistent with the observations that bcc $^4$He crystals are rough over their whole domain of existence. As for bcc $^3$He crystals, their roughening transition temperatures are considered in Sec. III.D.2.

#### 4. Surface tension of $^4$He crystals

As we have seen above, the surface stiffness of $^4$He crystals is known in various directions and it has a substantial anisotropy. The Moscow group has investigated the general shape of $\gamma$ in all directions (Andreeva *et al.*, 1989; Andreeva and Keshishev, 1991; Keshishev and Andreeva, 1991). The surface stiffness can also be extracted from the equilibrium shape of free-standing crystals, and Wulff (1901) has introduced a geometric construction of the equilibrium crystal shape from a polar plot of $\gamma$. Even values for the step energies can be extracted from the facet sizes on the equilibrium crystal shapes, but it has been observed that the facet sizes are hysteretic. They depend on the crystal history because, when growth proceeds from the motion of steps attached to the screw dislocations (see Sec. V), there is a threshold force below which the steps do not move (Nozières, 1992).

One should not forget either that only rough $^4$He crystal surfaces have high mobility. Even for the extraction of the stiffness values for rough surfaces, the inverse Wulff construction of $\gamma$ from an equilibrium crystal shape would not be easy. One would need to know the exact pressure difference from the melting pressure to obtain the absolute value of the surface stiffness. Furthermore, one would need a very good resolution on the measured shape to obtain its exact local curvature everywhere. Eventually, the crystal shape would be sensitive to defects. All these difficulties probably explain why the surface stiffness of classical crystals is rarely accurately known, so that an accurate experimental check of the universal relation is usually impossible.

The method of Andreeva *et al.* (1989) and Keshishev and Andreeva (1991) was different: they used the dispersion relation of crystallization waves to determine $\gamma$. Some of their results are shown in Figs. 27 and 28. Further analysis of these data was performed in order to extract the surface tension $\alpha$ (Andreeva and Keshishev, 1991; Edwards *et al.*, 1991). It was found that $\alpha$ typically varies from 0.16 to 0.18 erg/cm$^2$. The anisotropy of $\alpha$ is much smaller than for $\gamma$. The value of $\alpha$ is important for the study of the nucleation of solid helium, where it is the free energy of the liquid-solid interface which matters, not the stiffness (see Balibar, 2002, for a review).

#### 5. Step-step interactions

The shape of the facet edges at a crystal surface has attracted much attention. It is related to the interaction between steps. Consider a vicinal surface, that is, a surface tilted by a small angle $\phi$ with respect to a certain facet (the temperature has to be lower than the roughening temperature of that facet). If $\phi$ is small enough, the steps are well separated and we call this vicinal surface a "stepped surface" because its properties are de-

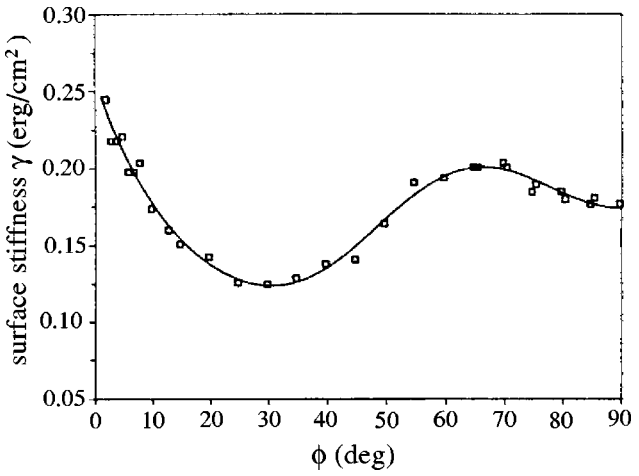


FIG. 27. Set of measurements of the surface stiffness $\gamma$ of hcp $^4$He crystals in the $(10\bar{1}0)$ plane. The angle $\phi=0$ corresponds to the (0001) plane and $\phi=90°$ to the $(11\bar{2}0)$ plane. From Andreeva and Keshishev, 1991.

termined by the steps. The energy of the stepped surface does not depend on the sign of $\phi$ and it can be expanded as

$$\alpha(\phi) = \left[ \alpha_0 + \frac{\beta}{d}\tan|\phi| + \frac{\delta}{d^3}\tan^3|\phi| \right]\cos\phi. \tag{27}$$

In this equation, we have assumed that the interaction energy between steps is a repulsion inversely proportional to the square of their mutual distance $l$, so that it can be written as $(\delta/d^2)\tan^2\phi$. From Eq. (27), one can derive the values of the two components of the stiffness tensor for such a vicinal surface:

$$\gamma_{//} = \frac{6\delta}{d^3}\phi \tag{28}$$

and

$$\gamma_{\perp} = \frac{\beta}{d}\frac{1}{\phi}. \tag{29}$$

Just as for a corrugated surface, it should be easy to bend the surface in one direction and very hard in the direction perpendicular to the first. The physics is simple: if one bends the surface in a plane perpendicular to the steps, one changes the distance between the steps. The energy cost depends on the interaction between steps, which is small if the steps are far apart (small $\phi$). In contrast, if one bends the surface along the steps, one forces the steps themselves to bend, that is, to increase their length. The associated cost is now a step energy, and the step bending is proportional to the inverse step density, consequently to $1/\phi$ (see Fig. 29).

Several kinds of interactions have been predicted to exist between steps. The dominant ones are the elastic interaction $\delta_{\rm el}$ and the entropic interaction $\delta_S$. Both of these vary as $1/l^2$ but with different coefficients. Let us start with the entropic interaction. It comes from a no-crossing condition. If two neighboring steps crossed, a

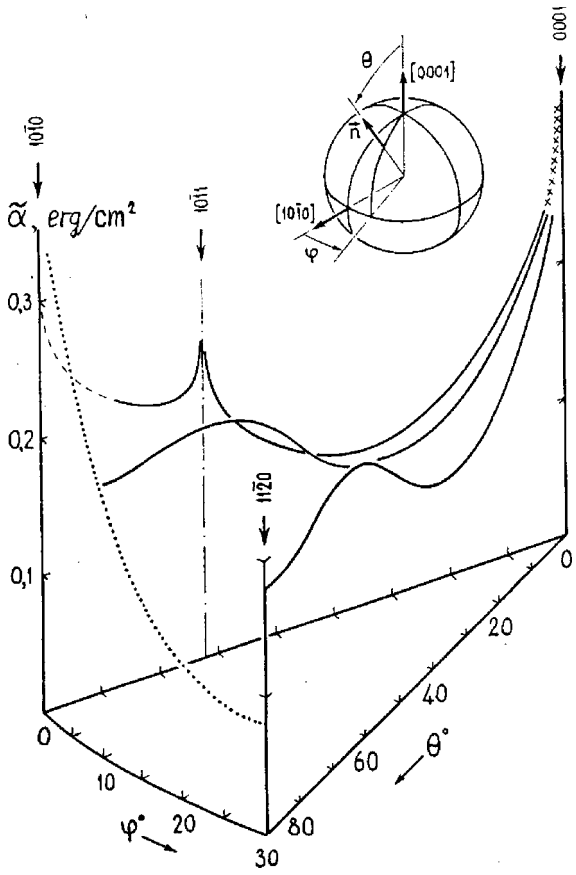


FIG. 28. General variation of the surface stiffness $\gamma$ of hcp $^4$He crystals, as measured from the dispersion relation of crystallization waves by Andreeva *et al.* (1989) and Keshishev and Andreeva (1991). From Andreeva and Keshishev, 1991.

local overhang would appear at the surface (see Fig. 30), and that is, of course, unlikely. Steps are thus confined by their neighbors, so that their long-wavelength fluctuations are cut and their entropy consequently reduced. This is a fundamental effect, which has an equivalent in one more dimension: the entropic repulsion between fluctuating membranes known as the "Helfrich interaction" (Helfrich, 1978). Its exact magnitude was first calculated from an analogy with one-dimensional Fermi particles, whose trajectories in a space-time plane are lines that do not cross (Jayaprakash and Saam, 1984; Bartelt *et al.*, 1990; Williams and Bartelt, 1991). After correction of a numerical error (see note 34 in Balibar and Nozières, 1994), the result of this calculation agreed with one obtained by a different method (Akutsu *et al.*, 1988):

$$\frac{\delta_S}{l^2} = \frac{\pi^2}{6}\frac{(k_B T)^2}{\beta\, l^2}. \tag{30}$$

This is another remarkable result, which is universal in the same sense as Eq. (11).

The elastic interaction was first calculated by Marchenko and Parshin (1980a). Its physical origin is the overlap of the strain fields around each step. The atoms in the step have a different environment from that of bulk atoms. As a consequence, there is a force doublet on

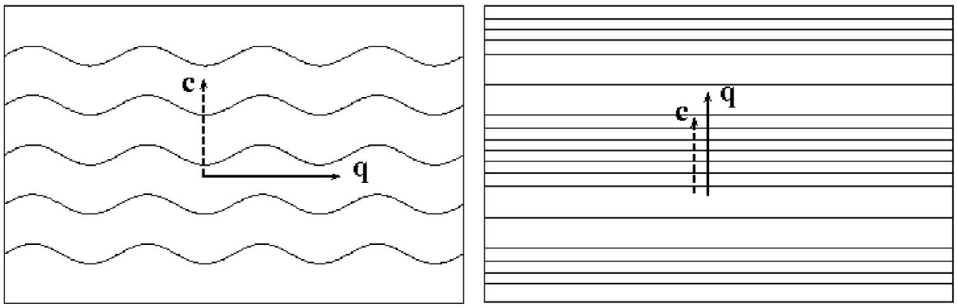


FIG. 29. Bending of a vicinal surface. It is easy to bend a vicinal surface in a plane parallel to the $c$ axis, but difficult in the plane perpendicular to it. For waves propagating with $q$ parallel to the projection of $c$, the relevant stiffness component $\gamma_{\|}$ is proportional to the interaction between steps and vanishes as the tilt angle $\phi$ tends to zero. In contrast, the component $\gamma_{\perp}$ is proportional to the step energy $\beta$ and diverges as $1/\phi$.

each step which induces a local strain field. Since the elastic energy is an integral of the square of the strain, the elastic energy of two steps is different from the sum of the elastic energies of two single steps: the cross term in the calculation gives the elastic interaction, which is repulsive for identical steps. Nozières (1992) wrote it as

$$\frac{\delta_{\rm el}}{l^2} = \frac{2}{\pi}\frac{(1-\sigma_P^2)(\vec{f}_1\cdot\vec{f}_2)}{E\,l^2}, \tag{31}$$

where $\sigma_P \simeq 1/3$ is the Poisson ratio, $E$ is the Young modulus ($3.05\times10^8$ erg/cm$^3$ for hcp $^4$He crystals), and $\vec{f}_{1,2}$ are the force doublets on each step. Each of these doublets is made of the local stretch of the surface $f^x$ and of the local torque $f^z$ which tends to twist the crystal.

As explained by Marchenko and Parshin (1980a), $f^z = \sigma^s d$, where $\sigma^s$ is a surface stress (Suttleworth, 1950; Marchenko and Parshin, 1980a; Andreev and Kosevich, 1981). In the case of $^4$He crystals, Edwards *et al.* (1991) estimated this surface stress to be 0.6 erg/cm$^2$ from the pressure dependence of the surface tension, and suggested measuring it by the transmission of phonons through the liquid-solid interface as a function of the direction of incidence. This does not look easy to do.

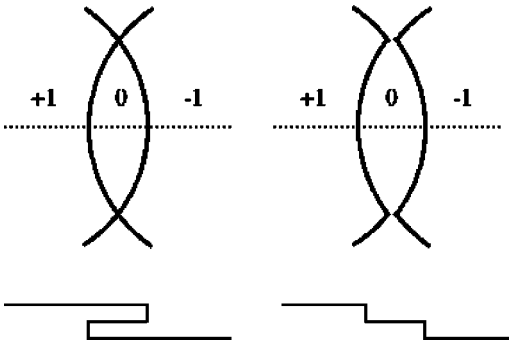


FIG. 30. No-crossing condition for steps. A crossing between steps (left) would induce a local overhang at the surface (cross section below). This is rather unlikely; thus the steps do not cross (right). The no-crossing condition for steps implies a reduction of the step entropy, hence a repulsive interaction.

Since $\sigma^s$ has to be comparable to the surface tension or surface stiffness, one can approximate $f^x$ as $\gamma$, and the elastic interaction as $\gamma^2/E\,l^2$.

Since they had not observed the anisotropy predicted by Eqs. (28) and (29), Andreeva *et al.* (1989) questioned the validity of the above reasoning. In fact, Rolley, Chevalier, *et al.* (1994; see also Rolley, Balibar, *et al.*, 1995 and Rolley, Guthmann, *et al.*, 1995) found this anisotropy when studying vicinal surfaces at lower temperature and with a smaller tilt angle. Both groups measured the surface stiffness from the dispersion of crystallization waves at surfaces with adjustable orientation. They rotated a cell containing a crystal with a large horizontal surface (see Fig. 14). Figure 39 below displays all their experimental results. Only the low-temperature and small-tilt-angle measurements by Rolley *et al.* showed the expected anisotropy of the surface stiffness tensor close to the $c$ facet. This experiment is described in greater detail in Sec. IV.B. Rolley's main results are twofold:

(1) At low temperature, the step energy is $\beta/d = (14\pm0.5)\times10^{-3}$ erg/cm$^2$ for ultrapure $^4$He crystals. In the presence of $^3$He impurities, Rolley *et al.* found a lower value of $\beta/d = (11\pm1)\times10^{-3}$ erg/cm$^2$, and they attributed the difference to adsorption, as explained in Sec. IV.C.8.

(2) The step-step interactions are consistent with the $1/l^2$ interactions predicted by Eqs. (30) and (31).

Eventually, hydrodynamic interactions were also calculated by Uwaha (1989, 1990). The fluctuations of steps induce flow fields that overlap if the steps are close to each other. Since the kinetic energy is quadratic in velocity, there is a hydrodynamic repulsion between steps. Uwaha first calculated this at $T=0$ and found a $1/l^2$ repulsion. At higher temperature, Uwaha predicted a crossover to $1/l$ interactions. Rolley, Guthmann, *et al.* (1995) could not verify Uwaha's predictions because these hydrodynamic interactions were too small under their experimental conditions.

### 6. Facet edges and related shape problems

The nature of step-step interactions has a direct effect on the equilibrium shape of crystals. As calculated by Jayaprakash *et al.* (1983) and Jayaprakash and Saam (1984), the shape of a crystal profile near the facet edge has to obey a power-law equation with a "3/2" exponent if the interaction energy is proportional to $1/l^2$. Suppose that the facet is some portion at $x<0$ of the horizontal plane $z=0$, then the shape of the crystal edge should be described by $z \propto x^{3/2}$. Jayaprakash *et al.* obtained this result by using Andreev's analysis of the Wulff construction (Wulff, 1901; Andreev, 1981). The "3/2" exponent is different from the mean-field exponent "2"; it relates the problem of a crystal shape to the Pokrovsky-Talapov transition of crystalline layers on incommensurate substrates (Gruber and Mullins, 1967; Jayaprakash *et al.*, 1983; Jayaprakash and Saam, 1984; Rottman *et al.*, 1984).

Several experimental attempts were made to check this new universal property. For $^4$He crystals, Carmi *et al.* (1987) found an exponent $1.55\pm0.06$ between 0.9 and 1.1 K; Gallet (1986) found $1.55\pm0.3$ from the fits in a small angular domain (from 0.14 to 0.18 rad) and a higher value at a larger tilt angle. Gallet also noticed that the fit of the exponent was so sensitive to the choice of the edge position $x=0$ that its error bar could not be small. Furthermore, it was noticed that, for large crystals and horizontal facets, gravity might change the exponent from "3/2" to "3" (Avron and Zia, 1988). Finally, Jayaprakash *et al.* (1984) and Rottman *et al.* (1984) discussed finite-size effects, which could be responsible for some rounding of the crystal profile very close to the facet edge. However, Parshin *et al.* (1988) showed by direct calculations of the crystal shape that the exponent "3/2" holds down to an atomic scale.

The most accurate experimental attempt was made in Helsinki. Babkin *et al.* (1995) measured the equilibrium profile of $^4$He crystals near the edge of the *c* facets, in the temperature interval from 0.05 to 0.7 K (Babkin *et al.*, 1995). They studied very-high-quality crystals, whose growth threshold was about 1 $\mu$bar, meaning an average density of screw dislocations or pinning centers of only $\sim 10$ cm$^{-2}$. They confirmed the "3/2" exponent but also obtained unexpected results.

Figure 31(a) shows a measured surface profile at 0.05 K. The facet is shown on the left side at $\zeta=0$. Far away from the edge the horizontal crystal profile follows the dashed line, the gravitational horizon. Figure 31(b) shows a magnified view of the same profile near the facet edge. There are two remarkable features. First, there is a discontinuity (marked by an arrow): the slope jumps from $\phi_{c1}=0.43$ mrad to $\phi_{c2}=2.3$ mrad, indicating a separation between two regions with distinct properties. In the region on the right-hand side the profile could be fit with the form $\zeta \sim x^{\theta}$, with $\theta$ between 1.3 and 1.8, in agreement with the "3/2" prediction. As in Gallet's analysis, the large error bar in the determination of the exponent comes from the uncertainty in the determination of the facet edge position. As for the region on the left side, which should be a flat facet, it appeared curved at that scale. The deviation from a flat plane was well represented by an exponential law $\zeta \propto \exp(-x/x_0)$, where $x$ was calculated from the facet edge and $x_0$ was a temperature-dependent quantity.

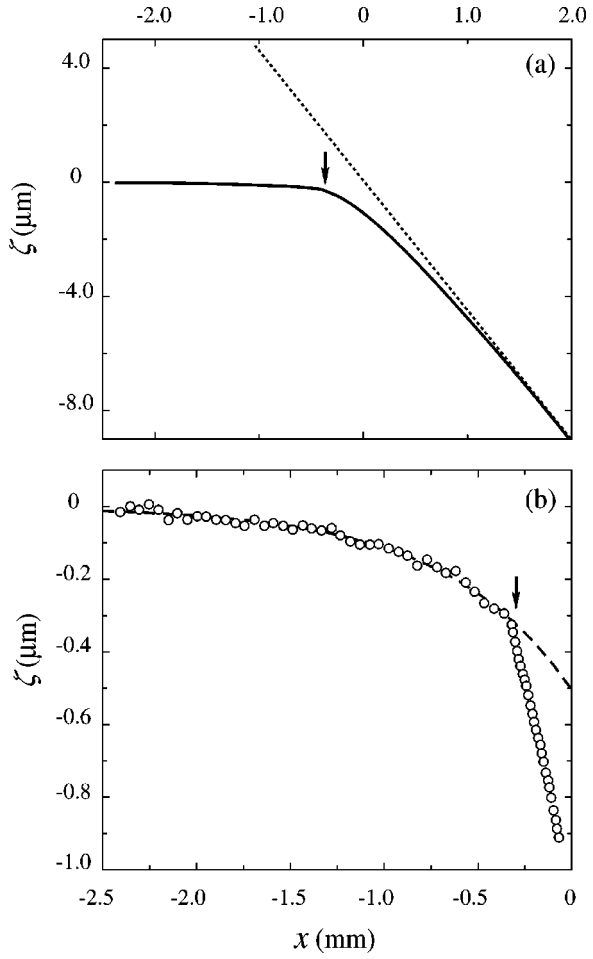


FIG. 31. Surface profile of a $^4$He crystal at 0.05 K (a) in a wide angular region $0 \leqslant \Theta \leqslant 4.5$ mrad; the dashed line corresponds to the gravitational horizon and the arrow indicates the slope discontinuity, and (b) at small $\Theta$ (magnified view); the dashed line is an exponential fit (see text). From Babkin *et al.*, 1995.

Several ideas have been proposed to explain this surprising curvature. Due to the presence of dislocations, there is a finite density of steps on the facet, and these steps could be polarized by the growth (Uwaha and Nozières, 1987); they could also be pinned by defects (Thuneberg, 1997), and the flatness of the facet could be affected by these phenomena. However, the density of dislocations and other pinning defects in these crystals looked too small for these explanations to apply. Another possibility was that the sixfold symmetry of the facet was broken, so that two different surface states could exist, with the same surface energy but with different orientations of the surface stress tensor; this would lead to a logarithmic interaction between steps (Marchenko, 1981a; Alerhand *et al.*, 1988), with an exponential bending of facets and a slope discontinuity as observed in the experiment. However, the origin of the

symmetry breaking, if real, is unknown, so that this explanation looks rather speculative. Before accepting this explanation, one would like some independent observations to be made and some physical arguments to be found in support of the idea that a reconstruction of the *c* facet takes place, leading to a new surface state.

Eventually, another explanation was proposed, which involved the existence of thermally excited dislocation loops at the interface (Andreev, 1990). This idea created a lively discussion on the effect of dislocations, dislocation loops, and point defects of different kinds on the long-range order in 3D and 2D systems, and on surface roughening in particular (Andreev, 1995; Bowley and Armour, 1997; Thuneberg, 1997; Armour *et al.*, 1998; Andreev and Melnikovsky, 2001). Andreev introduced the idea of thermodynamical equilibrium plasticity and argued that even point defects might destroy faceting. However, Armour *et al.* came to the conclusion that closely spaced pairs of dislocations with opposite signs could only slightly reduce the temperature of the roughening transition. They also predicted that, if the dislocations are randomly distributed, the interface will seem to have a glassy, nonfaceted low-temperature state. It undergoes a super-roughening transition with a singularity in the interfacial energy $\alpha$ but the transition does not manifest itself in the macroscopic shape, which is averaged over disorder (Toner and DiVincenzo, 1990; Korshunov, 1993).

To our knowledge, the whole issue is still an open problem. Turning back to Babkin's experiments, the activation energy of Andreev's loops was later estimated by the Helsinki group (Saramäki *et al.*, 1998), who found it larger than 18 K, and this looks too high to produce any observable effect at temperatures as low as 0.05 K. Thus no satisfactory explanation exists for the curvature of the *c* facets observed by Babkin *et al.*, nor for the slope discontinuity at the edge of the facets.

Additional support for the existence of $1/l^2$ interactions was obtained in $^3$He from the growth of stepped crystal surfaces (see Sec. V.A.3).

#### 7. Roughening and layering transitions

As already mentioned in Sec. II.C, $^4$He crystals grow epitaxially on clean graphite substrates. Maynard and his group carefully studied the variation of the thickness of the adsorbed film of solid $^4$He as a function of pressure and temperature (Ramesh and Maynard, 1982; Ramesh *et al.*, 1984). As shown in Fig. 32, the shape of the adsorption isotherms evolves with temperature. At high enough temperature the coverage is a continuous function of pressure $P$. As $P$ approaches the equilibrium pressure $P_{\mathrm{eq}}$, the coverage increases; it shows structures but evolves continuously. At low temperatures, the isotherms show jumps in thickness, that is, first-order transitions between films with integer numbers of atomic layers. Each of these *layering transitions* has a critical temperature $T_{cn}$, which depends on the number $n$ of layers.

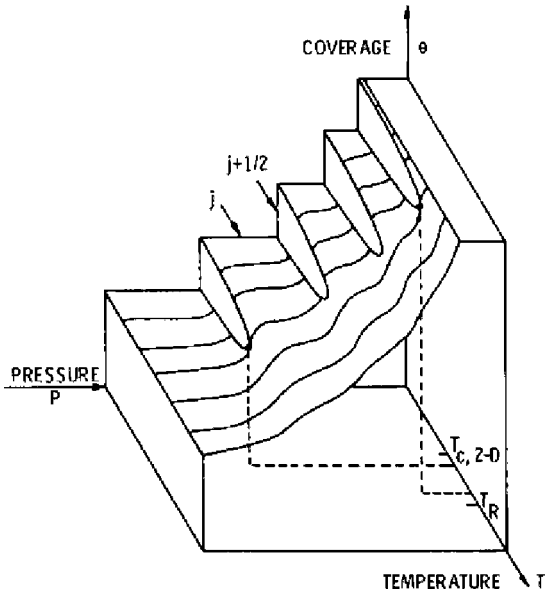


FIG. 32. Adsorption isotherms of solid $^4$He on graphite. At low temperature, the coverage shows jumps, that is, first-order transitions, between successive layers indexed with the integer number $j$ by Ramesh *et al.* (1984). The first-order transitions have critical end points at successive temperatures $T_c$ which depend on the number of atomic layers. From Ramesh *et al.*, 1984.

This phenomenon was related to roughening by Huse (1984) and by Nightingale *et al.* (1984) because the physics is similar: the liquid-solid interface can either be anchored by the lattice potential, in which case it occupies positions corresponding to an integer number of layers adsorbed on the graphite substrate, or it is free to occupy any position. However, the critical layering transitions are different from the roughening transition because of the van der Waals attraction, which confines the interface fluctuations. For the first layer, for example, the attraction is so strong that atoms can be in the first or in the second layer only. In this case, the system is strictly equivalent to the 2D Ising model, with a second-order phase transition, not with a Kosterlitz-Thouless transition. As the film thickness increases, the van der Waals attraction becomes weaker and the critical layering transition should evolve into the roughening transition. More precisely, Huse and Nightingale *et al.* predicted that $T_{cn}$ will tend linearly to $T_R$ as a function of $[\ln(n)]^{-2}$. This prediction was qualitatively verified by Ramesh *et al.* (1984), as shown in Fig. 33, at a time when the roughening transition temperature of $^4$He crystals was not yet accurately known. It would be very interesting to extend Ramesh's measurements beyond eight layers, the maximum thickness in Ramesh's experiment, in order to obtain a better check of this prediction.

Later the same group (McKenna *et al.*, 1992) discovered a surprising phenomenon. As temperature was lowered below 0.5 K, their fourth sound measurement technique showed the existence of a feature at a half-filling of solid $^4$He layers. It seemed that layers were being completed in two stages, not in a single one as was ex-

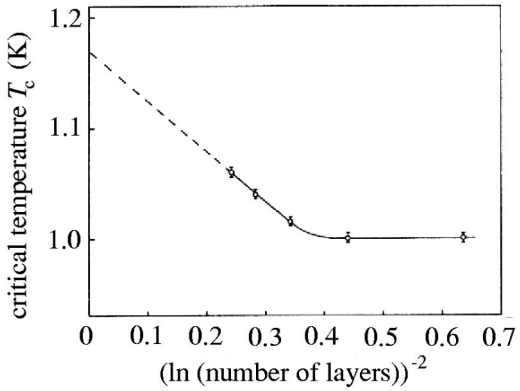


FIG. 33. Extrapolation of the critical layering transition temperatures $T_c(n)$ in $^4$He as a function of the number $n$ of layers, more precisely $(\ln n)^{-2}$. According to Huse (1984) and Nightingale *et al.* (1984), $T_c$ tends to the roughening temperature $T_R$ at infinite thickness. From Ramesh *et al.*, 1984.

pected. McKenna *et al.* first proposed that this observation was due to the existence of quantum kinks, whose mobility drastically changed when thermal rotons disappeared or when $^3$He impurities adsorbed on the steps. They then suggested another possible interpretation, namely, that some reconstruction of the (0001) surface could occur if one forced a half-filling of layers. Such ideas were also proposed by Gridin *et al.* (1984), who observed similar features in adsorption isotherms. The whole issue looks interesting and as yet undecided.

### D. $^3$He crystals

#### 1. Surface tension of $^3$He crystals

In $^3$He, crystallization waves can propagate only at submillikelvin temperatures. At higher temperatures the surface stiffness of $^3$He crystals can be measured from the equilibrium crystal shape, but it is difficult because the crystal shape can be easily distorted by defects, impurities, or temperature gradients. The crystal size should be larger than the capillary length $l_c \approx 1$ mm. Owing to the large latent heat of crystallization, the relaxation time of the crystal shape is very long (many hours or even days), except in the vicinity of the melting curve minimum ($T_{\min}=320$ mK), where the latent heat vanishes.

Rolley *et al.* (1989) have performed measurements between 140 and 330 mK. Figure 34(a) shows a $^3$He crystal in equilibrium at 320 mK. As shown in Figure 34(b), the measured profile fits very well with a single value of the surface stiffness $\gamma$. The stiffness is close to isotropic and consequently equal to the surface tension $\alpha$, as usually found for bcc structures. Moreover, the measured value $\alpha=0.060\pm0.011$ erg/cm$^2$ does not depend on temperature within the experimental accuracy. Rolley, Balibar, and Graner (1994) later estimated the anisotropy of $\gamma$ from the shape of quasispherical liquid inclusions inside crystals. Good fits were obtained with $\gamma(\phi)=\gamma_0[1+\epsilon\cos(4\phi)]$ and $\epsilon=0.02\pm0.01$, as found with other bcc crystals.

An important observation is the absence of visible facets above 140 mK on $^3$He crystals. More recently, the surface stiffness of $^3$He crystals has been measured down to 80 mK by the Helsinki group (Todoshchenko *et al.*, 2005). They used a Fabry-Pérot type of interferometer (see Sec. II.B.2) and observed the whole crystal shape, not only the profile. The results of Todoshchenko *et al.* confirm those by Rolley *et al.* (1989).

#### 2. Roughening transitions in $^3$He

In 1986, Rolley *et al.* first observed the (110) facets in $^3$He below 80 mK (see Fig. 35) and in 1989 up to 100 mK. Later two other types of facets [(100) and (211)] were seen by Wagner *et al.* (1996) in the millikelvin range, during growth of the crystals from the $A$ phase of superfluid $^3$He (see Fig. 36). More recently, the Helsinki group observed altogether 11 different types of facets at 0.55 mK (Alles *et al.*, 2001; Tsepelin *et al.*, 2001; see Fig. 37). With their interferometer, facets could be observed even when they occupied a small fraction of an otherwise rounded surface. With the same setup it was observed that at least three types of facets exist up to 55 mK (Todoshchenko *et al.*, 2003).

From all these publications, it appears that the maximum temperatures at which facets can be seen in $^3$He are definitely lower than expected from the universal relation [Eq. (11)]. This was already noticed by Rolley *et al.* (1989), who predicted that, for the (110) facets, $T_R$ should be about 260 mK. Table I shows the maximum temperatures at which facets have been observed by the Helsinki group and a simple estimate of the corresponding roughening temperatures. For this estimate, the criti-

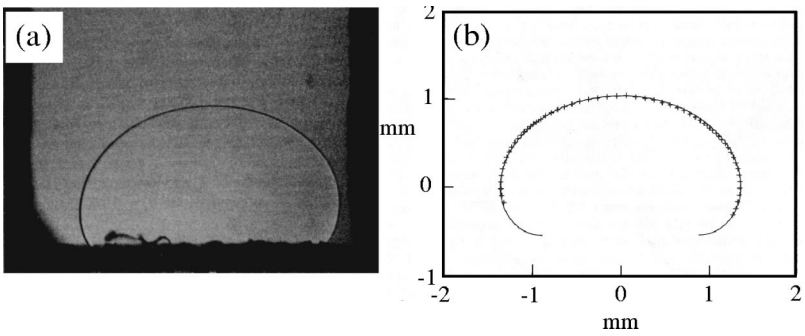


FIG. 34. $^3$He surface: (a) $^3$He crystal in equilibrium at 320 mK; (b) a fit of the surface profile with the Laplace equation, which yielded the value of the surface tension $\alpha=0.06$ erg/cm$^2$ for $^3$He crystals. From Rolley *et al.*, 1989.

FIG. 35. $^3$He crystals growing at 70 mK. The facets are the (110) surfaces. From Rolley *et al.*, 1986.

cal variation of $\gamma$ was neglected: Eq. (11) with $\gamma = 0.06$ erg/cm$^2$ and the respective values of the step height for each orientation were used.

In order to explain this discrepancy, Rolley *et al.* (1989) invoked dynamic roughening. Since a $^3$He atom is lighter than a $^4$He one, they noted that the zero-point motion of atoms in the crystal lattice is even larger in $^3$He than in $^4$He: $0.37a$ in $^3$He compared to $0.24a$ in $^4$He, according to Pierre *et al.* (1985) where $a$ is the lattice constant. From this they concluded that the coupling of the liquid-solid interface to the crystal lattice should be even weaker in $^3$He than in $^4$He. This is because the lattice potential is expected to decrease exponentially with the interface width (Iordanskii and Korshunov, 1984; Nozières, 1992). As a consequence, step energies should be so small in $^3$He that it would be nearly impossible to see facets on equilibrium crystal shapes, as noticed in all experiments. As for the growth shapes, they would reveal the existence of facets only if the growth

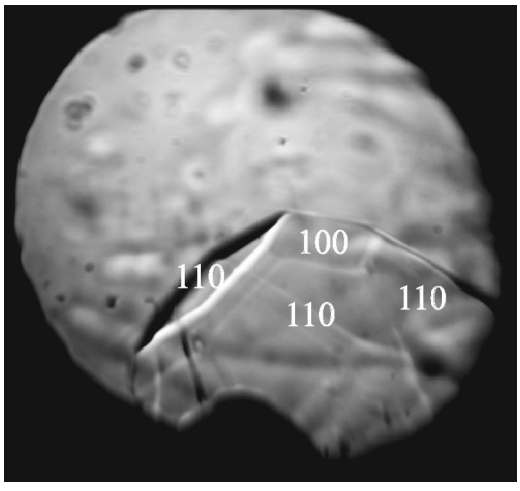


FIG. 36. Growing $^3$He crystal at 2.2 mK. Three types of facets, [(110), (100), and (211)], were identified from a comparison of this image with computer simulations. The (211) facets are barely visible in between some of the two neighboring (110) facets. From Wagner *et al.*, 1996.

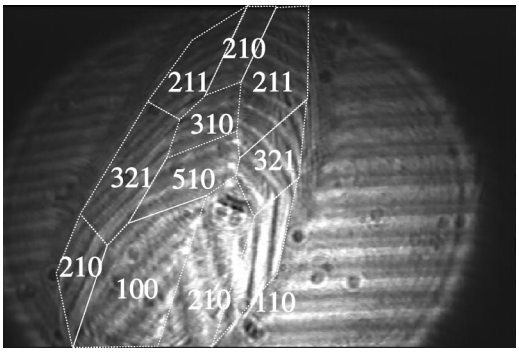


FIG. 37. Interferogram of a growing $^3$He crystal at 0.55 mK, revealing seven different types of facets which are labeled with Miller indices. From Alles *et al.*, 2001.

speed were slow enough to avoid dynamic roughening. Within this model, Rolley *et al.* used Eq. (21) to estimate the step free energy for the (110) facets at 100 mK, and found $\beta_{110} \approx 1.2 \times 10^{-11}$ erg/cm. Under these conditions, the correlation length had to be $\xi_{110} \approx 3 \times 10^{-6}$ cm, larger by two orders of magnitude than the lattice constant of $^3$He crystals. Such an extremely weak coupling leads to very wide steps, and it is possible. Its verification is in progress by the Helsinki group.

There appeared a serious difficulty when Tsepelin *et al.* (2002b) measured the step free energies of different facets in $^3$He at 0.55 mK, where the solid is ordered in its antiferromagnetic state and is in a contact with the $B$ phase of superfluid $^3$He. They found $\beta_{110} = 6.6 \times 10^{-10}$ erg/cm, about 50 times more than Rolley's estimate at 100 mK. If the coupling is really weak, it seems impossible to imagine that the step free energy increases that much from 100 to 0.55 mK. Moreover, Tsepelin's value is about one-third of the product $\gamma d = 1.8 \times 10^{-9}$ erg/cm, indicating strong coupling at low temperature. Another indication of strong coupling at low

TABLE I. The roughening transition in bcc $^3$He crystals. The calculated roughening transition temperatures ($T_{\mathrm{calc}}$) are systematically larger than the maximum temperatures at which facets have been observed ($T_{\mathrm{obs}}^{\mathrm{max}}$); different facets are represented by their respective Miller indices.

| Miller index | $T_{\mathrm{calc}}$ (mK) | $T_{\mathrm{obs}}^{\mathrm{max}}$ (mK) |
|---|---|---|
| 110 | 260 | 100 |
| 100 | 130 | 55 |
| 211 | 86.6 | 55 |
| 310 | 52 | 0.55 |
| 111 | 43.3 | 0.55 |
| 321 | 37.1 | 0.55 |
| 411 | 28.8 | 0.55 |
| 210 | 26 | 0.55 |
| 510 | 20 | 0.55 |
| 431 | 20 | 0.55 |
| 311 | 11.8 | 0.55 |

temperature comes from the comparison of the step energy values on successive facets: Tsepelin *et al.* (2002a, 2002b) showed that the $1/l^2$ law seems to hold down to interstep distances $l$ of order $d$, at variance with a large step width (see Sect. V.A.3).

Altogether, these measurements lead to a series of unanswered questions concerning $^3$He. Is the liquid-solid interface strongly or weakly coupled to the crystal lattice? Is it possible that the strength of this coupling changes with temperature? What could be the effect of the superfluid transitions on the surface properties of a crystal? What about the magnetic ordering transition in the solid? Could it be that the RG theory of roughening does not apply to $^3$He for some unknown reason? The whole issue is currently under investigation in Helsinki and in Leiden, where systematic measurements are in progress over the whole temperature range from 120 mK down to the lowest temperatures.

## IV. DYNAMICS OF ROUGH SURFACES

### A. Crystallization waves and the unusual growth dynamics of rough $^4$He surfaces

In 1978, Andreev and Parshin realized that at low temperatures, when all individual degrees of freedom are frozen, the melting and crystallization of helium are quantum collective processes, which can proceed without energy dissipation. Therefore the liquid-solid interface could oscillate as freely as the surface of a nonviscous classical liquid (Andreev and Parshin, 1978). As we shall see, the dispersion relation of crystallization waves is similar to that of ordinary surface waves because the potential energy is due to the same gravity and surface-tension terms. One difference is that the mass flow, hence the kinetic energy, comes from the difference between the crystal density $\rho_C$ and the liquid density $\rho_L$: any growth or melting leading to a displacement of the interface requires a mass flow in the liquid, which is proportional to the difference $\delta\rho=\rho_C-\rho_L$. Another difference is that since a crystal is anisotropic, crystallization waves are also anisotropic. Eventually, the attenuation of ordinary surface waves originates in viscous dissipation in the bulk liquid, while for crystallization waves it is mainly a surface mechanism.

In order to derive the dispersion relation, one proceeds as follows. Let us call $\zeta(x)$ the displacement of the crystal surface from its average horizontal position. Mass conservation implies a velocity $v_L$ in the liquid, which is related to the velocity $\dot{\zeta}$ of the surface by

$$v_L = \frac{\rho_L - \rho_C}{\rho_L}\dot{\zeta}. \tag{32}$$

If there is no dissipation, the difference in chemical potential $\delta\mu=\mu_L-\mu_C$ is zero at the interface. Since the chemical potentials $\mu_{C,L}$ are taken per unit mass, they obey

$$\frac{\partial\mu}{\partial P} = \frac{1}{\rho}. \tag{33}$$

Furthermore, the mechanical equilibrium at the interface implies that

$$P_C - P_L = \left(\alpha + \frac{\partial^2\alpha}{\partial x^2}\right)\frac{\partial^2\zeta}{\partial x^2} = \gamma_x\frac{\partial^2\zeta}{\partial x^2}, \tag{34}$$

where $\alpha$ is the surface tension and $\gamma_x$ the surface stiffness in the $x$ direction. The two above equations can be combined as

$$\left(\frac{1}{\rho_L} - \frac{1}{\rho_C}\right)(\delta P_L - \rho_L g\zeta) + \frac{1}{\rho_C}\gamma_x\frac{\partial^2\zeta}{\partial x^2} = 0. \tag{35}$$

Finally, at low enough frequency, these waves propagate with velocities much smaller than the sound velocity, so that the liquid can be considered as incompressible, and the equations for a potential flow are

$$v_L = \nabla\psi, \tag{36}$$

$$\delta P_L = -\rho_L\dot{\psi}. \tag{37}$$

For a sinusoidal wave $\zeta(x,t)=\zeta_0\exp(iqx-i\omega t)$, one finds a potential $\psi=\psi_0\exp(iqx-i\omega t-qz)$, where $z$ is the vertical coordinate, and one obtains the dispersion relation

$$\omega^2 = \frac{\rho_L}{\delta\rho^2}\gamma_x q^3 + g\frac{\rho_L}{\delta\rho}q. \tag{38}$$

The first term describes the capillary waves, which are anisotropic because $\gamma_x$ depends on orientation; it dominates at high frequencies (short wavelengths). The second term involves $g$, the acceleration of gravity. As usual, the crossover from capillary to gravitational waves occurs for wavelengths larger than the capillary length

$$l_c = \sqrt{\frac{\gamma}{\delta\rho g}}. \tag{39}$$

Equation (38) was first verified by Keshishev *et al.* between 70 Hz and 5 kHz (see Fig. 38) and later by Rolley, Chevalier, *et al.* (1994). From such graphs, very accurate measurements of the surface stiffness could be made in different crystalline directions (see, for example, Figs. 27 and 28).

Supposing now that growth and melting dissipate a small amount of energy, then a finite velocity $v$ of the liquid-solid interface produces a small difference in the chemical potential difference $\delta\mu$ between the solid and liquid. The dissipation can be described by the growth coefficient $k$ in the equation

$$v = k\delta\mu. \tag{40}$$

As a consequence, Eq. (35) has to be replaced by the more general form

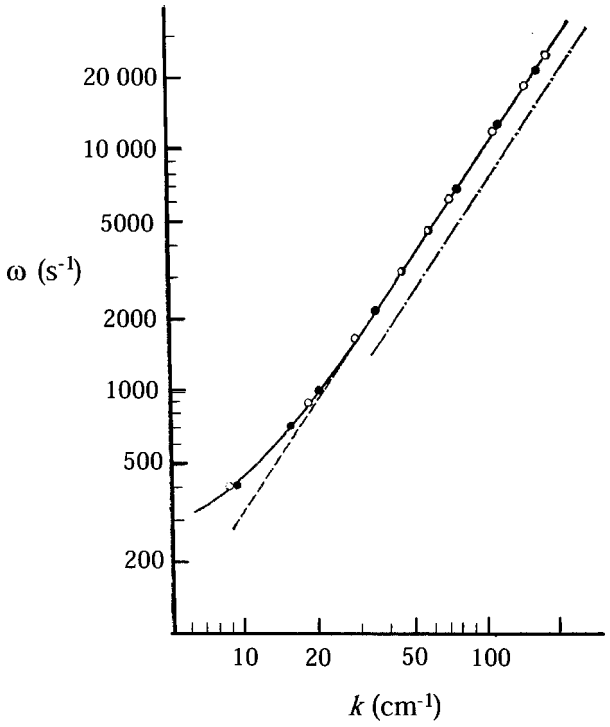


FIG. 38. Measurements by Keshishev *et al.* (1981) of the dispersion of crystallization waves in $^4$He. At high enough frequencies, a 3/2 power law was found, in a very good agreement with Eq. (38). Below about 20 cm$^{-1}$, the slight deviation from the 3/2 power law indicates a crossover to gravitational waves. From Keshishev *et al.*, 1981.

$$\left(\frac{1}{\rho_L}-\frac{1}{\rho_C}\right)(\delta P_L-\rho_L g\zeta)+\frac{1}{\rho_C}\gamma_x\frac{\partial^2\zeta}{\partial x^2}=\frac{1}{k}\dot{\zeta}, \tag{41}$$

and the dispersion relation acquires an imaginary term:

$$\omega^2=\frac{\rho_L}{\delta\rho^2}q^3+g\frac{\rho_L}{\delta\rho}q-\frac{\rho_C\rho_L}{\delta\rho^2}\frac{i\omega q}{k}. \tag{42}$$

Keshishev *et al.* (1979) obtained the first measurements of the dissipative coefficient $k$ from the damping of the waves (see, for example, Fig. 15). A more elaborate theoretical description of the dissipative coefficients is presented in Sec. IV.C.1, together with a comparison with several experiments. Corrections to the above equations have been calculated by Uwaha and Baym (1982), who considered the effect of compressibility at high frequency (see Sec. IV.C.9). Other corrections have to be introduced if the crystal is under stress (Balibar, Edwards, and Saam, 1994) (see Sec. VI.A).

### B. Crystallization waves at $^4$He vicinal surfaces

Rolley *et al.* (Rolley, Chevalier, *et al.*, 1994; Rolley, Balibar, *et al.*, 1995; Rolley, Guthmann, *et al.*, 1995) studied crystallization waves at vicinal surfaces, that is, on surfaces with an orientation close to that of the faceted ones. They were interested in the properties of stepped surfaces, which are particular vicinal surfaces in which steps are well separated and control the surface properties of crystals. They measured the energy of steps at the (0001) surfaces as well as their mutual interactions.

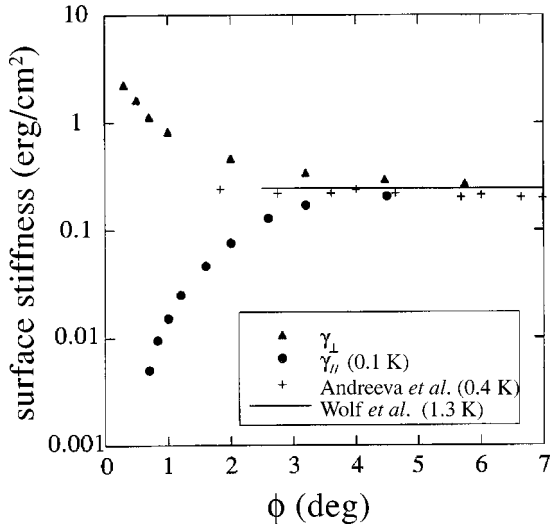


FIG. 39. Stiffness of the stepped surfaces of $^4$He crystals. As measured by Rolley, Balibar, and Graner (1994) and Rolley, Guthmann, *et al.* (1995), the stepped surfaces show a large anisotropy as their tilt angle $\phi$ with respect to a high-symmetry plane tends to zero. One component of the surface stiffness tensor tends to zero while the other diverges, as predicted by Eqs. (28) and (29). From Rolley, Guthmann, *et al.*, 1995.

As described in Sec. II.C, they were able to rotate their crystals in two perpendicular directions and study the case in which the wave vector $q$ was parallel to the projection of the $c$ axis at the surface, as well as the case in which $q$ was perpendicular to it. They obtained the angular variation of the two corresponding components $\gamma_{\|}$ and $\gamma_{\perp}$ of the surface stiffness tensor. Figure 39 shows that $\gamma_{\|}$ decreases while $\gamma_{\perp}$ increases as the surface approaches the (0001) basal plane.

Rolley, Balibar, *et al.* (1995) compared this behavior with the predictions of Eqs. (28) and (29). As shown in Fig. 40, the component $\gamma_{\perp}$ was found to be inversely proportional to the tilt angle $\phi$ so that they could deduce the low-temperature value

$$\beta_0/d=(14\pm0.5)\times10^{-3}\ \text{erg/cm}^2 \tag{43}$$

of the step energy. This was found to be close to the value ($17\times10^{-3}$ erg/cm$^2$) that had been predicted with the parameters of the RG theory. Although these parameters had been adjusted by comparing with measurements close to the roughening transition temperature, the extrapolation of the theory far from the roughening transition was considered to be a good approximation because the value of the parameter $t_c$ indicated weak coupling even at low temperature. For a more accurate calculation of $\beta_0$, one would need to go beyond the first approximations of the Nozières's theory. One attempt has been made by Hazareesing and Bouchaud (2000), who used "functional renormalization," a more elaborate method.

Rolley, Chevalier, *et al.* (1994) and Rolley, Guthmann, *et al.* (1995) also showed that the $\phi$ dependence of the

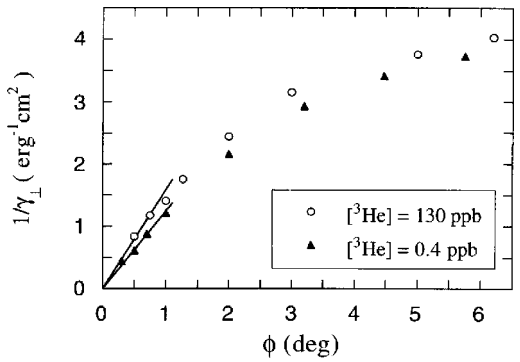


FIG. 40. Surface stiffness coefficient $\gamma_\perp$ as a function of the tilt angle $\phi$. With this measurement, Rolley, Balibar, *et al.* (1995) verified that $\gamma_\perp$ is inversely proportional to $\phi$, as predicted by Eq. (29); from the initial slope, they measured the step free energy $\beta/d=0.014$ erg/cm$^2$ for ultrapure $^4$He (0.011 erg/cm$^2$ with 130 ppb of $^3$He impurities). From Rolley, Balibar, *et al.*, 1995.

component $\gamma_\parallel$ approached the prediction of Eq. (28). They could make measurements down to $\phi=0.7°$ (see Fig. 41), but they found that this angle was not small enough to reach the linear behavior characteristic of well-separated steps. This is because the steps were confirmed to be very wide. As can be seen from Fig. 39, the surface stiffness components depart from the roughly isotropic value of 0.245 erg/cm$^2$ only below $\theta_c \approx 2.5°$. This finding agreed with the prediction of the RG theory of a crossover angle $\theta_c \approx d/6L_0 \approx 1/24$ rad [see Eq. (25)]. Andreeva *et al.* (1989) had questioned the existence of the stepped behavior but, after the work of Rolley *et al.*, this behavior was shown to exist only at a rather small $\phi$ and at low enough temperature for the wide steps to be well separated [remember that an estimate of the step width was given with Eq. (10), $w \approx 4\xi \approx 2L_{\max}$].

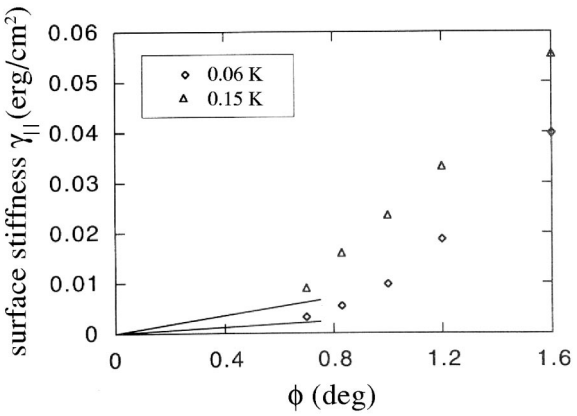


FIG. 41. Surface stiffness coefficient $\gamma_\parallel$ as a function of the tilt angle $\phi$. Rolley, Chevalier, *et al.* (1994) and Rolley, Guthmann, *et al.* (1995) verified that $\gamma_\parallel$ vanishes as $\phi$ tends to zero. They could not measure it at an angle small enough to verify the linear asymptotic behavior predicted by Eq. (28), but their measurements are consistent with Eqs. (30) and (31) (solid lines). From Rolley, Guthmann, *et al.*, 1995.

Although the steps were not fully separated at $\phi=0.7°$, Rolley *et al.* compared their measurements with the predictions for the interaction between two steps at a distance $l=d/\phi$ apart. In his mean-field theory, Andreev had assumed a $\phi$-independent value of $\gamma_\parallel$, implying a $1/l$ interaction between steps (Andreev, 1981; Andreev and Knizhnik, 1982); this was clearly ruled out. Rolley *et al.* compared their results with the prediction of entropic and elastic interactions which varied as $1/l^2$ (see Sec. III.C.5). From the temperature variation and the known value of $\beta_0$, they found good agreement with the entropic interaction, in particular with Akutsu's universal coefficient $(\pi^2/6)$ in Eq. (30), which had been a matter of debate for some time (Akutsu *et al.*, 1988). From an estimate of the temperature-independent term in the interaction, they found agreement with the prediction of Marchenko and Parshin (1980a) for the elastic interaction if the surface stress was roughly equal to the surface stiffness, $\gamma_0=0.245$ erg/cm$^2$. It would be useful to measure this interaction at a smaller tilt angle for the steps to be better separated, and to extend the theory of the step-step interactions to the case in which, steps being close to each other, their interaction depends on their structure, primarily on their width.

### C. Surface dissipation in $^4$He

#### 1. Heat and mass flow: The Onsager matrix

After Keshishev *et al.* (1979, 1981) measured the damping of crystallization waves, several authors undertook to calculate the dissipation at the liquid-solid interface (Castaing and Nozières, 1980; Huber and Maris, 1981; Andreev and Knizhnik, 1982; Bowley and Edwards, 1983). Keshishev *et al.* found that the inverse attenuation length of the waves varied as $\omega^{1/3}$, in agreement with Eq. (42). This corresponds to a damping rate proportional to the wave vector $q$ and confirms that dissipation takes place at the crystal surface; a viscous dissipation in the bulk would lead to a damping proportional to $q^2$. Furthermore, they found that the growth resistance $k^{-1}$ could be decomposed as a sum of three terms:

$$k^{-1} = A_0 + B_0 T^4 + C_0 \exp\left(-\frac{\Delta}{T}\right). \tag{44}$$

The constant term $A_0$ was not reproducible from one crystal to another and was therefore attributed to defects or impurities; the two other terms were attributed to the scattering of phonons and rotons by the moving liquid-solid interface.

Andreev and Parshin (1978) assumed that the dissipation was due to the total reflection of phonons and rotons, and they first predicted that the growth resistance should be proportional to $T^4$ in the low-temperature limit. Andreev and Knizhnik (1982) later distinguished "ballistic" and "hydrodynamic" regimes. The *ballistic regime* corresponds to a situation in which the size of the system is smaller than the mean free path $l_{mf}$ of excitations. In this case the interface moves with respect to an

excitation gas that is at rest in the frame of the experimental cell. For crystallization waves, this means $ql_{mf}>1$, or $\omega\tau>1$ if $\tau$ is the collision time of the excitations. In the opposite limit, the excitations move with the interface and the dissipation is due to the viscosity of the excitation system in the adjacent bulk phases; it does not take place at the interface. This is a remarkable situation. The transformation of the condensate into a crystalline phase is accompanied by no dissipation at all at the interface. In a classical system, the sticking atoms have to release their momentum and consequently some kinetic energy, so that some dissipation occurs at the interface.

Castaing and Nozières (1980) formulated the whole problem in the frame of an Onsager matrix relating currents to the differences in chemical potential ($\delta\mu=\mu_L-\mu_C$) and in temperature ($\delta T=T_L-T_C$) between the two phases. More precisely, they linearized the relation between the two forces $\delta\mu/T$ and $\delta T/T^2$, and the mass current $J$ and heat current $J_E$ flowing through the interface. They were followed by numerous authors who used different notations. In order to avoid confusion with the lattice spacing $a$ and the sound velocity $c$, we here define the Onsager matrix coefficients $A$, $B$, and $C$ by the following relations:

$$\frac{\delta\mu}{T}=AJ+BJ_E, \tag{45}$$

$$\frac{\delta T}{T^2}=BJ+CJ_E. \tag{46}$$

Since the Onsager matrix is symmetric, its cross coefficient $B$ is the same in these two equations. Furthermore, the condition that the dissipation, that is, the entropy production

$$\dot{S}=J\left(\frac{\delta\mu}{T}\right)+J_E\left(\frac{\delta T}{T^2}\right) \tag{47}$$

be positive requires $B^2<AC$. In the absence of mass current ($J=0$), one sees that the coefficient $C$ describes the thermal resistance of the interface, known as the *Kapitza resistance* $R_K=(\delta T/J_E)$. The two quantities are related by

$$R_K=CT^2. \tag{48}$$

As for the growth coefficient $k$, which was introduced above, this general formulation shows that two different cases have to be distinguished. The growth is called *adiabatic* if there is no heat current ($J_E=0$). In this case, the *adiabatic growth coefficient* (also called the *adiabatic interface mobility*) is

$$k_E=\frac{1}{\rho_C AT}. \tag{49}$$

If the growth is "isothermal" in the sense that $\delta T=0$, then the *isothermal growth coefficient* is different and given by

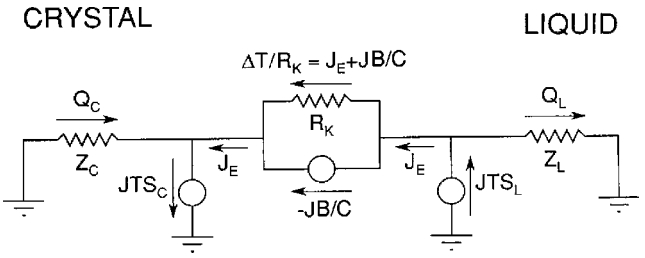


FIG. 42. Diagram of entropy conservation at the liquid-solid interface during growth, as represented by Balibar, Edwards, and Saam (1991) following Nozières and Uwaha (1987). From Balibar, Edwards, and Saam, 1991.

$$k_T=\frac{k_E}{1-B^2/AC}. \tag{50}$$

The cross coefficient $B$ describes the way the two entropies are shared between the two sides of the interface during growth. Its physical meaning was clarified by Balibar, Edwards, and Saam (1991), who used the previous work of Nozières and Uwaha (1987). They represented the flow of heat and entropy at the interface as shown in Fig. 42. In this figure, $Q_C$ is the heat flow from the walls into the crystal and $Q_L$ is the heat flow from the liquid into the walls. One has

$$Q_C=JTS_C-J_E, \tag{51}$$

$$Q_L=JTS_L-J_E. \tag{52}$$

Furthermore, the heat current $J_E$ which flows through the interface can be expressed as

$$J_E=\frac{\delta T}{R_K}-J\frac{B}{C}, \tag{53}$$

so that

$$Q_C=J(TS_C+B/C)-\delta T/R_K, \tag{54}$$

$$Q_L=J(TS_L+B/C)-\delta T/R_K. \tag{55}$$

One now understands that $\delta T/R_K$ is the heat that is *conducted* through the interface, and that $(-B/CT)$ is the entropy per unit mass that is *carried* through the interface by the mass current $J$.

#### 2. The growth resistance: Phonon contribution

Bowley and Edwards (1983) were the first to calculate the growth resistance $k_T^{-1}$ in the low-temperature limit where they assumed phonons to dominate and be ballistic. The dissipation is the work of the phonon radiation pressure at the moving interface: as it moves, the interface perturbs the distribution of phonons, and it is the relaxation of the perturbed distribution towards equilibrium which produces entropy. As a first step, and following Castaing and Nozières (1980), they assumed that, due to the high mobility of the interface at low temperature, all phonons were totally reflected at the interface (see the next subsection). They also neglected mode conversion and found that

$$k^{-1} = \frac{\hbar \pi^2}{30 \rho_C} \left( \frac{k_B T}{\hbar} \right)^4 \left[ \frac{1}{c_L^4} + \frac{2}{c_t^4} + \frac{1}{c_l^4} \right], \tag{56}$$

where $c_L$ is the sound velocity in the liquid, and $c_t$ and $c_l$ are the velocities of the transverse and longitudinal sounds, respectively, in the crystal. At low temperature, the above equation predicts that the growth resistance will be dominated by the phonons with the smallest velocity, the transverse phonons in the crystal. The result of Bowley and Edwards (1983) is more general than that obtained by Andreev and Knizhnik (1982), who only calculated the contribution from phonons in the liquid.

Equation (56) also explains the anisotropy of the growth resistance: it depends on the sound velocities in the crystal. Finally, Bowley and Edwards showed that the effect of phonon transmission was small, a reduction of the growth resistance by about 3%; they also showed that the effect of mode conversion is even smaller.

How does the above theory compare with experiments? Equation (56) predicts that the growth resistance will be proportional to $T^4$ with a coefficient between 3.06 and 3.32 cm $s^{-1}$ $K^{-4}$. Keshishev *et al.* (1981) had found $2.6T^4$ for one crystal and $3.4T^4$ for another crystal. The agreement is obviously good, but a precise comparison would need to know the exact orientation of these crystals. Furthermore, Keshishev's data were taken in the temperature range from 0.36 to 0.59 K, where the phonons in the crystal are not expected to be ballistic (Golub and Svatko, 1980). This was later confirmed by Wang and Agnolet (1992a), who observed that, below 0.25 K, the coefficients varied from crystal to crystal in the range from 2.7 to 3.5. They also found a systematic drop of this coefficient above 0.25 K, where the crystal phonons entered a hydrodynamic regime, so that, progressively, only the contribution from the liquid phonons was left. The crossover from a ballistic to a hydrodynamic regime of crystal phonons was also the explanation for the frequency dependence of the damping of crystallization waves, which was measured by Rolley, Guthmann, *et al.* (1995).

### 3. Rotons and kinks

At even higher temperatures, none of the phonons are ballistic and their contribution to the growth resistance is negligible; the thermodynamics of liquid $^4$He is dominated by rotons. Rotons are totally reflected at the interface because their velocities are very different from that of phonons in the crystal. There are two different types of reflections because there are two sorts of rotons, which were named $R^+$ and $R^-$ by Wyborn and Wyatt (1990). $R^+$ rotons have their momentum parallel to their group velocity, while $R^-$ rotons have it antiparallel. A normal reflection corresponds to rotons staying in the same category and an "Andreev reflection"[4] corresponds to the opposite case, when there is conversion from one type into another. Assuming ballistic rotons

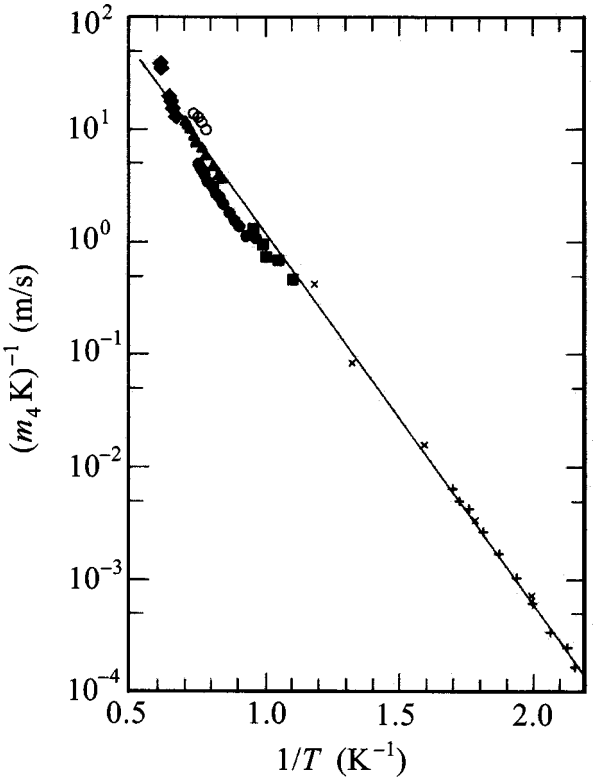


FIG. 43. Contribution of rotons to the growth resistance $k^{-1}$ of solid $^4$He labeled $(m_4 K)^{-1}$, as calculated by Bodensohn *et al.* (1986): +, experiments of Keshishev *et al.* (1981); ×, experiments of Castaing *et al.* (1980); ●, ■, ◆, experiments of Bodensohn *et al.* (1986); solid line, best fit with a simple exponential function [Eq. (59)]. The phonon contribution has been subtracted in the case of Keshishev's measurements. From Bodensohn *et al.*, 1986.

and a fraction $\xi_A$ of Andreev reflections, Bowley and Edwards (1983) found a roton contribution to the growth resistance:

$$k_{\rm rot}^{-1} = (1 - \xi_A) \frac{\hbar (q_0/\hbar)^4}{4\pi^2 \rho_C} \exp(-\Delta/k_B T) \tag{57}$$

$$\simeq 2.36 \times 10^5 (1 - \xi_A) \exp(-7.21/T) \text{ cm/s}, \tag{58}$$

where $q_0$ is the roton minimum wave vector; this result agreed with the experimental results of Keshishev *et al.* (1981) if $\xi_A \simeq 0.3$ to 0.4. However, they also pointed out an important difficulty, which remained as a puzzle for several years (Castaing, 1984; Edwards *et al.*, 1990). As shown in Fig. 43, all experiments (Castaing *et al.*, 1980; Keshishev *et al.*, 1981; Bodensohn *et al.*, 1986) agreed with each other and showed a unique exponential increase of the growth resistance over the whole temperature range from 0.45 to 1.7 K.

Bodensohn *et al.* (1986) gave a simple law for the growth resistance:

$$k^{-1} = 2.4 \times 10^5 \exp(-7.8/T) \text{ cm/s}, \tag{59}$$

which was close to Eq. (58). But the roton-roton mean free path was certainly smaller than the wavelength of

[4] See Deutscher, 2005.

Keshishev's waves; it was also smaller than the size of the experimental cell used by Castaing *et al.* (1980), who measured the temperature dependence of the sound transmission (see below). As for Bodensohn *et al.* (1986), they measured the relaxation of a surface deformation by charging the liquid-solid interface and applying an adjustable electric field to it. The size of their experimental cell was much larger than the roton mean free path. If rotons had been in a hydrodynamic regime, they would have moved with the interface, and the growth resistance would have been much smaller.

Castaing (1984) first proposed that rotons were moving with the interface, but were scattered by the lattice potential, which was immobile with respect to the cell walls. This possibility was considered more generally by Korshunov (1986a, 1986b). Castaing also questioned the validity of the assumption by Andreev and Knizhnik (1982) of a fraction $\xi_A=1$ of Andreev reflections of rotons. Later, Edwards *et al.* (1990) proposed that, at the atomic scale of rotons, rough helium surfaces could have a large density of microscopic steps with moving kinks (note that these microscopic steps should not be confused with the macroscopic steps considered in Sec. III). Even if the roton distribution moved with the interface, the kinks would move with respect to it. Edwards *et al.* developed a theory for the roton-kink collisions, in which the kink mass $m_k$ was an important parameter. This mass was introduced by Kosevich and Kosevich (1981) as a consequence of the flow of superfluid towards the kink, which acts as a moving sink. The existence of a kink mass implies the existence of a surface inertia $m_I$, which is proportional to $m_k$.

Furthermore, as explained by Puech and Castaing (1982), the surface inertia has a direct effect on the transmission coefficient $\tau$ of phonons through the liquid-solid interface and consequently on its Kapitza resistance (see below). Edwards *et al.* (1991) carefully discussed the boundary conditions that have been introduced in the series of articles by Nozières and Wolf (1988) and Wolf and Nozières (1988) in order to calculate the phonon transmission. From a fit of both $\tau$ and the roton contribution to the growth resistance $k_{\rm rot}^{-1}$, Edwards *et al.* (1990) obtained a kink mass

$$m_k^0 = 0.002 m_4 \tag{60}$$

at $T=0$, in agreement with the prediction $m_k \simeq m_4(v_L/v_C-1)^2/2\pi$ of Kosevich and Kosevich (1981). They also found that this mass increased with temperature (see Fig. 44). This time, they found good agreement with the measurements of $k_{\rm rot}^{-1}$ if the fraction $\xi_A$ was nearly zero. Their latest theoretical result was

$$k_{\rm rot}^{-1} = (0.25 + 0.3T)(2.36 \times 10^5)\exp(-7.21/T) \tag{61}$$

in cm/s again and in a good agreement with all available experimental results (see Fig. 43). As explained in the next section, the value of the surface inertia was confirmed by the series of experiments done by Poitrenaud and her group.

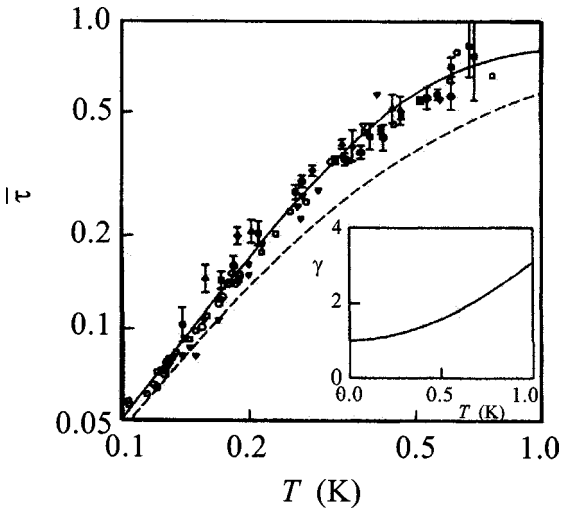


FIG. 44. Transmission coefficient of thermal phonons through the liquid-solid interface of $^4$He: filled symbols, measurements of Wolf, Edwards, and Balibar (1983); open symbols, measurements of Puech and Castaing (1982); dashed curve, calculation of Edwards *et al.* (1990) using a temperature-independent surface inertia $m_I^0=2.1\times10^{-10}$ g/cm$^3$. A better fit (solid curve) was obtained with a temperature-dependent inertia $m_I=\gamma m_I^0$, where $\gamma=m_k(T)/m_k^0$ is the kink mass ratio shown in the inset. From Edwards *et al.*, 1990.

Andreev and Knizhnik (1982) had assumed that $\xi_A=1$ after considering that rotons were reflected by a plane rigid boundary. In their model, Edwards *et al.* (1990) considered a rough surface with a large density of moving kinks, a rather different picture which implied $\xi_A\simeq0$. Note finally that all these comparisons use the theoretical value of the isothermal growth coefficient $k_T$, but experiments only measure some approximation of $k_T$. For example, Balibar, Edwards, and Saam (1991) explained that, in the experiment by Bodensohn *et al.* (1986), there should be a small temperature difference across the interface, so that, in fact, an effective growth resistance

$$k_{\rm eff}^{-1} = k_T^{-1} + \frac{\rho_C R_K}{T}(TS_C)^2 \tag{62}$$

was measured, where $S_C$ is the crystal entropy per unit mass. Consequently a small negative correction should be applied to their measurements of $k_T^{-1}$, from −20% at 0.9 K to −2% at 1.4 K.

#### 4. Sound transmission and surface inertia

As we now understand, one cannot calculate the growth coefficient or the Kapitza resistance without calculating the sound or phonon transmission. Castaing and Nozières (1980) had first noticed that the high mobility of the liquid-solid interface of $^4$He strongly affects the transmission of sound through it. They showed that the transmission probability $\tau$ from the liquid to the solid is related to the interface mobility $k$ by

$$\tau^{-1} = \frac{Z_C + Z_L}{2Z_C} + \frac{kZ_L\rho_C}{2}\left(\frac{\rho_C - \rho_L}{\rho_C\rho_L}\right)^2, \tag{63}$$

where the quantities $Z_C$ and $Z_L$ are the acoustic impedances in the crystal and in the liquid, respectively. If the liquid-solid interface were immobile, the transmission probability would be equal to the usual impedance ratio $2Z_C/(Z_C+Z_L)$. In contrast, if the interface were infinitely mobile, it would move in phase with any acoustic wave or incident phonon, so that there would be no difference in chemical potential across it. The pressure in the solid would always be equal to the equilibrium melting pressure, and no sound would be transmitted. In reality, we have seen above that the mobility $k$ is limited by interactions with the thermal excitations (phonons and rotons), so that $\tau$ depends on temperature.

Furthermore, Marchenko and Parshin (1980b) showed that, if the incidence angle of the incoming phonon is nonzero, a capillary wave is produced at the interface, which couples to the phonons in the solid. As a result, they found the probability $\tau$ to be proportional to the square of the phonon frequency, and consequently the Kapitza resistance to be proportional to $T^{-5}$ instead of $T^{-3}$, the usual behavior. Eventually, as we saw above, the interface has a nonzero inertia so that it cannot respond immediately to any perturbation. This was first predicted by Kosevich and Kosevich (1981), who proposed a hydrodynamic origin for this inertia. They found that the dispersion relation of crystallization waves departs from Eq. (38) when their wavelength is comparable to the average distance between steps. Puech and Castaing (1982) later explained that the local rearrangement of atoms passing from the liquid to the solid would induce the existence of a surface inertia even if $\rho_C$ were equal to $\rho_L$.

The surface inertia was measured by Poitrenaud and her group (Poitrenaud and Legros, 1989; Poitrenaud *et al.*, 1991; Amrit *et al.*, 1995a, 1995b). They measured the transmission of sound as a function of frequency (in the range from 10 to 70 MHz), crystal orientation, and temperature. Figure 45 shows that at low enough temperature the surface inertia limits the mobility of rough surfaces so that the transmission of sound is larger at higher frequency. They wrote the acoustic impedance $\zeta_I$ for the interface as

$$\zeta_I = \left(\frac{\rho_C\rho_L}{\rho_C - \rho_L}\right)^2\left[\frac{1}{\rho_C k} + i\frac{\omega m_I}{\rho_L\rho_C}\right], \tag{64}$$

where $m_I$ is the surface inertia or dynamic mass per unit area. The real part of the impedance is due to the finite value of $k$, while the imaginary term originates in the inertia $m_I$. This inertia was related to the kink mass $m_k(T)$ by Edwards *et al.* (1990):

$$m_I = \frac{m_k n_k}{\sigma_C n_s \zeta}. \tag{65}$$

In the above equation, the cross section $\sigma_C$ is related to the surface of a kink $\sigma$ by $\sigma_C = \sigma\rho_L/\rho_C$, $n_s$ is the density of steps at the crystal surface, and $n_k$ is the density of kinks on the steps; as for $\zeta$, it is a dimensionless roughness factor which depends on the density difference between the plus and minus kinks on steps [$\zeta = \sigma_C\langle(n_+ - n_-)^2\rangle$]. Amrit *et al.* (1995b) found good agreement between their measurements and the theory of Edwards *et al.* (1990), as shown in Fig. 46. According to their latest estimates, the inertia of rough surfaces is

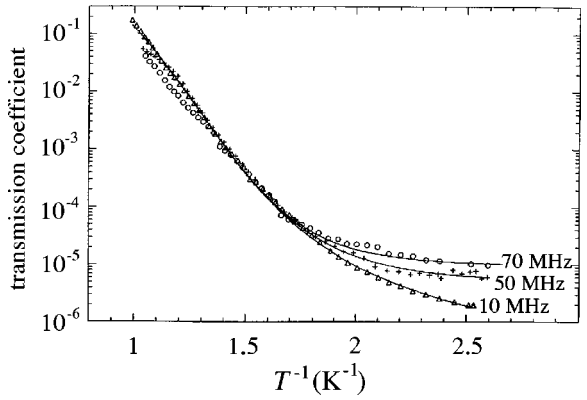


FIG. 45. Transmission coefficient of acoustic waves in $^4$He as a function of the inverse temperature $1/T$, at three different frequencies. These measurements by Amrit *et al.* (1995b) show that, at low enough temperature, the mobility of rough crystal surfaces is limited by the surface inertia, so that the transmission is larger at higher frequency. From Amrit *et al.*, 1995b.

$$m_I = (2.4 \pm 0.5) \times 10^{-10}\ \mathrm{g/cm^2}, \tag{66}$$

increasing by more than a factor of 10 as the surface orientation tends towards the direction of a facet.

#### 5. Heat flow: The Kapitza resistance

The Kapitza resistance $R_K$ can be expressed as

$$R_K = \frac{3}{4}\rho_L S_{\phi L} c_L \bar{\tau}, \tag{67}$$

where $\bar{\tau}$ is the average probability of phonon transmission from the liquid into the solid, and $S_{\phi L}$ is the phonon part of the liquid entropy (Maris and Huber, 1982). There have been three series of measurements on the Kapitza resistance. The first was made by Huber and Maris (1981, 1982). They used a heat-pulse technique at temperatures between 0.1 and 0.4 K and found significant variations from crystal to crystal, which they attributed to unknown changes in crystal orientation. Their results could be represented as $5\times10^8 T^5 < R_K^{-1} < 10^9 T^5$ erg s$^{-1}$ K$^{-1}$ cm$^{-2}$. This indicated a transmission probability for thermal phonons that was about $7T^2$, larger than that predicted (about $3T^2$) by the capillary theory of Marchenko and Parshin (1980b).

Similarly, Puech and Castaing (1982) and Puech *et al.* (1982) found that Marchenko's capillary effect was not sufficient to explain their experimental measurements on the Kapitza resistance, so that consideration of a surface inertia was necessary. For their final fit, shown in Fig. 44, Edwards *et al.* (1990) considered both the results of Puech *et al.* (1982) and the later results of Wolf, Ed-

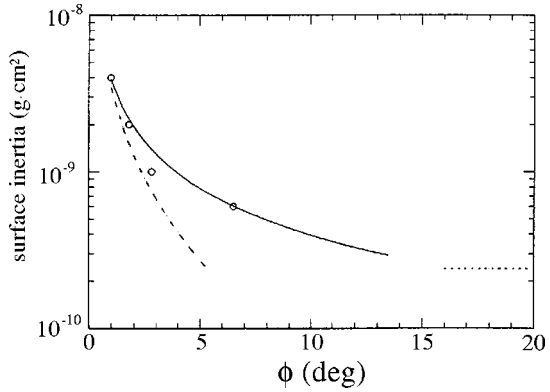


FIG. 46. Surface inertia of $^4$He crystals as deduced by Amrit *et al.* (1995b) from their sound transmission measurements. This graph shows the angular dependence of the inertia, which was found to be in a good agreement with the theory of Edwards *et al.* (1990) (solid line). The dashed line represents the theory of Kosevich and Kosevich (1981) in the limit of well-separated steps, that is, for a small tilt angle $\phi$. The horizontal dotted line indicates the surface inertia of rough surfaces at large $\phi$. From Amrit *et al.*, 1995b.

wards, and Balibar (1983). The experiment of Wolf *et al.* was primarily designed to measure the Onsager cross coefficient (see below). Its results for the transmission probability were summarized as $\tau=5.4T^2$ for rough surfaces. Wolf *et al.* found a somewhat larger value for a crystal surface close to the [0001] direction. As shown in Fig. 44, these results were well interpreted in terms of the calculated surface inertia (Edwards *et al.*, 1990). In summary, the Kapitza resistance of the liquid-solid interface in $^4$He is anomalous in the sense that its limiting behavior at low temperature is proportional to $T^5$ instead of $T^3$ for immobile surfaces. The coefficient of the $T^5$ law is well understood as being mainly due to the limitation of mobility by the surface inertia.

### 6. The Onsager cross coefficient

Wolf, Edwards, and Balibar (1983) designed an experiment to measure the Onsager cross coefficient $B$ from the difference in chemical potential $\delta\mu$ induced across the liquid-solid interface of $^4$He by a heat current flowing through it. For this, they had to know the changes in pressure and temperature on both sides of the interface. They obtained these by looking at level changes of the interfaces in a transparent box divided into two sides (see Fig. 47). The heat current was generated at the bottom of the box. It flowed up through the left side into the liquid. The right side was closed by a porous plug, which allowed a superfluid current to flow, and hence thermodynamic equilibrium to be reached, but no heat flow. The height changes were related to changes in pressure from the hydrostatic equilibrium in the liquid. The level on the right was different from that on the left because of a heat current flowing only through the left side.

From the difference in temperature, the Kapitza resistance $R_K$ was measured, as discussed above. From dimensional considerations, Bowley and Edwards (1983) expected the quantity $B\rho_C c_L T$ to be of order 1. They predicted a slight dependence on the mobility of the interface, which varied depending on whether the phonons were ballistic in both the liquid and the solid, or only in the liquid. For ballistic phonons on both sides, they predicted $B\rho_C c_L T=-1.6$ if the surface was immobile, and $-1.5$ if it was infinitely mobile; if phonons were ballistic in the liquid only, they predicted a smaller coefficient, $-0.7$ and $-0.6$, respectively, in the two above situations.

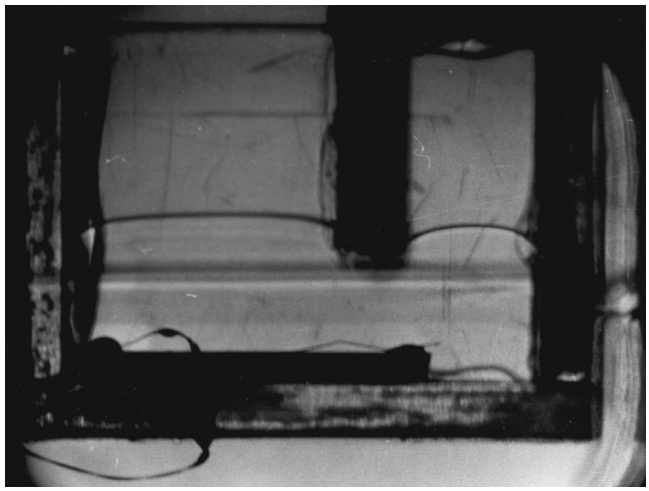

FIG. 47. Setup used by Wolf, Edwards, and Balibar (1983) to measure the Onsager cross coefficient $B$ and the Kapitza resistance $R_K$ at the liquid-solid interface of $^4$He. A heat current is applied at the bottom of a transparent box. It flows through the left side, which is open; the right side is closed by a superleak, which ensures thermodynamic equilibrium but does not allow any heat flow. The double horizontal gray line across the whole box is the liquid-solid interface outside the box. In this case ($J_E=0.503$ mW/cm$^2$ and $T=0.27$ K) it was about 2 mm below the levels inside the box. From the level changes on each side of the box, the pressure and the temperature of the crystal were measured, and $R_K$ and $B$ deduced. From Wolf, Edwards, and Balibar, 1983.

Wolf's experimental result was $-1.1\pm0.4$ in the temperature interval from 0.2 to 0.6 K, where the crystal phonons should have been in a hydrodynamic regime. This was considered to be in qualitative agreement with the predictions. A more precise analysis would be useful, but no other experimental measurement has been attempted.

### 7. Mobility of vicinal surfaces

When studying crystallization waves in $^4$He at vicinal surfaces, Rolley, Guthmann, *et al.* (1995) measured their damping and obtained the mobility of vicinal surfaces as a function of temperature and tilt angle. Figure 48 shows that the proximity of the $c$ facet has a strong influence on the growth rate. Furthermore, this influence extends over a much larger angular domain than for the surface stiffness, at least 15° compared with about 2.5°. For intermediate orientations ($2°<\phi<8°$), the temperature

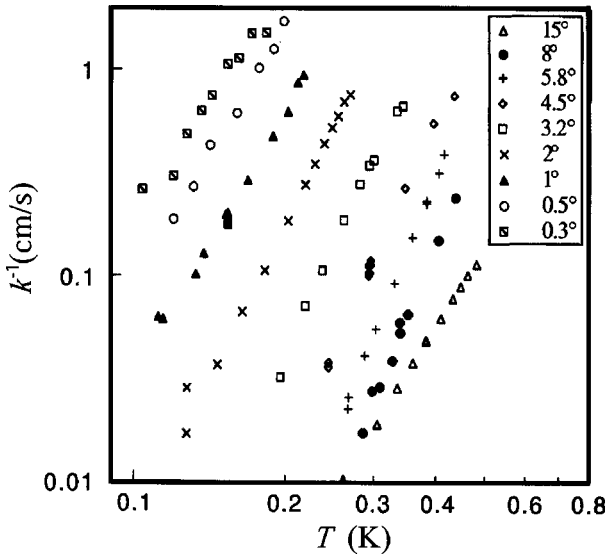


FIG. 48. Growth resistance of the vicinal surfaces of $^4$He crystals as a function of temperature and orientation, as measured by Rolley, Guthmann, *et al.* (1995); the angles measure a tilt with respect to the *c* facet. From Rolley, Guthmann, *et al.*, 1995.

dependence was also found to be closer to $T^6$ rather than $T^4$. Andreeva *et al.* had found qualitatively similar results in 1987–1992. This was surprising because Nozières and Uwaha (1987) had predicted a $T^3$ variation for the stepped surfaces.

In their analysis, Rolley, Guthmann, *et al.* (1995) explained all these results in terms of a crossover from coherent to incoherent scattering of phonons by steps. This scattering depends on the relative magnitudes of the step density $n_s$ and the phonon wave vector $q_{\rm ph}$. Phonons are scattered incoherently, that is, independently by the individual steps, if their wavelength is smaller than the typical spacing between steps, which would mean that the ratio $n_s/q_{\rm ph}$ is less than 1. A typical phonon wave vector is $q_{\rm ph}=2.7k_BT/\hbar c$ with $c\simeq 400$ m/s,

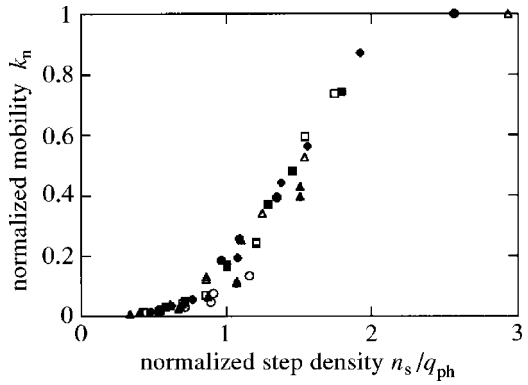


FIG. 49. Mobility of the vicinal surfaces of $^4$He crystals. Once the mobility of the vicinal surfaces is normalized by that of rough surfaces and plotted against $n_s/q_{\rm ph}$, the step density divided by the phonon wave vector, all measurements collapse on a single curve. From Rolley, Guthmann, *et al.*, 1995.

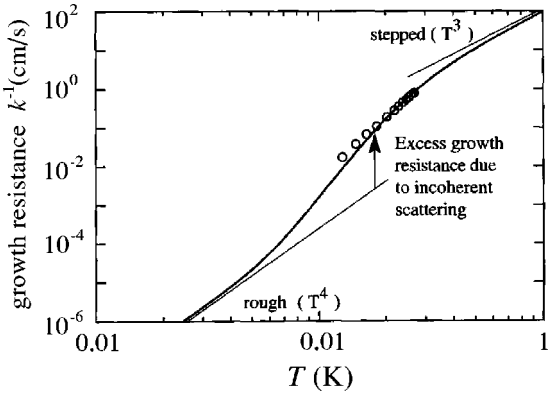


FIG. 50. Temperature dependence of the growth resistance of $^4$He crystals, for a vicinal surface tilted by 2° with respect to the *c* facet. In the crossover, which corresponds to the phonon wavelength's being comparable to the interstep distance, the growth resistance increases faster than $T^4$ (coherent scattering for rough surfaces or stepped surfaces at low temperature) and $T^3$ (incoherent scattering for stepped surfaces at higher temperature). From Rolley, Guthmann, *et al.*, 1995.

a typical sound velocity. Rolley *et al.* normalized the mobility $k$ of the vicinal surface by the typical mobility of a rough surface $k_{\rm rough}$ and plotted this normalized mobility as a function of $n_s/q_{\rm ph}$. Figure 49 shows that their results collapsed on a universal curve, in strong support of their initial idea.

Nozières and Uwaha (1987) had calculated $k^{-1}$ in the incoherent regime and found a $T^3$ law. In this incoherent regime the growth resistance is larger than in the coherent regime, because there is an additional channel for momentum exchange: in addition to the perpendicular momentum, the parallel component is not conserved during collision. Nozières and Uwaha also calculated an expression for the crossover to the coherent regime, which is $T^4$ as for rough surfaces, in which the average distance between steps is always smaller than the typical phonon wavelength. Rolley, Guthmann, *et al.* (1995) simplified Nozières's expression and found very good agreement with all their experimental results. At low temperature, the phonon wavelength is larger than the interstep distance, so that the scattering is coherent as for rough surfaces ($T^4$). As $T$ increases, incoherent scattering begins and the growth resistance increases even faster until it reaches a $T^3$ behavior (see Fig. 50). The crossover angle depends on temperature, of course, and it is larger than the crossover angle for the stiffness component $\gamma_\parallel$ because it has a different criterion, namely, $n_s/q_{\rm ph}\approx 1$ instead of $l/3w\approx 1$.

### 8. Effect of $^3$He impurities

The effect of $^3$He impurities on the surface properties of $^4$He crystals looks far from being completely understood, despite several attempts. $^3$He impurities affect both static and dynamic properties, which in many ways depend on both the temperature and the $^3$He concentration.

Landau *et al.* (1980) showed that $^3$He impurities changed crystal shapes. They later claimed that the roughening temperature was lowered by 20% when about 1 ppm of $^3$He was added (Carmi *et al.*, 1985, 1989). They attributed this effect to a lowering of the surface tension by 15% (at 1 K), which was caused by $^3$He adsorption but which was independent of the $^3$He concentration in the range from 0.8 to 150 ppm. They estimated the binding energy of $^3$He atoms to be about 10 K, but this looks rather large compared to 2.9 K, the theoretical estimate of Treiner (1993) for the binding energy on a solid substrate.

The binding energy was more directly estimated by Wang and Agnolet (1992b), who measured the surface stiffness of $^4$He crystals around 1 K for $^3$He concentrations ranging from 4.5 to 50 ppb. They found it to be 3.4 K. Further evidence of the existence of bound states for $^3$He atoms at the liquid-solid interface of $^4$He was obtained by Rolley, Guthmann, *et al.* (1995), who compared ordinary $^4$He containing 130 ppb of $^3$He with ultrapure $^4$He containing only 0.4 ppb. They found a change in the surface energy $\delta\alpha \approx -15\times10^{-3}$ erg/cm$^2$ at 0.2 K and nearly no change above 0.4 K. They also found that the step energy was lowered from $\beta/d = (14\pm0.5)\times10^{-3}$ erg/cm$^2$ in ultrapure $^4$He to $(11\pm1)\times10^{-3}$ erg/cm$^2$ in normal-purity $^4$He. In this experiment, most $^3$He impurities were probably bound to vortices in the heat exchangers and the exact concentration in the bulk liquid was not precisely known. The estimate of Rolley, Guthmann, *et al.* (1995) for the binding energy was 4.3 K at a rough surface, 10 mK more on a step. They also estimated the maximum amount of adsorbed impurities as 0.4 atomic layer. Clearly, these adsorption phenomena need more study.

The influence of $^3$He impurities on the growth resistance of $^4$He crystals is not completely clear either. After the early estimate of Castaing *et al.* (1982), Bowley and Edwards (1983) calculated the contribution to $k^{-1}$ of the scattering of $^3$He atoms by the moving interface. This was done for ballistic $^3$He atoms forming either a degenerate or a nondegenerate Fermi gas. Wang and Agnolet (1992b, 1994) found that the growth resistance increased exponentially in the region $0.2<T<0.3$ K for rather small concentrations (12–158 ppb). This effect looked much stronger than what Bowley and Edwards had calculated. It was attributed to the diffusion of $^3$He atoms in a $^4$He crystal. For this mechanism, Kagan and Kosevich (1986) calculated a growth resistance

$$k_{\rm diff}^{-1} = \frac{k_B T X_C}{m_4\sqrt{\omega D_C}}, \tag{68}$$

where $X_C$ is the concentration of $^3$He impurities in a solid and $D_C$ is their diffusion coefficient, $\omega$ is the frequency of the waves, and $m_4$ the mass of a $^4$He atom. From the phase diagram of helium mixtures (see Edwards and Balibar, 1989), $X_C$ was known to be related to the concentration $X_L$ in the liquid by

$$\frac{X_C}{X_L} = 2\left(\frac{1.696}{T}\right)^{3/2}\exp(-1.36/T), \tag{69}$$

and good agreement was found with the data.

Another series of measurements was performed by Suzuki *et al.* (1997) around 0.8 K and with higher concentrations (5 and 10 ppm). Suzuki *et al.* found that the growth resistance was larger by a factor of about 2 or 3 than in pure $^4$He, with no strong dependence on either the concentration or the temperature. Their results contradicted predictions by Burmistrov and Dubovskii (1993) who claimed that the additional dissipation was due to the flow of $^3$He in the liquid, in front of the moving interface, so that the growth velocity should strongly depend on $^3$He concentration and should be a nonlinear function of $\delta\mu$. Instead, Suzuki *et al.* proposed that the additional growth resistance was due to the flow of heat in the solid, so that the effective growth resistance was

$$k_{\rm eff}^{-1} = k_T^{-1} + \frac{\rho_C R_K}{T}(TS_L)^2. \tag{70}$$

This equation is similar to Eq. (62) but it contains the liquid entropy instead of the crystal entropy. Suzuki *et al.* justified this by claiming that, in the presence of 10 ppm $^3$He impurities, the thermal conductivity of the superfluid $^4$He was so much reduced that the heat could flow more easily in the crystal. This also deserves a more systematic study.

Eventually, the effect of $^3$He impurities on the Kapitza resistance was also investigated. Graf *et al.* (1984, 1985) studied mixtures with concentrations $X_3 = 110$, 190, 470, and 1500 ppm. By carefully fitting the time evolution of the solid and liquid temperatures after a heat pulse was applied in the crystal, they could measure three different quantities, namely, the heat conduction $\sigma_{CL}$ from the solid to the phonons in liquid $^4$He, the conduction $\sigma_{C3}$ to the $^3$He impurities, and the coupling $\Gamma_{L3}$ between the $^3$He and the phonons in liquid $^4$He. Their results confirmed their prediction of a direct coupling of crystal phonons with $^3$He impurities. Graf *et al.* explained that, if the surface is rough, and consequently mobile, a phonon incident from the solid side produces a large motion of the interface, which acts as a piston on the $^3$He atoms and directly transfers energy to them. Within this model, they estimated the additional thermal conductivity as

$$\sigma_{C3} = 9.4\times10^9 T^{7/2} X_3 \ {\rm erg\ s^{-1}\ cm^{-2}\ K^{-1}}. \tag{71}$$

With no adjustable parameter, this agreed with their experimental results. If, due to impurities, the liquid-solid interface had been smooth instead of rough, their theory predicted that $\sigma_{C3}$ would have the same temperature variation but with a magnitude of 100 times smaller. They also verified that $\sigma_{CL}$ varied proportionally to $T^5$, as expected for rough surfaces.

### 9. High-frequency and high-speed limitations

In the derivation of the spectrum of crystallization waves (Sec. IV.A), the compressibility of the liquid and

the elastic properties of the solid were neglected. However, other waves can propagate at the liquid-solid interface: in elastic Rayleigh waves, which involve no mass transfer between the liquid and the solid, the restoring force is provided by the elasticity of the solid. At long wavelengths, capillary effects are negligible and the spectrum of Rayleigh waves is exactly as if the solid were in contact with a vacuum (Marchenko and Parshin, 1980b). Indeed, as mentioned above, due to the very high mobility of the interface, the crystal oscillates at a constant chemical potential at the interface, hence at a constant pressure, exactly as if it were a crystal-vacuum interface. Capillary effects lead to a velocity dispersion but not to damping, since the sound velocity in liquid helium is larger than the velocity of transverse waves in solid helium. In contrast, the velocity of the surface acoustic waves on the helium facets (without melting) essentially depends on the properties of the liquid even in the long-wavelength limit.

Uwaha and Baym (1982) calculated the spectrum and the damping of surface waves at high frequency, when the two types of waves have comparable velocities and couple to each other. This happens for $q > 10^6$ cm$^{-1}$, which is still much less than the atomic wave vectors. For even shorter wavelengths the spectrum of these mixed waves becomes a linear one with a velocity slightly smaller than for Rayleigh waves without melting. The damping due to the growth resistance decreases with increasing $q$. An interesting feature is that in the limit of large $q$ the surface-tension term dominates in the boundary conditions. As a result, the elastic displacement of the crystal surface and the displacement due to crystallization almost compensate each other, and the total displacement of the surface becomes small compared to those in the liquid and solid.

In these calculations, as in calculations of the anomalous Kapitza resistance (Marchenko and Parshin, 1980b; Maris and Huber, 1982; Puech and Castaing, 1982), it was assumed that the crystallization and melting processes remain practically dissipationless even at very high frequencies, up to $\omega \sim 10^{10}$–$10^{11}$ rad/s. This poses an important question concerning possible high-speed and high-frequency limitations of the very concept of nondissipative crystallization. According to Andreev and Parshin (1978), such a limit is due to the finite probability of quantum tunneling of an individual helium atom across the liquid-solid interface, $\Omega \sim 10^{11}$–$10^{12}$ rad/s. As we have seen, experimental data on the Kapitza resistance in $^4$He agree well with the theory at temperatures up to at least 1 K and thus confirm that $\Omega$ is high compared to the characteristic frequency of thermal phonons at 1 K. Moreover, the analysis of Edwards *et al.* (1990) showed that the best fit was obtained with the hypothesis of very light quantum kinks: the width of their energy band was estimated to be 30 K! This value exceeds even the Debye temperature, which means that the concept of nondissipative crystallization has no specific frequency limitations in application to real helium.

As for the limitations on growth speed, the situation is different. Graf and Maris (1987) measured the transmission of high-amplitude sound waves across a rough superfluid-solid interface of $^4$He at temperatures from 0.1 to 1 K. They used these results to determine the growth coefficient $k$ as a function of the growth velocity $v$. They found that $k$ decreases rapidly as $v$ approaches a critical velocity $v_c$, which was found to be in the range from 1600 to 5100 cm/s for different samples. Surprisingly, this value is about ten times lower than the sound velocity. In terms of the above discussed $\Omega$, Graf's result would mean that $\Omega \approx v_c/a \approx 10^{11}$ rad/s; the width of the kink's energy band would be much smaller than 60 K.

Edwards *et al.* (1990) suggested the following mechanism for the decrease of the growth coefficient at high growth velocities: the kinks are accelerated by the driving force, so that their energy and density at the crystal surface deviate from the equilibrium values. This tendency is counteracted by thermal fluctuations and heat exchange with the surroundings, which result in additional dissipation, hence in a decrease of the growth coefficient. The following simple argument shows that this mechanism may be very important in the experiments of Graf and Maris, who used 2.15 MHz acoustic waves with pressure amplitudes up to 0.4 bar. Let us estimate the change in momentum of an individual kink $\delta q$ as a subject to a driving force $f = a^2(\rho_C - \rho_L)/\rho_L \delta P$: $\delta q \sim f/\omega = 3 \times 10^{-18}$ g cm/s. This is much higher than the atomic momentum $q \approx \pi\hbar/a = 10^{-19}$ g cm/s, so that the crystal surface should be very far from equilibrium unless an effective relaxation mechanism intervenes.

Of course, for a complete understanding of all the processes involved in the very rapid growth of helium crystals, more experiments are needed, in particular systematic studies with different surface orientations, including vicinal surfaces. Note also that the maximum growth velocity reached by Graf and Maris (1987), about 10 m/s, was exceeded in the experiments of Balibar *et al.* (2003). Using high-intensity ultrasound waves with a pressure amplitude up to 20 bar, they observed small crystals growing at 100 m/s, close to the sound velocity.

### D. The case of $^3$He

#### 1. High temperatures

The growth dynamics of $^3$He crystals is very different from that of $^4$He crystals. Above $T_c = 2.5$ mK, liquid $^3$He is a viscous Fermi liquid with low thermal conductivity. Furthermore, the latent heat of crystallization is large, so that the growth dynamics is limited by a large bulk resistance, as in classical systems. The surface resistance to growth could only be measured near $T_{\min} = 320$ mK, the minimum in the melting curve where the latent heat vanishes. As we shall see, this surface resistance is much larger in $^3$He than in $^4$He, because the excitations in the liquid are Fermi quasiparticles with a large momentum instead of phonons or rotons.

A rough theoretical estimate of the intrinsic growth coefficient $k$ in $^3$He was first given by Andreev and

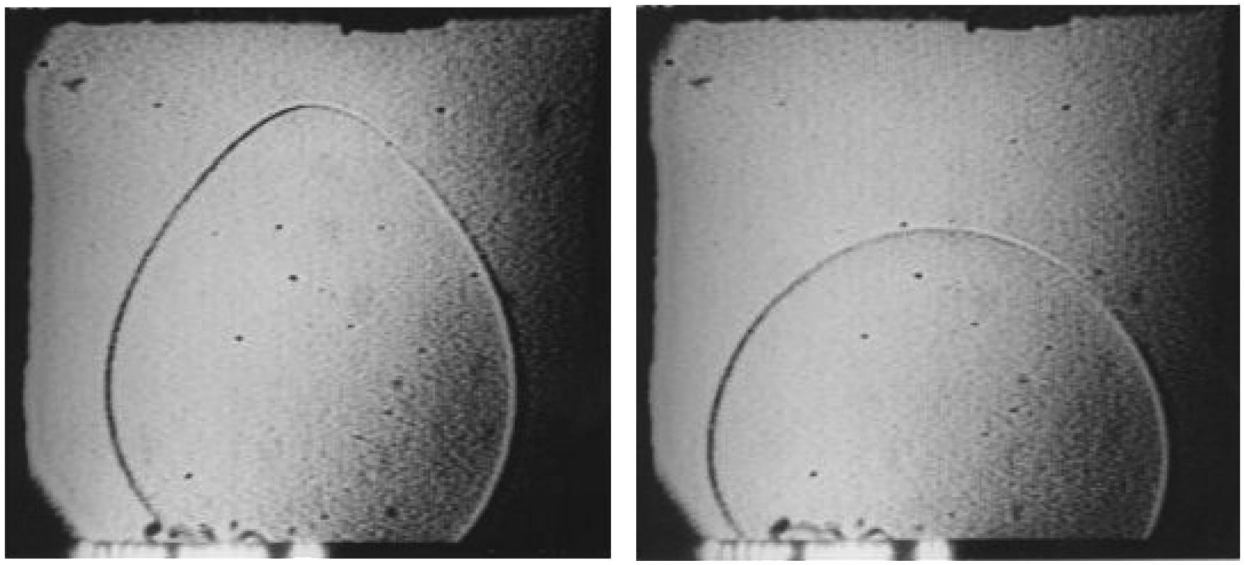

FIG. 51. $^3$He crystal relaxing towards its equilibrium shape. The time delay between the two photographs is 10 s. The temperature is close to $T_{\min}=320$ mK. From Graner, 1991.

Parshin (1978). Assuming that the dissipation comes from the collisions of Fermi quasiparticles in the liquid with the moving liquid-solid interface, they obtained $k \sim m_3/p_F$, the mass of a $^3$He atom divided by the Fermi momentum. They had assumed that the correlation time of the surface fluctuations is short compared to the average duration of an individual collision. However, both times should be comparable to the inverse exchange frequency in the liquid. In the opposite situation, the quasiparticles should interact with the crystal lattice rather than with the moving interface; with this assumption, Puech *et al.* (1986a) obtained

$$k = (3\tau_s/4)(m_3/p_F)[\rho_C\rho_L/(\rho_C - \rho_L)^2], \tag{72}$$

where $\tau_s$ is the sticking probability of quasiparticles at the crystal surface. Due to its large density factor, this equation predicts that the mobility is larger by about two orders of magnitude than first predicted by Andreev and Parshin (1978).

Accurate measurements were performed by Graner *et al.* (1989); they confirmed Puech's model and gave some information on other kinetic coefficients. Graner *et al.* recorded the shape relaxation of crystals near $T_{\min}$. The crystals evolved at a constant volume so that no heat had to flow into or out of the cell, even at temperatures slightly away from $T_{\min}$, where the latent heat was not strictly zero. Heat had to be transferred from the melting top of the crystal to its growing sides (see Fig. 51). In their analysis, they followed Puech *et al.* (1986a) and assumed that most of this latent heat was liberated on the liquid side, which meant $-B/C \approx TS_C$. This was justified by Puech *et al.* (1986a) and Graner *et al.* (1990) on the grounds that quasiparticles sticking to the solid exchange energy more easily with other quasiparticles in the liquid than with phonons in the solid, which have rather long wavelengths. Furthermore, since $Z_C \ll R_K \ll Z_L$, they assumed that the latent heat $L=T(S_L-S_C)$ mainly flowed through the interface and through the crystal, so that the effective growth resistance was

$$k_{\text{eff}}^{-1} = k_T^{-1} + \frac{R_K\rho_C}{T}L^2. \tag{73}$$

A fit with their experimental measurements (see Fig. 52) led Balibar, Edwards, and Saam (1991), and Graner *et al.* (1989, 1990) to the values

$$k_T = 0.18 \pm 0.04 \text{ s/m}, \tag{74}$$

which agreed with Eq. (72) if the sticking coefficient $\tau_s$ was about 0.1 at 320 mK, and

$$R_K(T = 320 \text{ mK}) = 1.3 \pm 0.3 \text{ cm}^2 \text{ K/W}. \tag{75}$$

Puech *et al.* (1986a) presented qualitative arguments that predicted the sticking probability $\tau_s$ to be proportional to $T$ in the low-temperature limit. This would be interesting to study. As for $R_K$, Graner *et al.* (1990) pro-

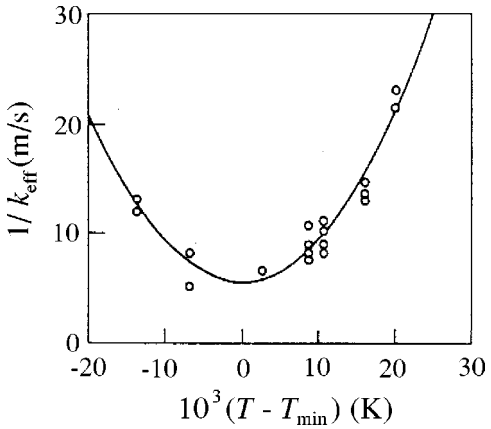


FIG. 52. Inverse mobility of the liquid-solid interface of $^3$He near the melting curve minimum at 320 mK. The solid line is a fit with Eq. (73). From Graner *et al.*, 1989.

posed that its relatively small value arises from the coupling between transverse phonons in the crystal and transverse zero sound in the Fermi liquid. Using a more direct method, Amrit and Bossy (1990) measured the Kapitza resistance over a much wider temperature domain ($50 < T < 200$ mK); they found that

$$R_K T^3 = 0.03 \text{ cm}^2 \text{ K}^4/\text{W}, \tag{76}$$

in a good agreement with the Graner's measurements (Graner *et al.*, 1989) and theoretical estimate (Graner *et al.*, 1990). They also performed careful pressure measurements when melting a crystal in a tube and obtained $k = 0.18 \pm 0.02$ s/m, confirming Graner's results (Amrit and Bossy, 1993).

In their discussion of the whole picture, Balibar, Edwards, and Saam (1991) emphasized the difference between $^3$He and $^4$He. In $^3$He, because of the low thermal conductivity of the liquid, an isothermal experiment is very hard to achieve, except when the latent heat is zero or at millikelvin temperatures where liquid $^3$He is superfluid. Furthermore, the adiabatic coefficient $k_E$ is very different from $k_T$, the isothermal one, because the quantity $(1 - B^2/AC)$ is very small ($\approx 3 \times 10^{-4}$ at 320 mK). In contrast, in $^4$He, $B^2/AC \ll 1$ so that $k_T \approx k_E$. In practice, the typical relaxation time of $^3$He crystals near 320 mK is comparable to that of $^4$He crystals at 1.2 K, but at 0.1 K, it is about three days in $^3$He and 3 $\mu$s for rough surfaces in $^4$He. This difference is due only to thermal effects. One can estimate the effect of viscosity in liquid $^3$He as

$$1/k \sim \frac{\nu}{R}\left(\frac{\rho_C - \rho_L}{\rho_L}\right)^2, \tag{77}$$

where $R$ is the characteristic size of a crystal and $\nu$ the kinematic viscosity of the liquid. This effect is relevant but small in the hydrodynamic regime, where the mean free path of the Fermi quasiparticles is small compared with the crystal size.

### 2. Low temperatures

Below $T_c$ liquid $^3$He becomes superfluid, but this transition does not result in an immediate change of the growth kinetics of crystals: due to the extremely high viscosity of the normal component, superfluid convection does not help in the heat transfer, the heat conductivity of the solid is very low, but the latent heat is still very large until the temperature is less than the magnetic ordering temperature $T_N$. As shown in Fig. 53 the mobility of rough surfaces of $^3$He crystals increases very fast below $T_N$. This figure shows data obtained by different authors at temperatures down to 0.55 mK (Nomura *et al.*, 1994; Akimoto *et al.*, 1998; Kawaguchi *et al.*, 2002; Tsepelin *et al.*, 2002a). It is likely that, even at the lowest temperature, the bulk dissipation still dominates the growth resistance (Jochemsen, 2002).

In all these experiments there was a net crystal growth, so that some latent heat had to be evacuated through the sintered heat exchangers to the thermal bath. Furthermore, the Kapitza resistance $R_K$ was small compared to the liquid thermal impedance (Feng *et al.*, 1993), and it could be neglected even if all the latent heat was liberated in the solid, as expected from arguments similar to those used above (in the very-low-temperature limit, one can neglect quasiparticles and magnons in the liquid, and the only remaining degrees of freedom are those of magnons in the solid). One can thus write

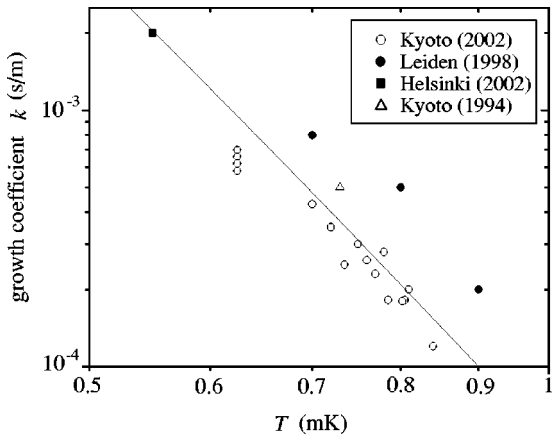


FIG. 53. Measurements of the growth rates of $^3$He crystals below $T_N = 0.93$ mK, the antiferromagnetic transition temperature of bulk solid $^3$He. The solid line shows the $T^7$ dependence.

$$k_{\text{eff}}^{-1} = k^{-1} + \frac{\rho_C}{T} Z_L L^2, \tag{78}$$

where $Z_L$ is the total impedance of the liquid including the impedance of the sinter. In the temperature range of Fig. 53, $Z_L$ is roughly temperature independent (Wellard *et al.*, 1982; Osheroff and Richardson, 1985; Vollhardt and Wölfle, 1990). Taking into account that $L \sim T^4$, we obtain a temperature dependence for the second term in Eq. (78) which is close to $T^7$ (solid line in Fig. 53). Note the rather large scatter of the data of different groups, which may be due to the different values of $Z_L$ in the experiments. As for the intrinsic growth resistance, it is expected to behave as $T^4$, about a thousand times more weakly (see below).

Below 0.4 mK the mean free path of Fermi quasiparticles becomes much larger than 1 cm, and the heat conductivity of the liquid $^3$He decreases exponentially, in proportion to the heat capacity of the liquid (Vollhardt and Wölfle, 1990; Feng *et al.*, 1993). The heat conduction across the liquid-solid interface also decreases exponentially. In contrast, the (magnon) heat conductivity of the solid remains almost constant (Osheroff *et al.*, 1991; Feng *et al.*, 1993). As a result, the crystal becomes thermally isolated from the liquid during growth, while its temperature is practically uniform and mainly depends on its thermal contact with the walls. Accordingly, the growth rate of such a crystal depends essentially on this thermal contact.

A different behavior is expected when the crystal changes shape at a constant volume. In this case the

total enthalpy of the crystal remains constant and no heat needs to be evacuated through the liquid or the sinter. The growth dynamics are then controlled by thermal magnons in the crystal, and the situation is similar to the case of $^4$He when phonons dominate; one only has to replace phonons by magnons (Andreev, 1982; Bowley and Edwards, 1983). Here too, one should distinguish the hydrodynamic regime from the ballistic one. In the hydrodynamic regime, where the magnon mean free path $l_m$ is much smaller than the characteristic size $R$ of the region where growth or melting takes place, one can write

$$\frac{1}{k} = \rho_C T S_C^2 Z_C, \tag{79}$$

where $Z_C \sim R/\kappa_C$ is the thermal impedance of the crystal. It has been found that $l_m \sim 1$ $\mu$m at 0.4 mK, and at lower temperatures $l_m$ increases as $T^{-2.5}$ or even faster (Osheroff *et al.*, 1991). This means that at sufficiently low temperatures one should expect thermal magnons to be ballistic and their interaction with the moving interface to be responsible for the growth resistance. In this case the growth resistance can be estimated (Korshunov and Smirnov, 1982; see also Andreev, 1996) as

$$\frac{1}{k} \approx \frac{1}{\rho_C \hbar^3}\left(\frac{k_B T}{c_m}\right)^4, \tag{80}$$

where the magnon velocity $c_m \approx 8$ cm/s (Osheroff and Yu, 1980; Osheroff *et al.*, 1991).

### 3. Crystallization waves in $^3$He

The possible observation of crystallization waves in $^3$He is a very interesting challenge. At temperatures far enough below $T_N$, thermal excitations disappear and one expects crystallization waves to propagate with a small damping. Let us estimate the temperature range where this could happen. As in $^4$He, the quality factor of the waves is

$$Q = 2k\frac{\omega}{q}\frac{(\rho_C - \rho_L)^2}{\rho_C \rho_L}, \tag{81}$$

where $q$ is the wave vector. Taking $k$ from Eq. (80), and $\gamma = 0.06$ erg/cm$^2$ from Rolley *et al.* (1989), one finds that for wavelengths of the order of 1 mm or shorter, $q > 10^2$ cm$^{-1}$, $Q \gg 1$ at $T < 0.2$ mK.

As in the case of $^4$He, there is a very weak, temperature-independent damping of crystallization waves in $^3$He caused by the decay of one quantum into two quanta with lower energies (Saam, 1973; Andreev and Parshin, 1978). Another damping mechanism is specific for $^3$He, namely, the Cherenkov radiation of magnons, whose velocity $c_m \approx 8$ cm/s is always smaller than the minimum phase velocity of crystallization waves (60 cm/s). This damping is much smaller than that resulting from the scattering of thermal magnons [(Eq. (80)], unless the temperature is lower than 10 $\mu$K (Korshunov and Smirnov, 1982).

In zero external magnetic field, the spin supercurrents that accompany the crystallization wave (Marchenko, 1981b; Korshunov and Smirnov, 1982) are too small to have any measurable effect on the dispersion relation. However, as shown by Andreev (1993), the situation changes in a nonzero field. In $^4$He, the kinetic energy of the wave is due to the mass flow, which is a consequence of mass conservation. In $^3$He, the spin conservation during phase transformation and the large difference in the magnetic susceptibilities $\chi_C$ and $\chi_L$ imply that spin currents are generated by growth or melting. Thus a magnetic contribution has to be added to the usual kinetic energy. The new magnetic terms being proportional to the square of the velocity of the interface, they constitute a magnetic kinetic energy. The dispersion relation is

$$\omega^2 = \frac{\gamma q^2}{M(q)} \tag{82}$$

with the effective mass

$$M(q) = \rho_L d_m \left(\frac{H}{H_0}\right)^2 + \frac{(\rho_C - \rho_L)^2}{\rho_L q}, \tag{83}$$

where

$$d_m = \frac{\chi_L {c_{mL}}^2}{\chi_C c_{mC} \Omega_c + \chi_L c_{mL} \Omega_L}, \tag{84}$$

and

$$H_0 = \frac{c_{mL}}{\chi_C}\sqrt{\rho_L \chi_L}. \tag{85}$$

In Eq. (84), $\Omega_C$ is the antiferromagnetic resonance frequency in the solid and $\Omega_I$ is the longitudinal NMR frequency in $^3$He-$B$; both frequencies are of the order of $10^5$ Hz; and $H_0$ is of the order of the exchange field in the solid ($\sim$1 T). The length $d_m$ is a few times shorter than the dipole length in the liquid, $l_D \sim 10^{-5}$ cm. This result was obtained for magnetic fields below 0.4 T, when the crystal is ordered in the antiferromagnetic state (and with superfluid $^3$He-$B$). The magnetic contribution dominates the effective mass $M$ when $H \gg H_0(\rho_C - \rho_L)/\rho_L$, in which case the dispersion relation is linear with a velocity

$$s = \frac{H_0}{H}\sqrt{\frac{\gamma}{\rho_L d_m}}. \tag{86}$$

It is important to note that neither the spin supercurrents nor the mass currents contribute to the dissipation. Therefore the damping should depend on the growth coefficient given by Eq. (80). Since the $Q$ factor increases proportionally to $\sqrt{M}$, working with nonzero field should allow one to observe crystallization waves in $^3$He at temperatures slightly higher than in zero field. The whole issue is an exciting challenge.

## V. DYNAMICS OF SMOOTH SURFACES

### A. Basic growth mechanisms

Contrary to rough ones, smooth surfaces grow layer by layer, from the transverse displacement of steps, so that the velocity $v$ is usually a nonlinear function of the driving force $\delta\mu$. Either these steps are nucleated, or screw dislocations emerge on the facet, so that steps are already present. These two different growth mechanisms are well known in the physics of classical crystals, and both have been observed in helium. As we shall see, a few other growth modes have been observed in helium, whose physical origins are not as yet clear.

#### 1. 2D nucleation

In order to nucleate a new terrace on a dislocation-free facet, one needs to create a step. The free energy of a terrace with a radius $R$ is

$$F(R) = 2\pi R\beta - \pi R^2 d\rho_C \delta\mu. \tag{87}$$

The maximum free energy is reached for the critical radius $R_c = \beta/(d\rho_C\delta\mu)$; it is the nucleation barrier

$$E = \frac{\pi\beta^2}{d\rho_C\delta\mu}. \tag{88}$$

In their experimental study, Wolf *et al.* (1985) distinguished three different regimes. At high temperature and with a large driving force, terraces should nucleate everywhere at a high rate, so that the crystal surface is covered by terraces. This is the "dynamic roughening." At very low temperature, and with a moderate driving force, the nucleation probability should be small and the completion of each layer results from the growth of terraces nucleated one by one. In this case, the growth rate should be simply proportional to $\exp(-E/T)$, where $E$ is given by the above equation. In practice, this mechanism is difficult to observe because, at low temperature, it is dominated by spiral growth from Frank-Read pairs of dislocations. There is a small temperature domain in the vicinity of $T_R$ where terraces nucleate simultaneously at different places and have time to grow on the surface.

One thus has to consider the coalescence of terraces. There is a characteristic time in this process, which is $a/v$, the time for the completion of one layer if the growth velocity is $v$. The density of terraces is the product of this time $\tau$ and the nucleation rate $\Gamma$, so that the average distance between terraces is $1/(\Gamma\tau)^{1/2}$. Within a time $\tau$ the terraces grow by an amount $v_{\rm step}\tau$. Coalescence occurs for $v_{\rm step}\tau = 1/(\Gamma\tau)^{1/2}$, and one finds that $\tau$ is proportional to the cubic root of $\Gamma$. Thus the Arrhenius factor in the growth velocity has to contain $\exp(-E/3T)$ instead of $\exp(-E/T)$. This explains the factor of 3 in Eq. (24). This growth mode was apparently observed by Wolf *et al.* (1985) and Gallet *et al.* (1987), who used this model to extract the step free energy of $c$ facets in $^4$He.

In the limit of zero temperature, Eq. (24) predicts that the growth rate will vanish exponentially, but there is a nonzero probability of nucleation by quantum tunneling in a system like $^4$He where dissipation can be neglected. The probability of quantum tunneling under the barrier $E(\delta\mu)$ has been calculated by Andreev (1982), and Uwaha (1983). In the quasiclassical approximation the tunneling exponent depends on both the potential barrier and the kinetic energy of the system. The latter is due to the motion of the liquid, which accompanies the formation of the nucleus. One finds

$$\Gamma_Q \sim \exp\left[-B\frac{\beta^{5/2}}{\hbar d\rho_C{}^{3/2}(\delta\mu)^2}\right], \tag{89}$$

where $B$ is a number of order unity. In principle, this process could be observed with $\delta p \sim 1$ bar in the case of the $c$ facets in $^4$He. Note that the quantum growth rate depends more strongly on $\delta\mu$ than the classical one.

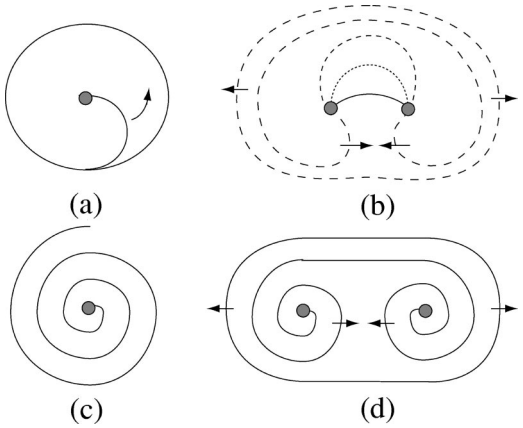


FIG. 54. Spiral growth of a crystal induced by screw dislocations. Growth of (a) a single dislocation under a small excess pressure and (b) a Frank-Read source. At higher growth rates the dislocation winds around itself to produce a spiral as shown in (c) for a screw dislocation and (d) for a Frank-Read source. From Ruutu *et al.*, 1998.

#### 2. Spiral growth

Spiral growth from Frank-Read sources was introduced by Burton *et al.* (1951) and reviewed by Chernov (1984). Figure 54 shows the main features of this phenomenon. It is important to realize that the growth rate does not depend on the number of sources, but is determined by the activity of each source. As explained by Burton *et al.* (1951), this is a consequence of the no-crossing condition for steps (see Fig. 30). Furthermore, the average distance between moving steps is usually very large compared to their height; thus the step velocity is much larger than the growth velocity of the facet itself. Since the step mobility is comparable to the mobility of rough surfaces, a facet grows much more slowly than a rough surface under the same $\delta\mu$. This in turn explains why the existence of facets is revealed by a slow growth (see Fig. 20). As a result, in the spiral growth regime, bulk dissipation is usually negligible and the growth is governed by the step dynamics only.

If one relates the step mobility $k_s$ to the step velocity $v_s$ by $v_s = k_s \delta\mu$, and if one assumes that $k_s$ is isotropic, then the asymptotic spacing between spiraling arms is

$$L \approx \frac{19}{K} \frac{\rho_L}{\rho_C - \rho_L} \frac{\beta}{d\,\delta p}, \tag{90}$$

where $K$ is the number of elementary steps produced by one dislocation (for the $c$ facet in $^4$He, $K=2$; Burton *et al.*, 1951). The facet velocity $v$ is $v_s d/L$, or

$$v \approx \frac{K}{19} \frac{(\rho_C - \rho_L)^2 d^2}{\rho_L^2 \rho_C \beta} k_s (\delta p)^2. \tag{91}$$

In helium, the step mobility has been the subject of a number of theoretical (Andreev and Parshin, 1978; Nozières and Gallet, 1987; Parshin, 1998; Ruutu *et al.*, 1998) and experimental studies (Rolley, Guthmann, *et al.*, 1995; Ruutu *et al.*, 1996, 1998; Tsepelin *et al.*, 1999). When discussing the step motion in $^4$He, Andreev and Parshin (1978) first considered a $T=0$ situation, in which all thermal processes are frozen out. They suggested that steps are rough, even in this limit, due to the existence of zero-point quantum kinks. A classical step should be smooth at $T=0$ because the creation of kinks or pairs of kinks requires overcoming a finite energy barrier (Nozières, 1992). However, in $^4$He, kinks can easily tunnel from site to site and consequently form delocalized quasiparticles with a finite bandwidth $\Delta_k$. Andreev and Parshin (1978) estimated that $\Delta_k \approx \hbar\Omega \approx 1-10$ K, where $\Omega$ is the tunneling frequency at the interface. They concluded that the bandwidth could be larger than the energy $\epsilon_{k0}$ of a localized kink, so that a finite density of quantum kinks could exist at $T=0$. As explained in Sec. IV.C.3, this model was also used by Edwards *et al.* (1990, 1991), who found an even larger bandwidth, about 30 K. It is generally accepted now that quantum kinks can induce a quantum roughness of steps at $T=0$. In their article, Andreev and Parshin further proposed that, similarly, there should be a finite density of zero-point steps leading to quantum roughening of the surface at $T=0$. However, we have seen in Sec. III.C.2 that this cannot be true. At $T=0$, the step energy is always positive, whatever its quantum fluctuations. Within their quantum solid-on-solid model, Iordanskii and Korshunov (1984) found that the step energy $\beta$ decays as $\exp(-c\sqrt{\Delta_k/\epsilon_{k0}})$ and is always positive; $c$ is a number of order unity.

If quantum roughening of steps occurs in all directions, then their mobility should be roughly isotropic. If the steps are smooth in some high-symmetry directions, then a large anisotropy of the step mobility ought to be observed. No experiment has as yet been attempted to verify such ideas. At $T \neq 0$, the step mobility has to be limited by interactions with thermal excitations, as seen for rough surfaces. This was calculated by Nozières and Uwaha (1987) in the case of well-separated steps. They considered the dissipation from the scattering of phonons. As already mentioned in Sec. IV.C.7, Nozières and Uwaha predicted a crossover from a $T^3$ behavior for incoherent scattering to a $T^4$ behavior for coherent scattering, when the separation between steps is less than the phonon wavelength. This crossover was observed by Rolley, Guthmann, *et al.* (1995).

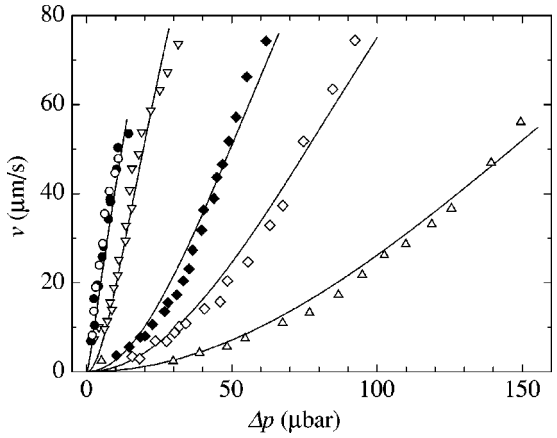


FIG. 55. Velocity of the $c$ facet on $^4$He crystals as a function of the driving pressure $\Delta p$: ○, $T=2$ mK; ●, 20 mK; ▽, 50 mK; ◆, 100 mK; ◇, 150 mK; △, 200 mK. Solid lines are guides to the eye. From Ruutu *et al.*, 1996.

In the theory of Nozières and Uwaha all internal degrees of freedom of the step were ignored—the step was assumed to be "cold." At very low temperatures in $^4$He this could be true only in the limit of a small driving force $\delta\mu$. At large $\delta\mu$ kinks on the step become accelerated and can reach the maximum possible velocity in the middle of the energy band before they release the excess kinetic energy. This is the phenomenon of quantum localization by an external field, which shows up in the quantum diffusion of vacancies and impurities in solid helium (Andreev, 1982), in the electrical conductivity of superlattices (Esaki, 1992), and in other systems with narrow-band quasiparticles. In the regime of localization, the rate of energy dissipation $W_l = \rho_C d v_s \delta\mu$ does not depend on the driving force; it is determined by the emission of phonons at collisions of "hot" kinks with each other (Ruutu *et al.*, 1998). Thus $v_s \sim 1/\delta\mu$, and

$$k_s = \frac{W_l}{\rho_C d (\delta\mu)^2}. \tag{92}$$

Ruutu *et al.* (1998) gave the following rough estimate for $W_l$:

$$W_l \sim 10^{-3} \left( \frac{\rho_C - \rho_L}{\rho_L} \right)^4 \frac{\rho_L n_k^2 a^6 \Delta_k^8}{\hbar^3 (k_B \theta_D)^5}. \tag{93}$$

The spiral growth of $^4$He crystals has been studied by Ruutu *et al.* (1996, 1998). Figure 55 shows the results of Ruutu *et al.* (1996) for the $c$ facet between 2 and 200 mK. The facet velocity rapidly increases when temperature decreases. A quadratic dependence on the pressure difference $\delta p$ is expected in the regime of constant mobility [Eq. (91)]; however, it is observed only at high temperatures and low velocities. At low temperatures the dependence is almost linear and it becomes even weaker at higher velocities. These results show that the classical

picture of the step motion fails under these conditions, where one should take into account nonlinear effects in the step dynamics.

The experiments of Ruutu *et al.* have shown that, at low temperatures, the step velocities may be very high: for instance, using $v=20$ $\mu$m/s, $\delta p=4$ $\mu$bar, and Eq. (90), one obtains a step velocity $v_s \approx 200$ m/s, close to the sound velocity. This means that at all temperatures, at least down to 2 mK, the density of kinks on a step is very high, of the order of the atomic density; otherwise the kink velocity would exceed the sound velocity, which is impossible. Moreover, one can estimate the lower limit of $\Delta_k$ by assuming, as usual, that $\epsilon_k = -\Delta_k \cos(pa/\hbar) + \text{const}$. Then $v_k = \Delta_k a/2\hbar \sin(pa/\hbar)$, and $\Delta \geqslant 2\hbar v_k/a \approx 10$ K (with $v_k = 200$ m/s). With such a large value of $\Delta_k$, and considering that the density of kinks shows no tendency to decrease down to 2 mK, it seems that for all step orientations there is a high density of very mobile quantum kinks.

Furthermore, at such high velocities, the step inertia should be taken into account. As we have seen in Sec. IV.C.3, the step inertia originates from the hydrodynamic flow around it; the hydrodynamic mass of a step per unit length can be written as (Kosevich and Kosevich, 1981)

$$m_s = \frac{(\rho_C - \rho_L)^2 d^2}{\pi \rho_L} \ln \frac{R}{\xi}, \tag{94}$$

where $R$ is the characteristic large scale of the system and where, for spiral growth, $R \sim L$. The kinetic energy may exceed the step energy at rest, $\beta$; for example, at $v_s = 200$ m/s, it should be five times larger. When accounting for the step inertia, one can write the step motion equation in the Euler variables as

$$m_s \left( \frac{\partial v_s}{\partial t} + v_s \frac{\partial v_s}{\partial n} \right) = \rho_C d \left( \delta\mu - \frac{v_s}{k_s} \right) - \frac{\beta^*}{r_c(\vec{r})}, \tag{95}$$

where $n$ is the normal to the step, $r_c(\vec{r})$ is the local radius of curvature of the step, and $\beta^* = \beta + m_s v_s^2/2$ (Ruutu *et al.*, 1998).

In addition to the usual quadratic growth, Eq. (95) provides two new growth regimes: the "inertial" regime at very low temperatures with a linear dependence,

$$v = K \frac{\rho_C d^2 \delta\mu}{2\pi\sqrt{2 m_s \beta}}, \tag{96}$$

and the regime of localization at high driving forces, where the growth rate saturates:

$$v \approx K \frac{W_l d}{19\beta}. \tag{97}$$

In Fig. 55 the low-temperature inertial regime can be clearly seen. The step mass obtained from these data $m_s = (4-5) \times 10^{-18}$ g/cm agrees quite well with the hydrodynamic mass given by Eq. (94). As for the regime of localization, there is a tendency to saturation only at the highest growth velocities, which allows one to estimate

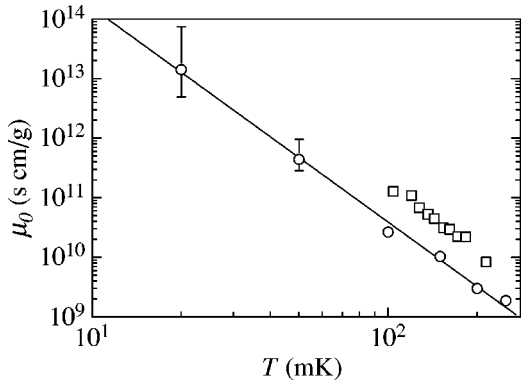


FIG. 56. Step mobility on $^4$He crystals as a function of temperature: ○, results of Ruutu *et al.* (1998), which follow the $T^{-3}$ law predicted by Nozières and Uwaha (1987); □, results of Rolley, Guthmann, *et al.* (1995), who measured a slightly larger mobility, probably because the phonon scattering was intermediate between coherent and incoherent in their experiment. From Ruutu *et al.*, 1998.

$W_l$ roughly as $(1-3) \times 10^{-3}$. With this value of $W_l$, one obtains from Eq. (93) $\Delta_k \approx 10$ K (at $n_k a = 1$), in agreement with previous estimates.

The quadratic regime with constant mobility can also be seen in Fig. 55 at low velocities and higher temperatures. The corresponding step mobility was obtained by using Eq. (91); it is shown in Fig. 56 as a function of temperature (circles). As one can see, the temperature dependence of the measured mobility is very close to $T^{-3}$ between 20 and 200 mK, as predicted by Nozières and Uwaha (1987). The absolute values of $k_s$ also agree well with this estimate. At lower temperatures, down to 2 mK, the mobility was too high to be measured. Note that in these experiments the spacing of the spiral arms was much larger than the wavelength of thermal phonons, and therefore the phonons scattered incoherently from the steps. Figure 56 shows a comparison with the effective mobility obtained by Rolley, Guthmann, *et al.* (1995) for a vicinal surface tilted by 0.3° (squares). The difference is probably due to the fact that in Rolley's situation the phonon scattering was intermediate between coherent and incoherent.

At low temperatures, where the effect of phonon scattering is weak, the step mobility becomes very sensitive to the presence of $^3$He impurities. There should be two contributions to the dissipation: one from impurities dissolved in the bulk liquid $^4$He and another from impurities adsorbed at the interface (Parshin, 1998). Both contributions depend on the way the step is "seen" by the $^3$He atoms, more precisely, on the relation between the characteristic wavelength of impurities and the effective width of the step. In the interesting case of relatively short wavelengths, the impurities probe the step profile. The nondegenerate 3D gas gives a contribution

$$\frac{1}{k_s} = \frac{d\sqrt{2 m_3 T}}{\pi \xi_i} n_3, \tag{98}$$

where $m_3$ and $n_3$ are the effective mass and the concentration of $^3$He atoms in the liquid $^4$He, respectively, and

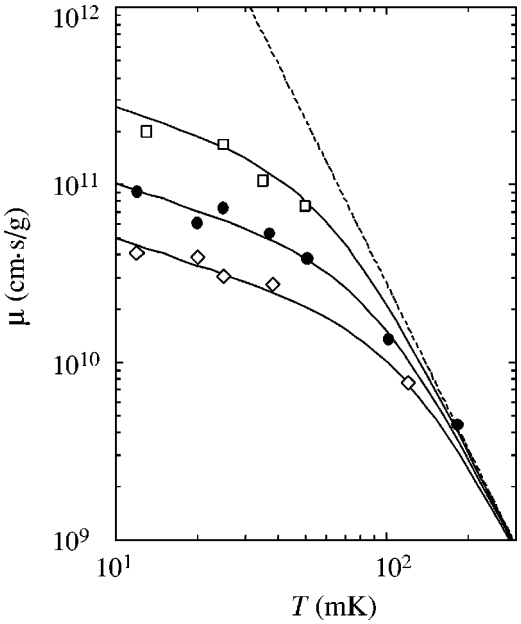


FIG. 57. Step mobilities $\mu$ on the $c$ facets of $^4$He crystals calculated from measurements with different $^3$He concentrations: □, 40 ppm; ●, 110 ppm; ◇, 220 ppm; dashed line, data taken with regular $^4$He (0.1 ppm); solid lines, theoretical curves. From Tsepelin *et al.*, 1999.

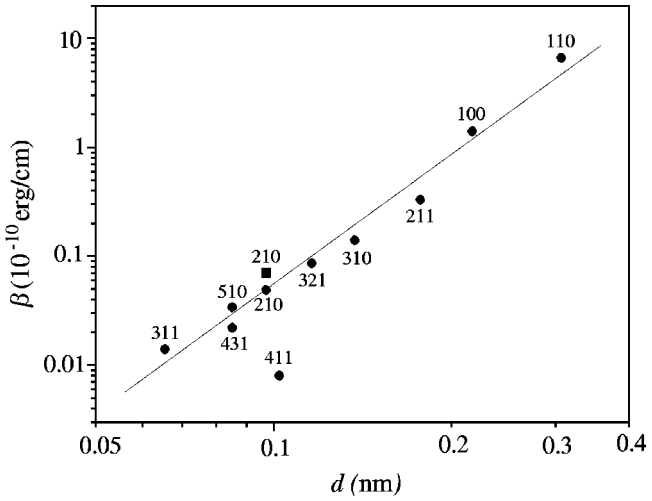


FIG. 58. Step free energies of different facets at 0.55 mK, plotted versus corresponding step heights. From Tsepelin *et al.*, 2002b.

$\xi_i$ plays the role of some kind of correlation length for the step profile as seen by the impurity. This formula has been checked by Tsepelin *et al.* (1999). Their results are shown in Fig. 57; they agree reasonably well with the above prediction, except that the value of $\xi_i = 8$ nm looks unexpectedly high.

One more nonlinear effect in the step dynamics may originate in the Cherenkov emission of various excitations by a moving step (phonons and rotons in $^4$He, Fermi quasiparticles and magnons in $^3$He, etc.). This happens when the step velocity exceeds the phase velocity of excitations. If the intensity of the emission is sufficiently strong, the step mobility drops below some critical velocity $v_c$. This may limit the growth velocity more than the inertia if $v_c$ is low (if $m_s v_c^2/2\beta < 1$) (Ruutu *et al.*, 1998). In this case, the solution of Eq. (95) yields

$$v = \frac{\rho_C v_c d^2}{2\pi(\beta + m_s v_c^2/2)} \delta\mu. \tag{99}$$

As for the radiation in the localization regime, the Cherenkov radiation is due to the coupling of the step motion with other degrees of freedom in the bulk phases, or in the interface itself. According to Ruutu *et al.* (1998), this coupling is rather weak in the case of $^4$He rotons because the momentum of rotons is large. In contrast, the radiation of phonons is expected to be strong, but the corresponding critical velocity is too high, $m_s v_c^2/2\beta \approx 5$. Thus the observed linear dependence of the growth velocity is most probably due to the inertia.

In order to avoid misunderstanding, we note here that Cherenkov emission is due to coherent motion of a continuous step with respect to the liquid or solid. This process is quite different from the emission of phonons (and other quasiparticles) in the regime of localization, where the step could even be at rest as a whole, but be very hot with respect to its internal degrees of freedom.

### 3. Facet growth in $^3$He

In $^3$He the critical velocities should be much lower than in $^4$He. This is because the magnon velocity $v_m$ in the solid is low, and because the pair-breaking velocity $v_{pb}$ is also low, approximately 7 cm/s (Osheroff and Yu, 1980; Feng *et al.*, 1993). The step-magnon coupling is expected to be rather strong because the moving step directly disturbs spins in the solid next to the interface. Therefore at $v_s > v_m$ the step mobility should be significantly lowered by the emission of magnons. As for the emission of quasiparticles in the liquid, this contribution is expected to be relatively weak due to the large value of the Fermi momentum, as in the case of rotons in $^4$He (Tsepelin *et al.*, 2002b).

The facet growth in $^3$He has been studied by several experimental groups (Feng, 1991; Nomura *et al.*, 1994; Akimoto *et al.*, 1998; Kawaguchi *et al.*, 2002; Tsepelin *et al.*, 2002b). In all measurements an almost linear dependence of $v(\delta\mu)$ was observed for overpressures of the order of a few mbar. This was interpreted as a spiral growth with a step velocity limited by the magnon velocity. In all but one case (Tsepelin *et al.*, 2002b) the crystal orientation was unknown. Despite this uncertainty all data agree quite well with each other. Using Eq. (99), and neglecting the kinetic energy of the steps, one can estimate the value of $\beta$ for facets growing in this regime. One finds a few times $10^{-10}$ erg/cm.

The most complete data were obtained by Tsepelin *et al.* (2002b). They were able to measure the growth velocities of ten different types of facets and to calculate the corresponding values of $\beta$ (see Fig. 58). Figure 58 shows that the dependence of $\beta$ on the step height $d$ is approximately $\beta \propto d^4$. This was expected for vicinal fac-

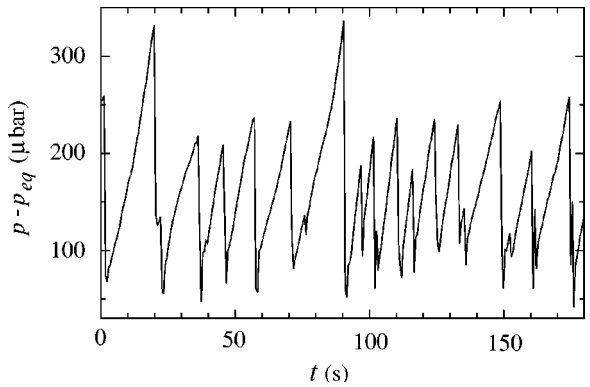


FIG. 59. Pressure trace indicating a burstlike growth of $^4$He crystals. From Ruutu *et al.*, 1996.

ets with an elastic interaction between steps, but somewhat surprisingly the $d^4$ law extends down to a very small interstep distance. This indicates that the steps are narrow at low temperature in $^3$He, meaning that the coupling to the crystal lattice is strong. Strong coupling is also indicated by the magnitude of the step energy, which is comparable to the surface energy $\gamma d$, as already discussed in Sec. III.D.2. There is no clear interpretation of this surprising finding as yet.

### B. Unusual growth modes of $^4$He facets

As explained above, a facet can grow only by 2D nucleation in the absence of screw dislocations, and this requires a typical overpressure of 1 bar. However, Ruutu *et al.* (1996) have found a burstlike growth mode occurring on the *c* facets of dislocation-free $^4$He crystals, when the overpressure was slowly increased up to some fraction of a mbar. Each rapid growth event was signalled by a drop of about 0.1 mbar in the overpressure (see Fig. 59).

The nature of this burstlike growth mode is not as yet clear. One possibility is that, while the overpressure $\delta p$ is increasing, the facet touches the side wall (which is somewhat rough) at randomly distributed points. This could happen at $\delta p \sim \rho\gamma/l_r\delta\rho$, where $l_r$ is the scale of the wall roughness. Then new terraces could be spontaneously emitted from the contact region, where the threshold for such emission can be estimated to be $\rho\beta/l_r\delta\rho$, a quantity much smaller than $\delta p$. The main difficulty is to explain why the observed values of $\delta p$ significantly increase with temperature or with the addition of $^3$He impurities. Both observations indicate that some dynamic process is involved, in which the energy dissipation is important. Here, accounting for the surface oscillations caused by mechanical vibrations of the cryostat might help. On the other hand, this growth mode could be a manifestation of some intrinsic property of the facet, not directly related to the cell walls. Further studies could clarify this issue, perhaps by using a cell with very smooth glass walls.

In the same series of experiments, a slow continuous movement of the *c* facet was found in between the fast events. The facets grew with typical velocities of 0.5 nm/s, changing approximately linearly with the overpressure. Increasing the temperature or adding $^3$He impurities slowed down this growth velocity. Andreev and Melnikovsky (2001) proposed that the crystal was growing "from the bottom," due to a flux of vacancies. If so, the growth velocity of a facet should depend on the crystal height. They also predicted the existence of a maximum in the temperature dependence of the growth velocity if these vacancies are thermally activated, but not if they are zero-point vacancies. It would be interesting to test these predictions experimentally.

An anomalously fast growth mode of facets was found in $^4$He crystals at high overpressures by Tsymbalenko (2000, 2003). The crystals were nucleated on a needle by applying an electrical pulse, without direct contact to the cell wall. At low overpressures, the crystals grew relatively slowly, apparently by the usual spiral mechanism. Above some threshold pressure value, which increased from about 1 mbar at 0.2 K to 14 mbar at 0.78 K, the crystals grew much faster, with velocities up to 3.5 m/s; this value is comparable to the maximum growth velocity found for rough surfaces by Graf and Maris (1987). The value of this pressure threshold, as well as its dependence on temperature and the concentration of impurities, is close to the values observed in Helsinki for the burstlike growth. This means that these two observations might have the same physical explanation (Tsymbalenko, 2003). Note, however, that in Tsymbalenko's experiments the crystal was touching only the needle, so that only one facet touched the wall, in contrast with the experiments of Ruutu *et al.*

The two above examples show that the growth dynamics of helium crystals far from equilibrium is not fully understood, and some important growth mechanisms may be still missing from the theory. One possibility was suggested by Parshin and Tsymbalenko (2003). Using the weak-coupling approximation, they considered the nonlinear dynamics of steps at a smooth superfluid-solid boundary, particularly the collisions of steps with opposite signs. In addition to the conventional annihilation of steps in such collisions, they found that under certain conditions transmission and reflection of steps could occur. The transmission of steps is similar to the transmission of sine-Gordon kinks and antikinks through each other; it becomes possible if the step velocity exceeds some threshold value, which can be estimated to be about 100 m/s in the case of $^4$He. This process results in a multiplication of preexisting steps and thus gives a qualitatively new mechanism for facet growth in the absence of renewable sources such as screw dislocations.

## VI. INSTABILITIES AND OTHER PROPERTIES

### A. A mechanical instability

If a nonhydrostatic stress is applied to a crystal, the planar shape of its surface becomes unstable and periodic grooves appear. This instability was first predicted

by Asaro and Tiller (1972), who suggested that it might be a precursor of fracture and corrosion, and later was independently predicted by Grinfeld (1986, 1993), who proposed to study it in $^4$He. It might also be connected to the spontaneous formation of quantum dots during the heteroepitaxy of semiconducting materials. The mechanism of the instability was further investigated by Nozières (1992) and by Balibar, Edwards, and Saam (1991), who explained that the deformation of the crystal surface allows some release of elastic energy at the expense of the surface energy, which can happen if the applied stress exceeds a certain threshold.

Consider a liquid-solid interface at $z=0$ and suppose that a stress tensor $\sigma_{ij}$ is applied, which induces a deformation $u_{ij}$. The stress would be called hydrostatic if its tensor were diagonal, with $\sigma_{xx}=\sigma_{yy}=\sigma_{zz}=-P(z)$. Suppose that an extra stress $\sigma_0$ is applied in the $x$ direction and that the crystal has fixed boundaries in the $y$ direction; then the equilibrium conditions at the interface are

$$\sigma_{zz} = -P_L, \quad \sigma_{xy} = \sigma_{yx} = 0, \tag{100}$$

$$\sigma_{xx} = \sigma_{zz} + \sigma_0, \quad u_{yy} = 0, \tag{101}$$

$$\sigma_{xx} = \sigma_{yz} = 0, \tag{102}$$

$$\frac{f_C - \sigma_{zz}}{\rho_C} = \mu_C^{\text{eff}} = \mu_L, \tag{103}$$

where the chemical potential of the crystal is generalized as $\mu_C^{\text{eff}}$ since the pressure in the crystal is not defined.

The extra uniaxial stress $\sigma_0$ shifts the equilibrium pressure in the liquid by an amount $\delta P_L$, which obeys

$$\delta\mu_C^{\text{eff}} = \frac{(1-\sigma_P^2)\sigma_0^2}{2\rho_C E} + \frac{\delta P_L}{\rho_C} = \delta\mu_L = \frac{\delta P_L}{\rho_L}, \tag{104}$$

where $\sigma_P$ is the Poisson coefficient and $E$ the Young modulus of the crystal. Due to gravity, the crystal melts down by an amount

$$\delta h = \frac{(1-\sigma_P^2)\sigma_0^2}{2Eg(\rho_C - \rho_L)}. \tag{105}$$

A corrugation of the surface appears with a wave vector

$$q^* = \sqrt{\frac{(\rho_C - \rho_L)g}{\gamma}} \tag{106}$$

if the uniaxial stress $\sigma_0$ exceeds the threshold

$$\sigma^* = \sqrt{\frac{\gamma E q^*}{1-\sigma_P^2}}. \tag{107}$$

Well beyond this threshold, gravity becomes negligible and all Fourier components of the surface deformation are unstable up to a maximum wave vector

$$q_m = \frac{2\sigma_0^2}{E\gamma}. \tag{108}$$

Bodensohn *et al.* (1986) noticed the formation of grooves at the surface of a $^4$He crystal after rapid cooling (see Fig. 60). Balibar, Edwards, and Saam (1991) proposed that the origin of the instability was the nonhydrostatic stress produced by cooling: above 1 K, the melting pressure varies significantly with temperature so that cooling down a crystal in a box with fixed boundaries should produce horizontal stresses. This hypothesis was proved to be correct, and the mechanical origin of the instability was clearly established by Thiel *et al.* (1992), who showed that grooves appeared during either cooling or warming, or after applying a horizontal stress with a piezoelectric bimorph. At nearly the same time, Torii and Balibar (1992) used piezoelectric cylinders to apply calibrated strains to $^4$He crystals. They first verified Eq. (105) (see Fig. 61). They also verified that an increasing number of grooves appears beyond the threshold $\sigma^*$ predicted by Eq. (107). However, no experiment has accurately tested Eq. (108), which predicts a wavelength $2\pi/q_m$ in the nanometer range for strains of a few percent (as found in semiconductor epitaxy).

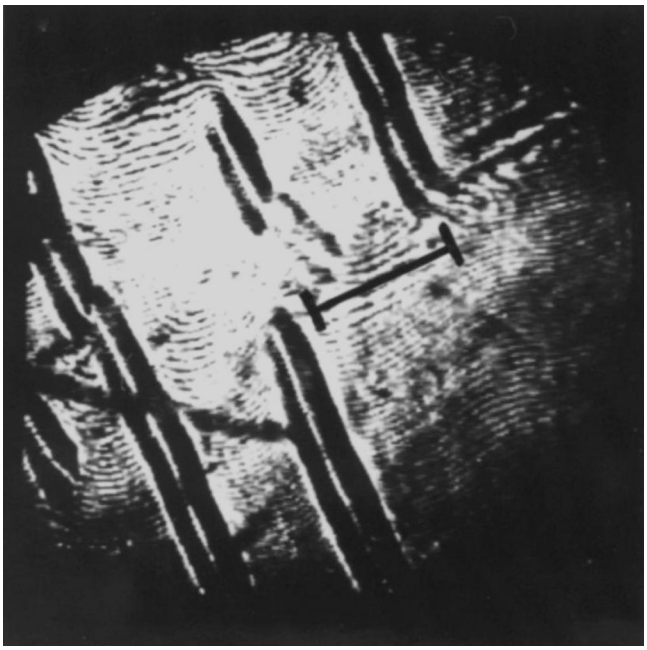

FIG. 60. Mechanical instability due to the appearance of stresses in a $^4$He crystal after a rapid quench in temperature around 1 K. The distance between parallel grooves which appear at the crystal surface is approximately $2\pi l_c \approx 6.3$ mm, the length of the scale bar on the image ($l_c$ is the capillary length). From Bodensohn *et al.*, 1986.

Balibar, Edwards, and Saam (1991) also proposed that the crystallization waves are modified in the vicinity of this instability, but this has not yet been checked either. Thiel *et al.* (1992) and Torii and Balibar (1992) observed that the groove direction depends on the orientation of both the stress and the crystal: the wave vector tends to be aligned perpendicular to the (0001) planes and perpendicular to the uniaxial stress. These tendencies could be in conflict with each other.

### B. Hydrodynamic instabilities

Several interface instabilities have been considered, which originate from hydrodynamic phenomena. One of

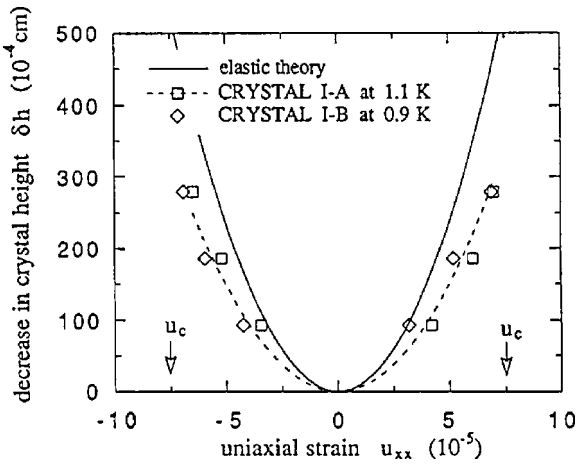


FIG. 61. Amount of melting produced when a uniaxial stress is applied to a $^4$He crystal in equilibrium with its superfluid phase; the experimental results (various symbols) are close to the prediction of Eq. (105) (solid line). An instability occurs at the threshold strain $u_c$ indicated by arrows. From Torii and Balibar, 1992.

these is the Kelvin-Helmholtz instability, which is comparable to the generation of sea waves by wind: in the presence of a tangential flow in the superfluid above a crystal surface, crystallization waves are generated. Assuming that the interface is horizontal, the critical velocity for this instability is (Parshin, 1985; Kagan, 1986; Uwaha and Nozières, 1986)

$$v_c = \left( \frac{4\gamma(\rho_C - \rho_L)g}{\rho_L^2} \right)^{1/4}. \tag{109}$$

Numerically, one finds $v_c = 4-5$ cm/s, depending on the surface orientation. Uwaha and Nozières (1986) considered the combined effect of a flow and electric charges; they showed that the critical velocity can be made arbitrarily small by letting the electrostatic force approach the critical threshold in the absence of flow. Maksimov and Tsymbalenko (2002) recently reported on the observation of the Kelvin-Helmholtz instability at a crystal surface; in their experiment, a jet of liquid helium was produced by injecting electrons with a tungsten needle. However, there could be another explanation for their observation: the flow could have been inhomogeneous and produced an inhomogeneous Bernoulli pressure, which would destabilize the surface.

A Kelvin-Helmholtz instability has been predicted for *facets* by Andreev (1994). He showed that in the presence of a superfluid flow parallel to the facet, the facet becomes unstable against the formation of pairs of steps aligned perpendicular to the superfluid velocity $v_{sf}$. As a result, the surface stiffness becomes finite in the direction of the superfluid flow, and the facet shape becomes cylindrical. The equilibrium density of steps was estimated as

$$n_s \sim \exp\left( -\frac{2\pi\beta}{\rho_L a v_{sf}^2} \right). \tag{110}$$

For a *c* facet on a $^4$He crystal the exponent in Eq. (110) is of the order of unity if $v_{sf} \approx 4 \times 10^3$ cm/s. This value is high, so that Andreev's instability looks difficult to observe.

Another hydrodynamic instability has been considered by van Saarlos and Weeks (1995) for rough surfaces. With ordinary liquids, Faraday (1831) explained that standing capillary waves can be excited by oscillating the liquid vertically. van Saarlos and Weeks suggested exciting standing crystallization waves at the horizontal liquid-solid interface by shaking the whole cell. At a given frequency, the instability threshold depends only on the growth coefficient $k$ and it is essentially the same for modes with different wave vectors $q$ (in the low-damping limit), thus providing an independent way to measure $k$. Moreover, the growth resistance and the surface stiffness being anisotropic, different patterns could be observed, not only the usual one, which has a triangular symmetry. van Saarlos proposed this experiment in order to obtain more information on both the surface properties of $^4$He crystals and the mechanisms of pattern selection in the Faraday instability.

Recently Nomura *et al.* (2003) have studied the effect of acoustic radiation pressure (Rayleigh, 1902) at a rough liquid-solid interface. When an acoustic wave was applied from the liquid side, it always induced melting of the crystal. When applied from the crystal side, melting was induced at high temperatures and crystallization was induced at temperatures below the inversion temperature $T_i$ which varied in the interval from 0.6 to 0.8 K, depending on the surface orientation. The acoustic radiation pressure theory (Borgnis, 1953) explains reasonably well the experimental observations at low temperatures, but additional melting mechanisms are needed to explain the high-temperature behavior, the origin of which is not as yet known.

### C. Dendrites

#### 1. Helium crystals in zero magnetic field

In a number of situations, the growth of helium crystals is governed by the diffusion of heat or mass in two adjacent bulk phases. Under sufficiently strong departure from equilibrium, dendritic instabilities have been observed and analyzed. Franck and Jung (1986) and Rolley, Balibar, and Graner (1994) have found some interesting differences between helium dendrites and more classical ones.

Franck and Jung (1986) studied the dendritic growth of pure $^4$He crystals at high pressure (from 210 to 4200 bars) and at high temperature (from 5.4 to 46 K). Under such conditions, liquid $^4$He is in the normal state; the structure of solid $^4$He is hcp below 1120 bars (where the melting temperature is 15 K) and fcc above. Franck and Jung found that the growth velocity of crystals was larger than predicted and also that the side branches appeared much further away from the dendrite tip than in ordinary crystals. They tried to make some quantitative comparison with existing theories but had to estimate many unknown quantities.

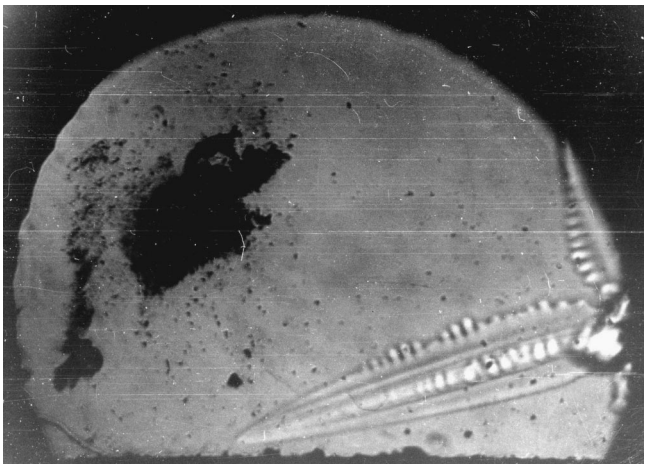

FIG. 62. $^3$He dendrite growing at 100 mK with a tip velocity of 30 $\mu$m/s. The cell width is 4 mm. Side branches appear at a distance of about 50 times the tip radius from this tip. From Rolley, Balibar, and Graner, 1994.

Rolley, Balibar, and Graner (1994) studied the dendritic growth of $^3$He crystals between 80 and 120 mK. Thanks to many other experiments of the same group, most of the relevant physical quantities were known, including the anisotropy of the surface stiffness. Like Franck and Jung, they found that the side branching instability was weak, so that these branches were often absent on dendrites with almost perfect parabolic shapes. On the fast-growing shapes of crystals they found the side branches appearing at a distance as far as $\approx 50\rho_t$ away from the tip, $\rho_t$ being the tip curvature radius (see Fig. 62). This is ten times farther than with ordinary crystals. They attributed this difference to the heat conductivity in the solid being much larger than in the liquid, an anomalous situation, but suggested further checks of this interpretation.

Rolley *et al.* (1986) noticed another difference between helium dendrites and other crystals: the latent heat released in the liquid under their experimental conditions had to go through the liquid-solid interface, whose thermal resistance $R_K$ was large, before being conducted through the solid, whose thermal impedance was small. This gave them a better understanding of the stability criterion for $^3$He dendrites, which selects the dendrite tip velocity. In the calculation of this criterion, Rolley, Balibar, and Graner (1994) showed that the usual ratio of the heat conductivities on both sides of the liquid-solid interface had to be replaced by an expression involving the surface resistance $R_K$. Once this was done, they found agreement with their measurement on the product $v_t\rho_t^2$ ($v_t$ being the tip velocity).

### 2. Melting process of highly magnetized solid $^3$He

The growth or melting of a solid is accompanied by mass and heat flows, which are due to the density and entropy differences between the two phases in contact. If the two phases have different magnetizations at equilibrium, a magnetization flow also appears. In the case of $^3$He, where the solid has a much larger susceptibility than the liquid, one can probe the magnetization flows on both sides of the interface as well as the magnetization transfer through the interface.

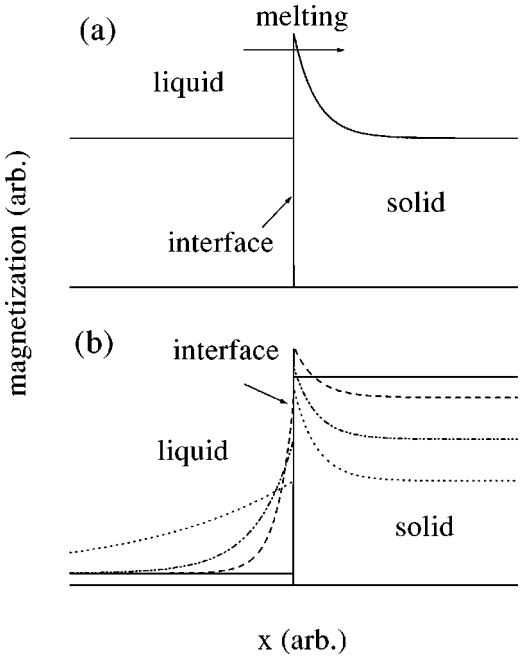


FIG. 63. Magnetization at the liquid-solid interface: (a) Sketch of the magnetization profile of a planar liquid-solid interface melting with a constant speed, as analyzed by Puech *et al.* (1986b). On the solid side, the magnetization profile falls off exponentially and there is no gradient on the liquid side. (b) Sketch of the buildup of magnetization profiles as concluded by Akimoto *et al.* (2000) at time $t=0$, when the melting is started (black line) and at three successive moments during the initial melting phase. While the boundary layer with increased magnetization is building up in the solid, a stabilizing gradient is also building up in the liquid. The magnetization of the bulk solid (at right) decreases due to the increase in temperature during the rapid melting experiment. Both pictures are drawn in a frame moving with the interface. From Akimoto *et al.*, 2000.

The melting of magnetized solid $^3$He was considered by Castaing and Nozières (1979). They proposed that when the solid is melted with a time scale shorter than the spin-lattice relaxation time (about 1000 s at a few tens of mK), a magnetization boundary layer builds up on the solid side of the interface. This boundary layer is simply due to the increased magnetization of the newly produced liquid, and that in turn enhances the magnetization in the solid near the interface. Later, Bonfait *et al.* (1984) suggested that, in analogy to the Mullins-Sekerka instability (Mullins and Sekerka, 1964), the buildup of this boundary layer would make the liquid-solid interface unstable, and this suggestion was backed up by a calculation of Puech *et al.* (1986b).

The situation, analyzed by Puech *et al.*, is sketched in Fig. 63(a). This kind of picture has been used in several theoretical considerations (Langer, 1980; Kassner, 1996). The analysis of Puech *et al.* shows that when a planar

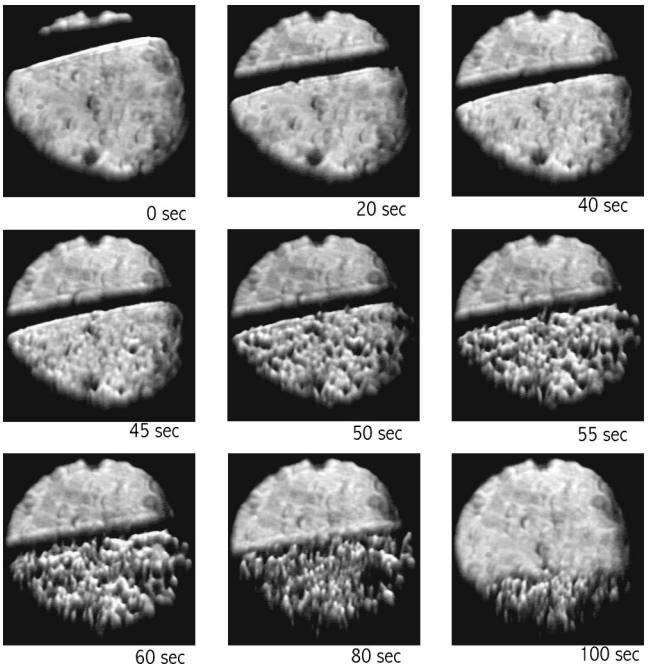


FIG. 64. Sequence of images during rapid melting of solid $^3$He in an 8.9-T magnetic field. The instability occurs about 45 s after cell decompression was started: cellular dendrites with a size of 50–100 $\mu$m appear in the vertical direction. From Marchenkov *et al.*, 1999.

interface propagates with a constant speed in the absence of magnetization gradients in the liquid, the interface will be unstable, with a typical growth time for the most unstable modes of the order of 0.1 s.

Experimentally, the melting of highly polarized solid $^3$He has been studied by different groups (Bonfait *et al.*, 1984; Vermeulen *et al.*, 1987; Marchenkov *et al.*, 1999; Akimoto *et al.*, 2000). The most recent experiments have been performed by Marchenkov *et al.* (1999) who found that if the solid $^3$He was melted sufficiently rapidly in an 8.9-T field and at 9 mK, instability of the interface occurred in several tens of seconds after melting was started. The solid formed many cellular dendrites, which were directed parallel to the applied magnetic field (see Fig. 64). No instability was observed during melting in low magnetic field or at high initial temperature (about 100 mK), even in an 8.9-T field.

In later experiments, the Leiden group applied a small magnetic field gradient and they were able not only to image the liquid-solid interface but also to measure the magnetization profile perpendicular to the interface (Akimoto *et al.*, 2000). These measurements revealed the buildup of a magnetization gradient on both the liquid and the solid sides of the interface during the first phase of the melting process [see Fig. 63(b)]. It was shown by Akimoto *et al.*, who extended the stability analysis of Puech *et al.*, that it is this gradient in the liquid which stabilizes the interface during the initial stage of melting. The interface becomes unstable only when the magnetization gradient on the liquid side is negligible, and after that the instability develops within a short time, as predicted by theory. These results agreed with numerical calculations performed by Plomp *et al.* (2001).

## VII. CONCLUSION: OPEN QUESTIONS

In conclusion, we wish to list a few open problems or unanswered questions that look interesting to us and deserve further study:

(1) Roughening in $^3$He. What is the roughening temperature of the (110) facets on $^3$He crystals? Is it possible that the coupling of the liquid-solid interface to the crystal lattice is weak at high temperature and strong at low temperature? How do the superfluid and the magnetic ordering transitions affect surface properties like the step energies of facets and the growth rate of crystals?[5]

(2) Roughening in $^4$He. New measurements of the step free energy near the roughening transition temperature of the *c* facets are necessary. If possible, independent measurements of the correlation length $\xi$ would allow clarification of some fundamental aspects of the renormalization-group theories. One would also like to know if more than three roughening transitions can be observed in $^4$He.

(3) Crystallization waves in $^3$He. These waves are predicted to propagate below about 0.2 mK. To excite and detect waves at such low temperatures is a real challenge. Of particular interest is the magnetic-field dependence of the kinetic energy of waves. In fact, the magnetic-field dependence of the dynamics of rough surfaces in $^3$He is unexplored experimentally.

(4) Fast dynamics of facets at very low temperature in $^4$He. The mechanisms of several different rapid growth modes have to be understood. Could it be possible that facets are so mobile at low temperature that the Kapitza resistance becomes anomalous on facets as well as at rough surfaces? If so, could one observe nonlinear crystallization waves on facets?

(5) Could one observe the competition between crystal anisotropy and stress anisotropy in the surface instability of stressed crystals? And could one study crystallization waves near the instability threshold?

This list only gives some feeling for the rich variety of problems that can be addressed when studying the surface of helium crystals. Some of them are of general interest, others are particular to helium and often surprising. Clearly, there is much to see at the surface of these crystals, probably more than has been covered in this review. We would have enjoyed telling Keesom about all this.

[5]During the preparation of this review Todoshchenko *et al.* (2004) proposed very interesting answers to some of the above questions.

## ACKNOWLEDGMENTS

S.B. and A.P. are grateful to Professor Mikko Paalanen and all members of the Low Temperature Laboratory (Helsinki) for their hospitality during the writing of this review. The authors acknowledge support from the EEC program ULTI III.

## NOTATIONS AND SYMBOLS

| | |
|---|---|
| $a$ | lattice constant |
| $A, B, C$ | Onsager's matrix coefficients |
| $(\,)_{C,L}$ | indices for crystal and liquid |
| $c_C, c_L$ | sound velocity in the crystal and in the liquid |
| $c_l, c_t$ | longitudinal and transverse sound velocity in the crystal |
| $d$ | step height |
| $E$ | Young modulus |
| $k$ | surface mobility or growth coefficient |
| $l_c$ | capillary length |
| $k_B$ | Boltzmann's constant |
| $k_s$ | step mobility |
| $m_I$ | interface inertia or mass per unit area |
| $m_k$ | kink mass |
| $q$ | wave vector |
| $R_K$ | Kapitza resistance |
| $T_R$ | roughening temperature |
| $t=(1-T/T_R)$ | reduced temperature |
| $u$ | strain |
| $U$ | lattice potential per cell $L\times L$ |
| $v$ | velocity |
| $V$ | lattice potential per unit area |
| $w$ | step width |
| $Z=\rho c$ | acoustic impedance |
| $\alpha$ | surface tension or free energy per unit area |
| $\beta$ | step energy |
| $\gamma$ | surface stiffness |
| $\Delta$ | roton gap energy |
| $\delta$ | interaction energy between steps |

## REFERENCES

Akimoto, H., R. van Rooijen, R. Jochemsen, G. Frossati, and W. van Saarloos, 2000, Phys. Rev. Lett. **85**, 1894.
Akimoto, H., R. van Rooijen, A. Marchenkov, R. Jochemsen, and G. Frossati, 1998, Physica B **255**, 19.
Akutsu, Y., N. Akutsu, and T. Yamamoto, 1988, Phys. Rev. Lett. **61**, 424.
Alerhand, O. L., D. Vanderbilt, R. D. Meade, and J. D. Joannopoulos, 1988, Phys. Rev. Lett. **61**, 1973.
Alles, H., and A. Y. Parshin, 2004, J. Low Temp. Phys. **135**, 665.
Alles, H., V. Tsepelin, A. Babkin, R. Jochemsen, A. Y. Parshin, and I. Todoshchenko, 2001, J. Low Temp. Phys. **124**, 189.
Amrit, J., and J. Bossy, 1990, Physica B **165-166**, 529.
Amrit, J., and J. Bossy, 1993, J. Low Temp. Phys. **92**, 415.
Amrit, J., P. Legros, and J. Poitrenaud, 1995a, J. Low Temp. Phys. **100**, 121.
Amrit, J., P. Legros, and J. Poitrenaud, 1995b, J. Low Temp. Phys. **101**, 971.
Andreev, A. F., 1981, Zh. Eksp. Teor. Fiz. **80**, 2042 [Sov. Phys. JETP **53**, 1063 (1981)].
Andreev, A. F., 1982, in *Progress in Low Temperature Physics*, Vol. 8, edited by D. F. Brewer (Elsevier Science, Amsterdam), p. 67.
Andreev, A. F., 1990, Pis'ma Zh. Eksp. Teor. Fiz. **52**, 1204 [JETP Lett. **52**, 619 (1990)].
Andreev, A. F., 1993, Pis'ma Zh. Eksp. Teor. Fiz. **58**, 740 [JETP Lett. **58**, 715 (1993)].
Andreev, A. F., 1994, Zh. Eksp. Teor. Fiz. **106**, 1219 [JETP **79**, 660 (1994)].
Andreev, A. F., 1995, Pis'ma Zh. Eksp. Teor. Fiz. **62**, 123 [JETP Lett. **62**, 136 (1995)].
Andreev, A. F., 1996, Czech. J. Phys. **46 S6**, 3043.
Andreev, A. F., and V. G. Knizhnik, 1982, Zh. Eksp. Teor. Fiz. **83**, 416 [Sov. Phys. JETP **56**, 226 (1982)].
Andreev, A. F., and Y. A. Kosevich, 1981, Zh. Eksp. Teor. Fiz. **81**, 1435 [Sov. Phys. JETP **54**, 761 (1981)].
Andreev, A. F., and I. M. Lifshitz, 1969, Zh. Eksp. Teor. Fiz. **56**, 2057 [Sov. Phys. JETP **29**, 1107 (1969)].
Andreev, A. F., and L. A. Melnikovsky, 2001, Zh. Eksp. Teor. Fiz. **120**, 1457 [JETP **93**, 1261 (2001)].
Andreev, A. F., and A. Y. Parshin, 1978, Zh. Eksp. Teor. Fiz. **75**, 1511 [Sov. Phys. JETP **48**, 763 (1978)].
Andreeva, O. A., and K. O. Keshishev, 1987, Pis'ma Zh. Eksp. Teor. Fiz. **46**, 160 [JETP Lett. **46**, 200 (1987)].
Andreeva, O. A., and K. O. Keshishev, 1990, Pis'ma Zh. Eksp. Teor. Fiz. **52**, 799 [JETP Lett. **52**, 164 (1990)].
Andreeva, O. A., and K. O. Keshishev, 1991, Phys. Scr. **T39**, 352.
Andreeva, O. A., K. O. Keshishev, and S. Y. Osip'yan, 1989, Pis'ma Zh. Eksp. Teor. Fiz. **49**, 661 [JETP Lett. **49**, 759 (1989)].
Armour, A. D., R. M. Bowley, and P. Nozières, 1998, J. Low Temp. Phys. **110**, 127.
Asaro, R. J., and W. A. Tiller, 1972, Metall. Trans. A **3**, 1789.
Avron, J. E., L. S. Balfour, C. G. Kuper, J. Landau, S. G. Lipson, and L. S. Schulman, 1980, Phys. Rev. Lett. **45**, 814.
Avron, J. E., and R. K. P. Zia, 1988, Phys. Rev. B **37**, 6611.
Babkin, A. V., H. Alles, P. J. Hakonen, A. Y. Parshin, J. P. Ruutu, and J. P. Saramäki, 1995, Phys. Rev. Lett. **75**, 3324.
Babkin, A. V., K. O. Keshishev, D. B. Kopeliovich, and A. Y. Parshin, 1984, Pis'ma Zh. Eksp. Teor. Fiz. **39**, 519 [JETP Lett. **39**, 633 (1984)].
Babkin, A. V., D. B. Kopeliovich, and A. Y. Parshin, 1985, Zh. Eksp. Teor. Fiz. **89**, 2288 [Sov. Phys. JETP **62**, 1322 (1985)].
Balibar, S., 2002, J. Low Temp. Phys. **129**, 363.
Balibar, S., and J. P. Bouchaud, 1992, Phys. Rev. Lett. **69**, 862.
Balibar, S., and B. Castaing, 1980, J. Phys. (France) Lett. **41**, L329.
Balibar, S., B. Castaing, and C. Laroche, 1980, J. Phys. (France) Lett. **41**, L283.
Balibar, S., X. Chavanne, and F. Caupin, 2003, Physica B **329-333**, 380.
Balibar, S., D. O. Edwards, and C. Laroche, 1979, Phys. Rev. Lett. **42**, 782.
Balibar, S., D. O. Edwards, and W. F. Saam, 1991, J. Low Temp. Phys. **82**, 119.
Balibar, S., F. Gallet, F. Graner, C. Guthmann, and E. Rolley, 1991, Physica B **169**, 209.
Balibar, S., C. Guthmann, and E. Rolley, 1993, J. Phys. I **3**,

1475.
Balibar, S., T. Mizusaki, and Y. Sasaki, 2000, J. Low Temp. Phys. **120**, 293.
Balibar, S., and P. Nozières, 1994, Solid State Commun. **92**, 19.
Bartelt, N. C., T. L. Einstein, and E. D. Williams, 1990, Surf. Sci. **240**, L591.
Bodensohn, J., K. Nicolai, and P. Leiderer, 1986, Z. Phys. B: Condens. Matter **64**, 55.
Boldarev, S. T., and V. P. Peshkov, 1973, Pis'ma Zh. Eksp. Teor. Fiz. **17**, 416 [JETP Lett. **17**, 297 (1973)].
Bol'shov, L. A., V. L. Pokrovski, and G. V. Umin, 1984, Pis'ma Zh. Eksp. Teor. Fiz. **39**, 145 [JETP Lett. **39**, 173 (1984)].
Bonfait, G., L. Puech, A. Greenberg, G. Eska, B. Castaing, and D. Thoulouze, 1984, Phys. Rev. Lett. **53**, 1092.
Borgnis, F. E., 1953, Rev. Mod. Phys. **25**, 653.
Bowley, R. M., and A. D. Armour, 1997, J. Low Temp. Phys. **107**, 225.
Bowley, R. M., and D. O. Edwards, 1983, J. Phys. (Paris) **44**, 723.
Burmistrov, S. N., and L. B. Dubovskii, 1993, Europhys. Lett. **24**, 749.
Burton, W. K., and N. Cabrera, 1949, Discuss. Faraday Soc. **5**, 33.
Burton, W. K., N. Cabrera, and F. C. Frank, 1951, Philos. Trans. R. Soc. London, Ser. A **243**, 299.
Carmi, Y., S. G. Lipson, and E. Polturak, 1985, Phys. Rev. Lett. **54**, 2042.
Carmi, Y., S. G. Lipson, and E. Polturak, 1987, Phys. Rev. B **36**, 1894.
Carmi, Y., E. Polturak, and S. G. Lipson, 1989, Phys. Rev. Lett. **62**, 1364.
Castaing, B., 1984, J. Phys. (France) Lett. **45**, L233.
Castaing, B., S. Balibar, and C. Laroche, 1980, J. Phys. (Paris) **41**, 897.
Castaing, B., A. S. Greenberg, and M. Papoular, 1982, J. Low Temp. Phys. **47**, 191.
Castaing, B., and P. Nozières, 1979, J. Phys. (Paris) **40**, 257.
Castaing, B., and P. Nozières, 1980, J. Phys. (Paris) **41**, 701.
Chavanne, X., S. Balibar, and F. Caupin, 2001, Phys. Rev. Lett. **86**, 5506.
Chernov, A. A., 1984, *Crystal Growth*, Vol. 3 of Modern Crystallography (Springer, Berlin).
Chui, S. T., and J. D. Weeks, 1976, Phys. Rev. B **14**, 4978.
Chui, S. T., and J. D. Weeks, 1978, Phys. Rev. Lett. **40**, 733.
Conrad, E. H., and T. Engel, 1994, Surf. Sci. **299**, 391.
Cuthbertson, C., and M. Cuthbertson, 1932, Proc. R. Soc. London, Ser. A **135**, 40.
Dash, G. J., 1982, Phys. Rev. B **25**, 508.
Deutscher G., 2005, Rev. Mod. Phys. **77**, 109.
Donnelly, R. I., and C. R. Barenghi, 1998, J. Phys. Chem. Ref. Data **27**, 1217.
Eckstein, Y., J. Landau, S. G. Lipson, and Z. Olami, 1980, Phys. Rev. Lett. **45**, 1805.
Edwards, D. O., and S. Balibar, 1989, Phys. Rev. B **39**, 4083.
Edwards, D. O., S. Mukherjee, and M. S. Pettersen, 1990, Phys. Rev. Lett. **64**, 902.
Edwards, D. O., M. S. Pettersen, and H. Baddar, 1991, in *Excitations in Two-Dimensional and Three-Dimensional Quantum Fluids*, edited by A. F. G. Wyatt and H. J. Lauter (Plenum, New York), p. 361.
Edwards, M. H., 1958, Can. J. Phys. **36**, 884.
Esaki, L., 1992, Phys. Scr. **T42**, 102.
Faraday, M., 1831, Philos. Trans. R. Soc. London **121**, 319.
Feng, Y. P., 1991, Ph.D. thesis (Stanford University).
Feng, Y. P., P. Schiffer, D. D. Osheroff, and M. C. Cross, 1993, J. Low Temp. Phys. **90**, 475.
Fisher, D. S., and J. D. Weeks, 1983, Phys. Rev. Lett. **50**, 1077.
Fradkin, E., 1983, Phys. Rev. B **28**, 5338.
Franck, J. P., and J. Jung, 1986, J. Low Temp. Phys. **64**, 165.
Gallet, F., 1986, Ph.D. thesis (Université de Paris).
Gallet, F., S. Balibar, and E. Rolley, 1987, J. Phys. (Paris) **48**, 369.
Gallet, F., P. E. Wolf, and S. Balibar, 1984, Phys. Rev. Lett. **52**, 2253.
Giorgini, S., and R. M. Bowley, 1995, J. Phys. I **5**, 815.
Golub, A. A., and S. V. Svatko, 1980, Fiz. Nizk. Temp. **6**, 957 [Sov. J. Low Temp. Phys. **6**, 465 (1980)].
Graf, M. J., R. M. Bowley, and H. J. Maris, 1984, Phys. Rev. Lett. **53**, 1176.
Graf, M. J., R. M. Bowley, and H. J. Maris, 1985, J. Low Temp. Phys. **58**, 209.
Graf, M. J., and H. J. Maris, 1987, Phys. Rev. B **35**, 3142.
Graner, F., S. Balibar, and E. Rolley, 1989, J. Low Temp. Phys. **75**, 69.
Graner, F., R. M. Bowley, and P. Nozières, 1990, J. Low Temp. Phys. **80**, 113.
Graner, G., 1991, Ph.D. thesis (Université de Paris).
Gridin, V., J. Adler, Y. Eckstein, and E. Polturak, 1984, Phys. Rev. Lett. **53**, 802.
Grinfeld, M. A., 1986, Dokl. Akad. Nauk SSSR **290**, 1358 [Sov. Phys. Dokl. **31**, 831 (1986)].
Grinfeld, M. A., 1993, J. Nonlinear Sci. **3**, 35.
Gruber, E. E., and W. W. Mullins, 1967, J. Phys. Chem. Solids **28**, 875.
Guthmann, C., S. Balibar, E. Chevalier, E. Rolley, and J. Sutra-Fourcade, 1994, Rev. Sci. Instrum. **65**, 273.
Hakonen, P. J., H. Alles, A. V. Babkin, and J. P. Ruutu, 1995, J. Low Temp. Phys. **101**, 41.
Harris-Lowe, R. F., and K. A. Smee, 1970, Phys. Rev. A **2**, 158.
Hazareesing, A., and J. P. Bouchaud, 2000, Eur. Phys. J. B **14**, 713.
Helfrich, W., 1978, Z. Naturforsch. A **33a**, 305.
Herring, C., 1953, in *Structure and Prorperties of Solid Surfaces*, edited by R. Gomer and C. S. Smith (University of Chicago, Chicago), p. 5.
Hoogeman, M. S., M. A. J. Klik, D. C. Schlösser, L. Kuipers, and J. W. M. Frenken, 2000, Surf. Sci. **448**, 142.
Huber, T. E., and H. J. Maris, 1981, Phys. Rev. Lett. **47**, 1907.
Huber, T. E., and H. J. Maris, 1982, J. Low Temp. Phys. **48**, 463.
Huse, D. A., 1984, Phys. Rev. B **30**, 1371.
Iordanskii, S. V., and S. E. Korshunov, 1983, Pis'ma Zh. Eksp. Teor. Fiz. **38**, 542 [JETP Lett. **38**, 655 (1983)].
Iordanskii, S. V., and S. E. Korshunov, 1984, Zh. Eksp. Teor. Fiz. **87**, 927 [Sov. Phys. JETP **60**, 528 (1984)].
Iordanskii, S. V., and S. E. Korshunov, 1985, J. Low Temp. Phys. **58**, 425.
Jayaprakash, C., C. Rottman, and W. F. Saam, 1984, Phys. Rev. B **30**, 6549.
Jayaprakash, C., and W. F. Saam, 1984, Phys. Rev. B **30**, 3916.
Jayaprakash, C., W. F. Saam, and S. Teitel, 1983, Phys. Rev. Lett. **50**, 2017.
Jochemsen, R., 2002, private communication.
Kagan, M. Y., 1986, Zh. Eksp. Teor. Fiz. **90**, 498 [Sov. Phys. JETP **63**, 288 (1986)].
Kagan, M. Y., and Y. A. Kosevich, 1986, Zh. Eksp. Teor. Fiz.

**91**, 826 [Sov. Phys. JETP **64**, 487 (1986)].
Kardar, M., G. Parisi, and Y. C. Zhang, 1986, Phys. Rev. Lett. **56**, 889.
Kassner, K., 1996, *Pattern Formation in Diffusion-Limited Crystal Growth* (World Scientific, Singapore).
Kawaguchi, Y., T. Ueno, Y. Kinoshita, Y. Sasaki, and T. Mizusaki, 2002, J. Low Temp. Phys. **126**, 27.
Keesom, W. H., 1926, Commun. Phys. Lab. Univ. Leiden **184**, 17.
Keshishev, K. O., and O. A. Andreeva, 1991, in *Excitations in Two-Dimensional and Three-Dimensional Quantum Fluids*, edited by A. F. G. Wyatt and H. J. Lauter (Plenum, New York), p. 387.
Keshishev, K. O., A. Y. Parshin, and A. V. Babkin, 1979, Pis'ma Zh. Eksp. Teor. Fiz. **30**, 63 [JETP Lett. **30**, 56 (1980)].
Keshishev, K. O., A. Y. Parshin, and A. V. Babkin, 1981, Zh. Eksp. Teor. Fiz. **80**, 716 [Sov. Phys. JETP **53**, 362 (1981)].
Keshishev, K. O., A. Y. Parshin, and A. I. Shal'nikov, 1982, in *Soviet Scientific Reviews*, edited by I. M. Khalatnikov, Section A: Physics Reviews, Vol. 4 (Harwood Academic, New York).
Knops, H. J. F., 1977, Phys. Rev. Lett. **39**, 766.
Knops, H. J. F., 1979, Phys. Rev. B **20**, 4670.
Korshunov, S. E., 1986a, Zh. Eksp. Teor. Fiz. **90**, 2118 [Sov. Phys. JETP **63**, 1242 (1986)].
Korshunov, S. E., 1986b, Zh. Eksp. Teor. Fiz. **91**, 1466 [Sov. Phys. JETP **64**, 864 (1986)].
Korshunov, S. E., 1993, Phys. Rev. B **48**, 3969.
Korshunov, S. E., and A. V. Smirnov, 1982, Zh. Eksp. Teor. Fiz. **83**, 2128 [Sov. Phys. JETP **56**, 1234 (1982)].
Kosevich, A. M., and Y. A. Kosevich, 1981, Fiz. Nizk. Temp. **7**, 809 [Sov. J. Low Temp. Phys. **7**, 394 (1981)].
Landau, J., S. G. Lipson, L. M. Määttänen, L. S. Balfour, and D. O. Edwards, 1980, Phys. Rev. Lett. **45**, 31.
Landau, L. D., 1965, *The Equilibrium Form of Crystals*, in *Collected Papers* (Pergamon, Oxford).
Langer, J. S., 1980, Rev. Mod. Phys. **52**, 1.
Lapujoulade, J., 1994, Surf. Sci. Rep. **20**, 195.
Leamy, H. J., G. H. Gilmer, and K. A. Jackson, 1975, in *Surface Physics of Materials*, edited by J. B. Blakeley (Academic, New York), p. 121.
Leiderer, P., 1995, Z. Phys. B: Condens. Matter **98**, 303.
Leiderer, P., H. Poisel, and M. Wanner, 1977, J. Low Temp. Phys. **28**, 167.
Maksimov, L. A., and V. L. Tsymbalenko, 2002, Zh. Eksp. Teor. Fiz. **122**, 530 [JETP **95**, 455 (2002)].
Manninen, A. J., J. P. Pekola, G. M. Kira, J. P. Ruutu, A. V. Babkin, H. Alles, and O. V. Lounasmaa, 1992, Phys. Rev. Lett. **69**, 2392.
Marchenko, V. I., 1981a, Pis'ma Zh. Eksp. Teor. Fiz. **33**, 397 [JETP Lett. **33**, 381 (1981)].
Marchenko, V. I., 1981b, Zh. Eksp. Teor. Fiz. **80**, 2010 [Sov. Phys. JETP **53**, 1045 (1981)].
Marchenko, V. I., and A. Y. Parshin, 1980a, Zh. Eksp. Teor. Fiz. **79**, 257 [Sov. Phys. JETP **52**, 129 (1980)].
Marchenko, V. I., and A. Y. Parshin, 1980b, Pis'ma Zh. Eksp. Teor. Fiz. **31**, 767 [JETP Lett. **31**, 724 (1980)].
Marchenkov, A., H. Akimoto, R. van Rooijen, R. Jochemsen, and G. Frossati, 1999, Phys. Rev. Lett. **83**, 4598.
Maris, H. J., and T. E. Huber, 1982, J. Low Temp. Phys. **48**, 99.
Markovitz, T., and E. Polturak, 2001, J. Low Temp. Phys. **123**, 53.
McKenna, M. J., T. P. Brosius, and J. D. Maynard, 1992, Phys. Rev. Lett. **69**, 3346.
Mochrie, S. G. J., 1987, Phys. Rev. Lett. **59**, 304.
Mullins, W. W., and R. F. Sekerka, 1964, J. Appl. Phys. **35**, 444.
Nightingale, P. M., W. F. Saam, and M. Schick, 1984, Phys. Rev. B **30**, 3830.
Nomura, R., H. H. Hensley, T. Matsushita, and T. Mizusaki, 1994, J. Low Temp. Phys. **94**, 377.
Nomura, R., Y. Suzuki, S. Kimura, and Y. Okuda, 2003, Phys. Rev. Lett. **90**, 075301.
Nozières, P., 1992, *Shape and Growth of Crystals, in Solids Far from Equilibrium*, edited by C. Godrèche (Cambridge University, Cambridge, UK).
Nozières, P., and F. Gallet, 1987, J. Phys. (Paris) **48**, 353.
Nozières, P., F. Pistolesi, and S. Balibar, 2001, Eur. Phys. J. B **24**, 387.
Nozières, P., and M. Uwaha, 1987, J. Phys. (Paris) **48**, 389.
Nozières, P., and D. E. Wolf, 1988, Z. Phys. B: Condens. Matter **70**, 399.
Osheroff, D. D., Y. P. Feng, and P. Schiffer, 1991, Physica B **169**, 204.
Osheroff, D. D., and R. C. Richardson, 1985, Phys. Rev. Lett. **54**, 1178.
Osheroff, D. D., R. C. Richardson, and D. M. Lee, 1972, Phys. Rev. Lett. **28**, 885.
Osheroff, D. D., and C. Yu, 1980, Phys. Lett. **77A**, 458.
Parshin, A. Y., 1985, *Crystallization Waves in* $^4$*He*, in Low Temperature Physics, edited by A. S. Borovik-Romanov (MIR, Moscow).
Parshin, A. Y., 1998, J. Low Temp. Phys. **110**, 133.
Parshin, A. Y., J. J. Saenz, and N. Garcia, 1988, J. Phys. C **21**, L305.
Parshin, A. Y., and V. L. Tsymbalenko, 2003, Pis'ma Zh. Eksp. Teor. Fiz. **77**, 372 [JETP Lett. **77**, 321 (2003)].
Pierre, L., H. Guignes, and C. Lhuillier, 1985, J. Chem. Phys. **82**, 496.
Pipman, J., S. G. Lipson, J. Landau, and N. Bochner, 1978, J. Low Temp. Phys. **31**, 119.
Plomp, E. R., R. van Rooijen, H. Akimoto, G. Frossati, R. Jochemsen, and W. van Saarloos, 2001, J. Low Temp. Phys. **124**, 169.
Poitrenaud, J., M. Boiteux, and J. Joffrin, 1991, Europhys. Lett. **14**, 673.
Poitrenaud, J., and P. Legros, 1989, Europhys. Lett. **8**, 651.
Puech, L., G. Bonfait, and B. Castaing, 1986a, J. Low Temp. Phys. **62**, 315.
Puech, L., G. Bonfait, and B. Castaing, 1986b, J. Phys. (Paris) **47**, 723.
Puech, L., and B. Castaing, 1982, J. Phys. (France) Lett. **43**, L601.
Puech, L., B. Hebral, D. Thoulouze, and B. Castaing, 1982, J. Phys. (France) Lett. **43**, L809.
Puech, L., B. Hebral, D. Thoulouze, and B. Castaing, 1983, J. Phys. (France) Lett. **44**, L159.
Ramesh, S., and J. D. Maynard, 1982, Phys. Rev. Lett. **49**, 47.
Ramesh, S., Q. Zhang, G. Torzo, and J. D. Maynard, 1984, Phys. Rev. Lett. **52**, 2375.
Rayleigh, J. W. S., 1902, Philos. Mag. **3**, 338.
Rolley, E., S. Balibar, and F. Gallet, 1986, Europhys. Lett. **2**, 247.
Rolley, E., S. Balibar, F. Gallet, F. Graner, and C. Guthmann, 1989, Europhys. Lett. **8**, 523.
Rolley, E., S. Balibar, and F. Graner, 1994, Phys. Rev. E **49**, 1500.
Rolley, E., S. Balibar, C. Guthmann, and P. Nozières, 1995,

Physica B **210**, 397.
Rolley, E., E. Chevalier, C. Guthmann, and S. Balibar, 1994, Phys. Rev. Lett. **72**, 872.
Rolley, E., C. Guthmann, E. Chevalier, and S. Balibar, 1995, J. Low Temp. Phys. **99**, 851.
Rottman, C., M. Wortis, J. C. Heyraud, and J. J. Métois, 1984, Phys. Rev. Lett. **52**, 1009.
Ruutu, J. P., P. J. Hakonen, A. V. Babkin, A. Y. Parshin, J. S. Penttilä, J. P. Saramäki, and G. Tvalashvili, 1996, Phys. Rev. Lett. **76**, 4187.
Ruutu, J. P., P. J. Hakonen, A. V. Babkin, A. Y. Parshin, and G. Tvalashvili, 1998, J. Low Temp. Phys. **112**, 117.
Saam, W. F., 1973, Phys. Rev. A **8**, 1918.
Saramäki, J. P., A. V. Babkin, P. J. Hakonen, R. M. Luusalo, and A. Y. Parshin, 1998, J. Low Temp. Phys. **110**, 141.
Savignac, D., J. Bodensohn, and P. Leiderer, 1983, in *75th Jubilee Conference on Helium-4*, edited by J. G. M. Armitage (World Scientific, Singapore), p. 156.
Savignac, D., and P. Leiderer, 1982, Phys. Rev. Lett. **49**, 1869.
Shal'nikov, A. I., 1961, Zh. Eksp. Teor. Fiz. **41**, 1059 [Sov. Phys. JETP **14**, 755(1962)].
Shal'nikov, A. I., 1964, Zh. Eksp. Teor. Fiz. **47**, 1727 [Sov. Phys. JETP **20**, 1161 (1965)].
Straty, G. C., and E. D. Adams, 1969, Rev. Sci. Instrum. **40**, 1393.
Suttleworth, R., 1950, Proc. Phys. Soc., London, Sect. A **63**, 444.
Suzuki, M., M. Thiel, and P. Leiderer, 1997, J. Low Temp. Phys. **109**, 357.
Sydoriak, S. G., R. L. Mills, and E. R. Grilly, 1960, Phys. Rev. Lett. **4**, 495.
Thiel, M., A. Willibald, P. Evers, A. Levchenko, P. Leiderer, and S. Balibar, 1992, Europhys. Lett. **20**, 707.
Thuneberg, E. V., 1997, J. Low Temp. Phys. **106**, 575.
Todoshchenko, I. A., 2004, private communication.
Todoshchenko, I. A., H. Alles, H. J. Junes, A. Y. Parshin, and V. Tsepelin, 2003, Physica B **329-333**, 386.
Todoshchenko, I. A., H. Alles, H. J. Junes, A. Y. Parshin, and V. Tsepelin, 2004, Phys. Rev. Lett. **93**, 175301
Todoshchenko, I. A., H. Alles, H. J. Junes, A. Y. Parshin, and V. Tsepelin, 2005, J. Low Temp. Phys. **138**, 811.
Toner, J., and D. P. DiVincenzo, 1990, Phys. Rev. B **41**, 632.
Torii, R. H., and S. Balibar, 1992, J. Low Temp. Phys. **89**, 391.
Treiner, J., 1993, J. Low Temp. Phys. **92**, 1.
Tsepelin, V., H. Alles, A. Babkin, J. P. H. Härme, R. Jochemsen, A. Y. Parshin, and G. K. Tvalashvili, 2001, Phys. Rev. Lett. **86**, 1042.
Tsepelin, V., H. Alles, A. Babkin, R. Jochemsen, A. Y. Parshin, and I. A. Todoshchenko, 2002a, J. Low Temp. Phys. **129**, 489.
Tsepelin, V., H. Alles, A. Babkin, R. Jochemsen, A. Y. Parshin, and I. A. Todoshchenko, 2002b, Phys. Rev. Lett. **88**, 045302.
Tsepelin, V., J. P. Saramäki, A. V. Babkin, P. J. Hakonen, J. J. Hyvönen, R. M. Luusalo, A. Y. Parshin, and G. K. Tvalashvili, 1999, Phys. Rev. Lett. **83**, 4804.
Tsymbalenko, V. L., 1995, Zh. Eksp. Teor. Fiz. **108**, 686 [JETP **81**, 373 (1995)].
Tsymbalenko, V. L., 2000, J. Low Temp. Phys. **121**, 53.
Tsymbalenko, V. L., 2003, Pis'ma Zh. Eksp. Teor. Fiz. **77**, 288 [JETP Lett. **77**, 243 (2003)].
Uwaha, M., 1983, J. Low Temp. Phys. **52**, 15.
Uwaha, M., 1989, J. Low Temp. Phys. **77**, 165.
Uwaha, M., 1990, J. Phys. (Paris) **51**, 2743.
Uwaha, M., and G. Baym, 1982, Phys. Rev. B **26**, 4928.
Uwaha, M., and P. Nozières, 1986, J. Phys. (Paris) **47**, 263.
Uwaha, M., and P. Nozières, 1987, J. Phys. (Paris) **48**, 407.
van Beijeren, H., 1975, Commun. Math. Phys. **40**, 1.
van Beijeren, H., 1977, Phys. Rev. Lett. **38**, 993.
van Rooijen, R., A. Marchenkov, H. Akimoto, O. Andreeva, P. van de Haar, R. Jochemsen, and G. Frossati, 2001, J. Low Temp. Phys. **124**, 497.
van Saarlos, W., and J. D. Weeks, 1995, Phys. Rev. Lett. **74**, 290.
Vermeulen, G., S. A. Wiegers, C. C. Kranenburg, R. Jochemsen, and G. Frossati, 1987, Can. J. Phys. **65**, 1560.
Vollhardt, D., and P. Wölfle, 1990, *The Superfluid Phases of Helium 3* (Taylor and Francis, London).
Wagner, R., P. J. Ras, P. Remeijer, S. C. Steel, and G. Frossati, 1994, J. Low Temp. Phys. **95**, 715.
Wagner, R., S. C. Steel, O. A. Andreeva, R. Jochemsen, and G. Frossati, 1996, Phys. Rev. Lett. **76**, 263.
Wang, C. L., and G. Agnolet, 1992a, Phys. Rev. Lett. **69**, 2102.
Wang, C. L., and G. Agnolet, 1992b, J. Low Temp. Phys. **89**, 759.
Wang, C. L., and G. Agnolet, 1994, Physica B **194-196**, 935.
Weeks, J. D., 1980, in *Ordering in Strongly Fluctuating Condensed Matter Systems*, edited by T. Riste (Plenum, New York/London), p. 293.
Wellard, N. V., P. W. Alexander, H. E. Hall, and J. R. Hook, 1982, Physica B & C **109**, 2096.
Williams, E. D., and N. C. Bartelt, 1991, Science **251**, 393.
Wilson, K. G., 1971, Phys. Rev. B **4**, 3174.
Wolf, D. E., and P. Nozières, 1988, Z. Phys. B: Condens. Matter **70**, 507.
Wolf, P. E., S. Balibar, and F. Gallet, 1983, Phys. Rev. Lett. **51**, 1366.
Wolf, P. E., D. O. Edwards, and S. Balibar, 1983, J. Low Temp. Phys. **51**, 489.
Wolf, P. E., F. Gallet, S. Balibar, E. Rolley, and P. Nozières, 1985, J. Phys. (Paris) **46**, 1987.
Wulff, G., 1901, Z. Kristallogr. **34**, 449.
Wyborn, G. M., and A. F. G. Wyatt, 1990, Phys. Rev. Lett. **65**, 345.